Modeling of the Wire-Driven Deflection Mechanism with Application in Ureteroscope

LEI, Man Cheong

A Thesis Submitted in Partial Fulfilment of the

Requirements for the Degree of

Master of Philosophy

in

Mechanical and Automation Engineering

The Chinese University of Hong Kong

August 2011

Thesis/Assessment Committee

Professor Liu Yunhui (Chair)

Professor Du Ruxu (Thesis Supervisor)

Professor Meng Max Qing Hu (Committee Member)

Abstract

Research and development of biomedical engineering boost in recent years. In which the increasing employment of endoscopy proves itself a trustworthy surgical technology to replace the traditional operations. The equipment endoscope enables the surgeon to perform non- or minimally invasive surgery for the sake of reducing the surgical risk as well as the patient's healing time. As the channels within a human body are tortuous, flexible endoscope is specially designed for the ease of passing through the channels and cavities. It allows the surgeon to not only observe but also carry out different therapeutic procedures within the patient's body. It can thank to the deflection mechanism embedded in it. Although many products have been bringing to the market for decades, there is no systematic study about the design or specification of the endoscopes. The purpose of this research is to configure the information on designing the deflection mechanism of a flexible ureteroscope which is particularly used in urological surgery.

This deflection mechanism is mostly wire-driven. It mainly consists of the control mechanism and the bending section. This study firstly presents the CAD models of different designs of the bending section. Then the critical parameters of the bending section are introduced. Those parameters directly constrain the effect of deflection of a ureteroscope. The geometry modeling and simulations are given with respect to different values of the parameters. It follows by the trajectory analysis of the bending section under different designs. Last but not least, the result of study reveals the way of application by adopting the information in the design of a flexible ureteroscope.

摘要

近年，生物醫學工程的研究和發展一日千里，其中內窺鏡治療法的廣泛採用證明了它有足夠的能力取代傳統的手術。這絕對歸功於內窺鏡治療法可大大減低手術風險以及病人的痊癒時間，因為這種新穎的治療法是屬於無創或微創手術，顧名思義，利用內窺鏡，醫生不用在病人身上留下傷口或只需開一個很小的洞，便能完成手術。軟管鏡可適應病人體內迂迴曲折的管道，醫生可透過它觀察病人體內的情況，並在患處施以適合的手術，這都有賴於軟管鏡內的偏轉機械結構。雖然在這幾十年來已經有不少產品投入市場，但在學術上還沒有很多對於設計或規範內窺鏡的有系統的研究，因此，這個研究的目的就是提供這個偏轉機械的資料以及規範它的設計參數和結構並以專門用於排泄系統上的軟輸尿管鏡作為研究對象。

這個偏轉機械結構很多時都是被設計成綫控的，它主要由一個控制結構和一組彎曲關節組成。這個研究首先給出幾種彎曲關節設計的 CAD 模擬圖，然後定出這個彎曲關節的重要參數，這些參數都直接限制了軟輸尿管鏡的可偏轉角度。根據給予不同參數值，可找出和建立對應的幾何模型和仿真，以及彎曲關節的軌跡研究。最後，根據研究結果，提出了一個軟輸尿管鏡的偏轉機械設計。

Acknowledgement

First of all, I want to give my wholehearted thanks to my parents. Having been studying in Hong Kong for years, this year I only spent very little time at home. I really feel sorry for them. Although I did not have too much time for them, they kept concerning about me every single day. It was my bad to let them worrying about me most of time. They even came to Hong Kong to visit me. I felt so warm but compunctious at the same time. I have to say thank you again for everything they do for me.

May I also express my big thanks to my supervisor, Prof. Ruxu Du and president of MedServ International, Mr. Fond Koo for their supports during my master study. They both are very nice gentlemen. They are willing to teach me how to carry out a research project as well as what practical factors should also be taken into consideration. Their guidance of the research eased me to double the result with effort halved.

Finally, I want to thank my friends who always support me either in school work or daily life. They all are the best treasures I gain in the Chinese University of Hong Kong.

Lei, Man Cheong, Michael

Table of Contents

1. Introduction

The wire-driven deflection mechanism is a snake-like mechanism which distinguishes itself from the common snake robots because of its wire-driven method. The common snake robot have motors assembled in all its joints and by controlling the motors, the robots are able to move like a snake. While this method is effective, it is also complex and expensive. The wire-driven deflection mechanism, on the other hand, can deflect by controlling the wires passing through the joints. Thus, the control plant can be removed from the moving part. As a result, it is simple, compact and inexpensive. According to literatures, however, few systematic studies on the wire-driven deflection mechanism have been founded.

This study focuses on the kinematics of the wire-driven deflection mechanism. Two types of configurations are studied: one is driven by one pair of wires and the other is driven by two pairs of wires.

This study is partially funded by a cooperation project between Institute of Precision Engineering (IPE) at the Chinese University of Hong Kong and MedServ International Co., U.S.A. In this project, I used the wire-driven deflection mechanism to design a flexible ureteroscope for MedServ. The design includes 3D modeling, kinematic analysis, 2D engineering drawing, and suggested manufacturing methods.

The rest of the thesis is organized as follows. First, Chapter 2 gives the introduction to ureteroscopy, configuration of the ureteroscope and existing problems of the current products in the market. Ureteroscopy is a new technology developed

about ten years ago. Based on literature and market survey, few particular studies have been found. In this chapter, the CAD models of different designs are built by Solidworks®. Chapter 3 focuses on the kinematic analysis. In Section 3.1, the model of the deflection mechanism is derived. In Section 3.2, MATLAB® simulations are conducted such that a better observation of the bending section when deflecting can be realized. Furthermore, in Section 3.3, the trajectory of the distal end is studied. It contains two configurations: a single pair of control wires and a double pairs of control wires. The static analysis of the deflection mechanism is given in Section 3.4.With the study in the previous chapters, the wire-driven deflection mechanism of a ureteroscope is designed and presented in Chapter 4. It mainly consists of the bending section and the control body, which are presented in Sections 4.1 and 4.2 respectively. The conclusion in Chapter 5 summarizes the work done in this study. Future work is also given.

2. Introduction to Ureteroscope

In recent years, the wire-driven deflection mechanism found many applications in the fields of biomechanics, robotics and manufacturing. The most significant one is the endoscope. There are many types of endoscopes, among them the flexible ureteroscope is perhaps the most difficult one because of its size (approximately 3 mm in diameter) and length (approximately 500 mm).

In this chapter, first, the introduction about ureteroscope is given and the design of a ureteroscope is presented. Next, in order to understand what the market uses, different designs of the bending section are studied. Afterwards, the existing problems of the products in the market are drawn, which helps to determine the directions to work on.

2.1 Ureteroscope

It is known that many people suffer from urological diseases mostly due to irregular living habits. Before the introduction of ureteroscopy, the patients had to endure the invasive surgeries which might cause a long time to fully recover. Thanks to the advance of technologies, the ureteroscopy treatment is much less painful.

According to literatures, the ureteroscopy was firstly introduced to be the treatment on different urological conditions in late 1970s. With the ureteroscopy, the patients are able to go home in one or two days after urologic treatment. Ureteroscopy is one of the endoscopic treatments mainly operating in the ureter. It

can not only provide the images in the urinary tracts but also perform therapeutical process such as renal calculi (kidney stone) removal or elimination. In recent decades, ureteroscopy has become the treatment of choice for a growing number of urological conditions, such as kidney stone. The area which can be performed the ureteroscopy includes ureter, uretha, urinary tracts and kidney.

Ureteroscopic treatment of renal calculi could not be achieved without the recent evolution in flexible ureteroscopes. Current flexible ureteroscopes allow access to the entire intrarenal collecting system in 94-100% of patients [1, 2]. At the same time, having an efficient method to destroy the renal calculi is also important. Fortunately, the introduction of the holmium: YAG laser for use as an intraluminal lithotripsy device in the early 1990s greatly improved the precision and effectiveness of ureteroscopic lithotripsy [3-6].

Ureteroscope is a kind of endoscopes which is particularly use in the urinary system. By different configurations, it can be classified as rigid, semi-rigid and flexible. In this study, we put the focus on the flexible ureteroscope. Fig. 1 shows the popular models used nowadays.

Around 1964, Marshall [7], Takagi et al. [8] and Bush et al. [9] developed the first set of flexible ureteroscopic procedures which could be regarded as the pioneer of the ureteroscopy. However, the earliest flexible ureteroscopes could only provide visualization of the upper urinary tract as there was no deflecting mechanism integrated in the design of the ureteroscope. Due to this limitation together with the

introduction of shock-wave lithotripsy, the flexible ureteroscope was not widely used until flexible fiber optics was well developed.

(a) Gyrus ACMI DUR-8 Elite

(b) Olympus URF-P5

Figure 1: Popular models using in the current ureteroscopy.

2.2 Configuration of flexible ureteroscope

A flexible ureteroscope basically consists of three parts, namely, the optical system, deflection mechanism, and the working channel. The optical system gives the image of the patient's intrarenal collecting system. The deflection mechanism allows the urologist to control the ureteroscope to access to the desired place. Last but not least, the working channel is a tunnel for surgical tools such as basket and laser.

2.2.1 The optical system

The development of flexible ureteroscope indeed has a very close relationship with the improvement of flexible fiber optics. Despite how good the deflection mechanism can be designed, there must be a corresponding fiber optics which allows

bending of light without losing any image information. Thus, the optical system is undoubtedly the soul of a ureteroscope. The optical system consists of two parts which are the image bundles and the light bundles. An image bundle is made of fiber optics which is bundled with identical orientation at each end. In order words, the fibers are bundled coherently. The light from each fiber within the image bundle will coalesce to transmit images. The fiber optics used to form a light bundle can be treated less restricted. They are bundled randomly because they are only used for providing excellent illumination at the distal end of the ureteroscope. Besides the use of fiber optics, small lenses are also used to attach the distal and proximal ends of the image bundle in order to create a telescope with magnified image.

One can easily see that the construction of the image bundle directly affects the ureteroscope. Provided that closer packing of more fibers can be achieved, the outer diameter of the ureteroscope can be reduced, or the working channel can be larger. Thus larger tools and / or more tools can be put inside the working channel.

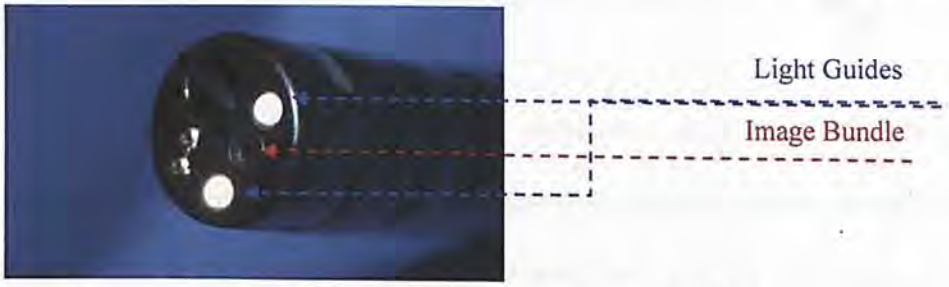

Figure 2: Light guides and image bundle at the tip of the ureteroscope.

2.2.2 Deflection mechanism

The deflection mechanism permits the surgeon to completely maneuver the flexible ureteroscope into the intrarenal collecting system. It basically consists of a

pair of control wires (guide wires) passing through the bending section and connecting the manually operated lever mechanism at the proximal end. Moving the lever up or down will pull the control wire to move the tip of the ureteroscope up or down. Both up or down deflection are in the same plane. Fig. 3 illustrates the basic configuration of the deflection mechanism.

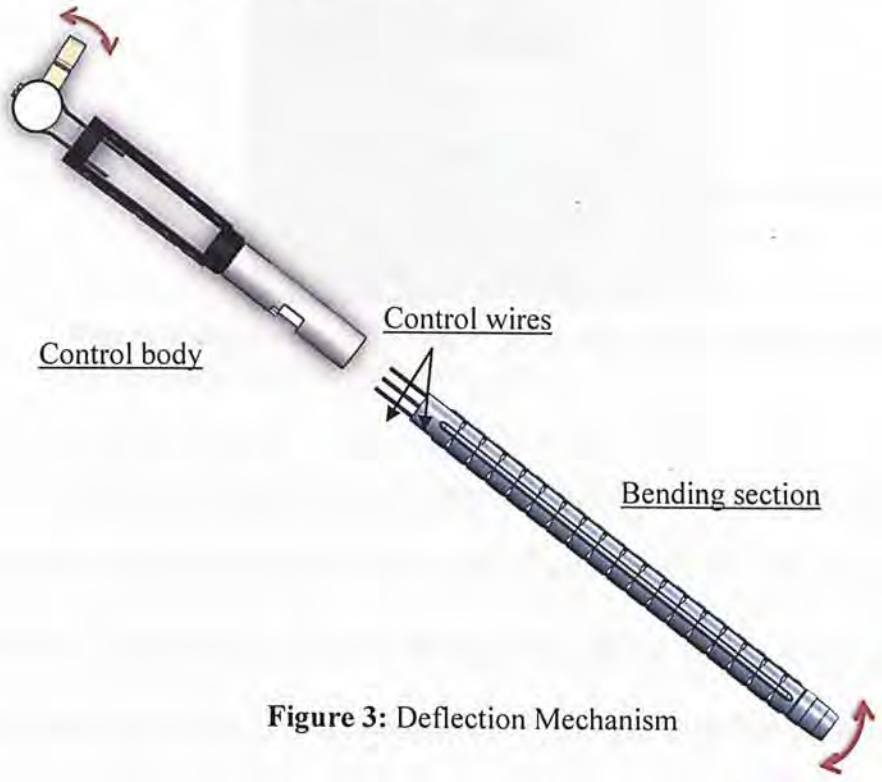

Figure 3: Deflection Mechanism

Depending on the design of the deflection mechanism, the deflection performed by the ureteroscope can be classified by three types: Primary active deflection, secondary active deflection and secondary passive deflection. Primary means the initial deflection of the bending section. Secondary means the further deflection based on the primary deflection. The point of deflection for primary and secondary are not the same. Active deflection means that the deflection is controlled by the surgeon. Passive deflection means that the deflection only happens when the surgeon push the ureteroscope ahead inside the ureter. Because of the existence of the bending section, the ureteroscope can access to certain place within the intrarenal

collecting system. The passive deflection simply follows the path of the urether to the lower urinary tract. Fig.4 demonstrates the primary active (tip) deflection and secondary passive deflection.

Figure 4: Demonstration of the primary active (tip) deflection and the secondary passive deflection. [10]

A study involving 30 patients reported that the average angle between the major axis of the ureter and the lower pole infundibula is 140° with a maximum of 175°[11]. It is illustrated in Fig. 5. Therefore most of the models in the market can deflect from upwards 175° to downwards 185°, i.e. Gyrus ACMI DUR-8. Table 1 lists out the specification of different models in the market.

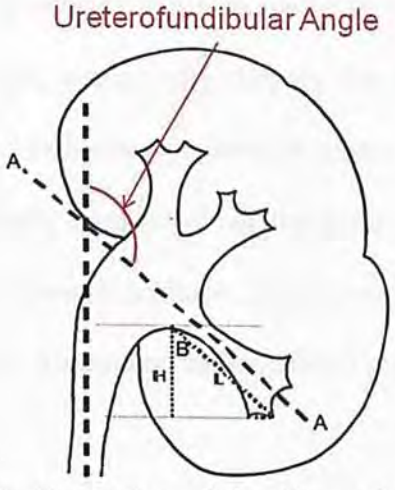

Figure 5: Illustration of the Ureterofundibular Angle (angle between the major axis of the ureter and the lower pole infundibula)

Characteristics	Gyrus ACMI			Olympus	Karl Storz	Richard Wolf		
	DUR-D (digital)	DUR-8	DUR-8 Elite	URF-P5	Flex-X2	7330 0.072	7325 0.172	7325 0.071
Tip diameter, Fr	8.7	6.75	6.75	5.3	7.5		6.8	6.0
Shaft diameter, Fr	9.3	8.6	8.6	8.4	8.4	9.0	7.5	8.8
Working length, cm	65	65	65	70	70	70	70	68
Channel size, Fr	3.6	3.6	3.6	3.6	3.6	4.5	3.6	3.6
Active deflection up, °	250	175	175	180	270	130	130	270
Active deflection down, °	250	185	185	275	270	160	160	270
Active secondary deflection, °	0	0	165	0	0	0	0	0
Angle of view, °	9	12	12	0	6	0	0	0
Field of view, °	80	80 ± 5	80 ± 5	90	90	65	65	65
Depth of field, mm		2–40	2–40	2–50	2–50	2–40	2–40	2–40
Magnification	Zoom capabilities	30×	30×	52×	40×	50×	50×	50×

Table 1: Characteristics of the currently available flexible ureterscopes [11]

2.2.3 Control wires (Guidewires)

In order to bend the tip of the ureteroscope, the most frequently component, control wires are used. The control wire is a solid wire with a coiled spring wire tightly wrapped around it. Because of frequently use, it also sustains the most stress in the ureteroscope. To decrease the friction between the wire and the wall of the bending section, the outer surface of the wire can be treated with various coatings such as Telfon and polytetrafluoroethylene. There is also an alternative design of the control wire which uses polyurethane plus hydrophilic polymer to replace the coiled spring wire. Such construction is especially slippery that is particularly helpful for negotiating tortuous segments of ureter, ureteral strictures, and bypassing impacted ureteral stones. The commonly used length of the control wire is 150cm and the minimum diameter can be 0.2mm. In addition, if the control wire mounts at different places of the bending section, it would result in different part of deflection.

Figure 6: Different control wires including (from left to right) polytef (Teflon)-coated, hydrophilic-coated, angled-tip, and J-tipped. [10]

2.2.4 Working channel

The working channel is a place prepared for the ureteroscopic instruments. They are used to perform a series of ureteroscopic procedures especially for renal calculi removal. The instruments include a variety of laser, baskets, grasping forceps and loops. From Table 1, the diameter of the working channel of all the models is 3.6 Fr (1.2mm). Therefore the instruments are usually designed no larger than 1mm in terms of the diameter.

2.3 Problems of the existing products

According to Hudson's study [12], in order to let the ureteroscope pass the urethra and ureter easier, the outer diameter of the bending section of the ureteroscope should be as small as possible. Refer to the specifications of different models of ureteroscopes in the market, their outer diameters range from 2.5mm to 3.0mm. The design of the bending section in this paper proposes that the outer diameter is possibly reduced to 2.4mm. However, the outer diameter can hardly reduce more because at least one image guide, two light guides and one working

channel are put inside the bending section. The sizes of these components are assumed to be standard. Thus, such improvement is considerably significant since it can further lower the chance for the ureteroscope harming the urinary system.

Besides, several groups of researchers, including Bratslavsky, Moran, and Afane et al.[13], evaluated the durability of different ureteroscopes which outer diameters were less than 3mm. It was found that those ureteroscopes needed repair after 6-15 procedures or 3-12.8 hours of use. In addition, due to the linkage between two parts in the bending section are mainly pin joints, it is not convenient to replace the broken parts. In other words, it would be great if the repairing time can be shortened and the damage to the good components can be avoided during repair. With such goal, the proposed design completely distinguishes from the conventional ones.

2.4 Designs of the bending section

Ureteroscopy is a relatively new urologic treatment. It is still in the developing stage. The improvement of a flexible ureteroscope highly depends on the improvement on the flexible fiber optics, together with the effort done by the endoscope manufacturers and urologists. Although rapid improvements on the design of ureteroscope can be seen recently, there are still some critical issues which block the way to the urologists' desired design. As the current flexible fiber optics has already been ideal enough to use in the ureteroscope, more effort should be put on the miniaturization and durability of it. Therefore, I want to make a design which is able to tackle some of the existing problems.

As shown in Table 1, there are mainly four companies dominating the market of ureteroscopes. However, among them, Olympus and Karl Storz are the real dominators since ACMI was purchased by Olympus and now focuses on the US market. Summarizing the products in the market, the design of the bending section contains two features. The first one is the configuration of the parts forming it. The second feature is the way to link the parts together. In section 2.4.1 to 2.4.3, three designs of the bending section: pin-joint bending section, wire-connected bending section and smart alloy bending section.

2.4.1 Pin-joint bending section

As mentioned in the paragraph above, the designs of the bending sections distinguish themselves by the method of connection. In this section, pin-joint will be introduced. It is also the most commonly used joints found in the designs of bending sections. Two types of pin-joint design are easily found, namely, rivet and spot-welding. Both have the advantage of stable assembling but are bad for maintenance. It is because they cannot be disassembled but be damaged in order to separate the adjacent parts. Fig.7isa pin-jointed bending section composing of alternatively identical parts which means two kinds of parts different in length are chosen to form the bending section by assembling with each other alternatively. Fig. 8 shows another pin-joint bending section which consists of two sub-sections. Different from the bending section in Fig. 7, the two parts with different lengths independently compose two subsections first. Then the two subsections are connected together to form a complete bending section. The number of parts chose in the subsections can be different. It depends on the desired extent of deflection that the bending section

can make. Detail of the relationship between the desired angle of deflection and the part of the bending section will be given in Chapter 3.

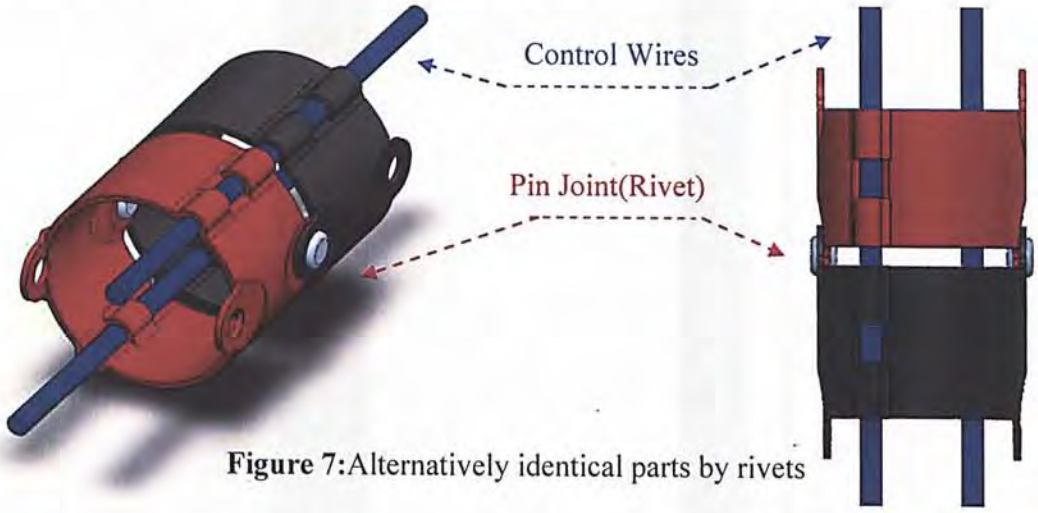

Figure 7: Alternatively identical parts by rivets

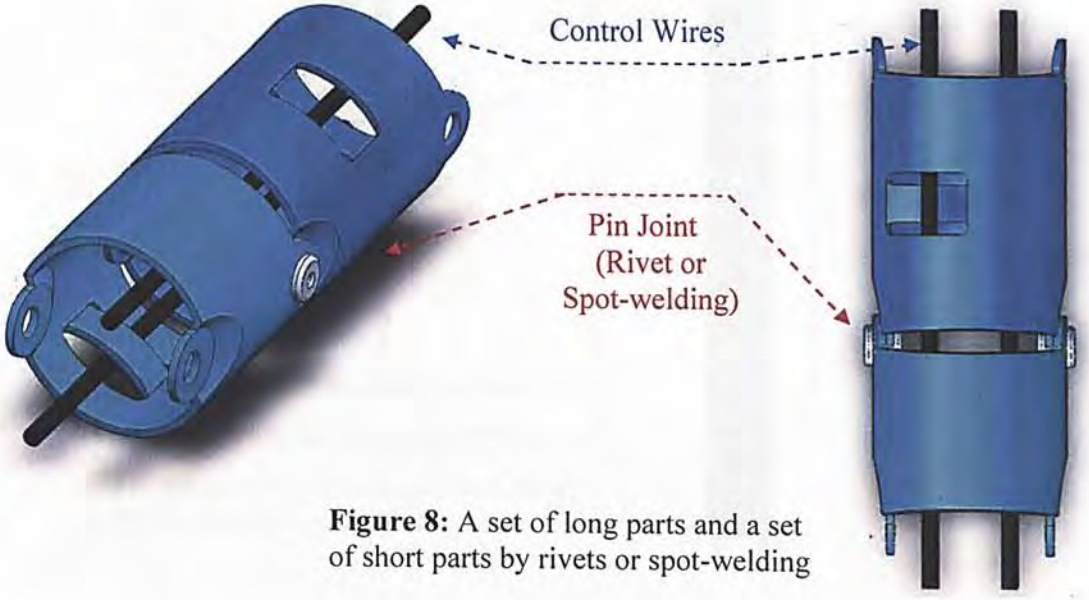

Figure 8: A set of long parts and a set of short parts by rivets or spot-welding

Fig.9shows the complete bending sections composing of designs in Fig. 7 and Figure 8 respectively. The bending section in Fig. 9(a) is formed by the red parts and black parts linking alternatively. Here the red part has shorter length than the black part. All the parts are linked as pin joints by using rivets. In Fig. 9(b), the bending section is composed of two sets of parts namely Part A and Part B. Part B

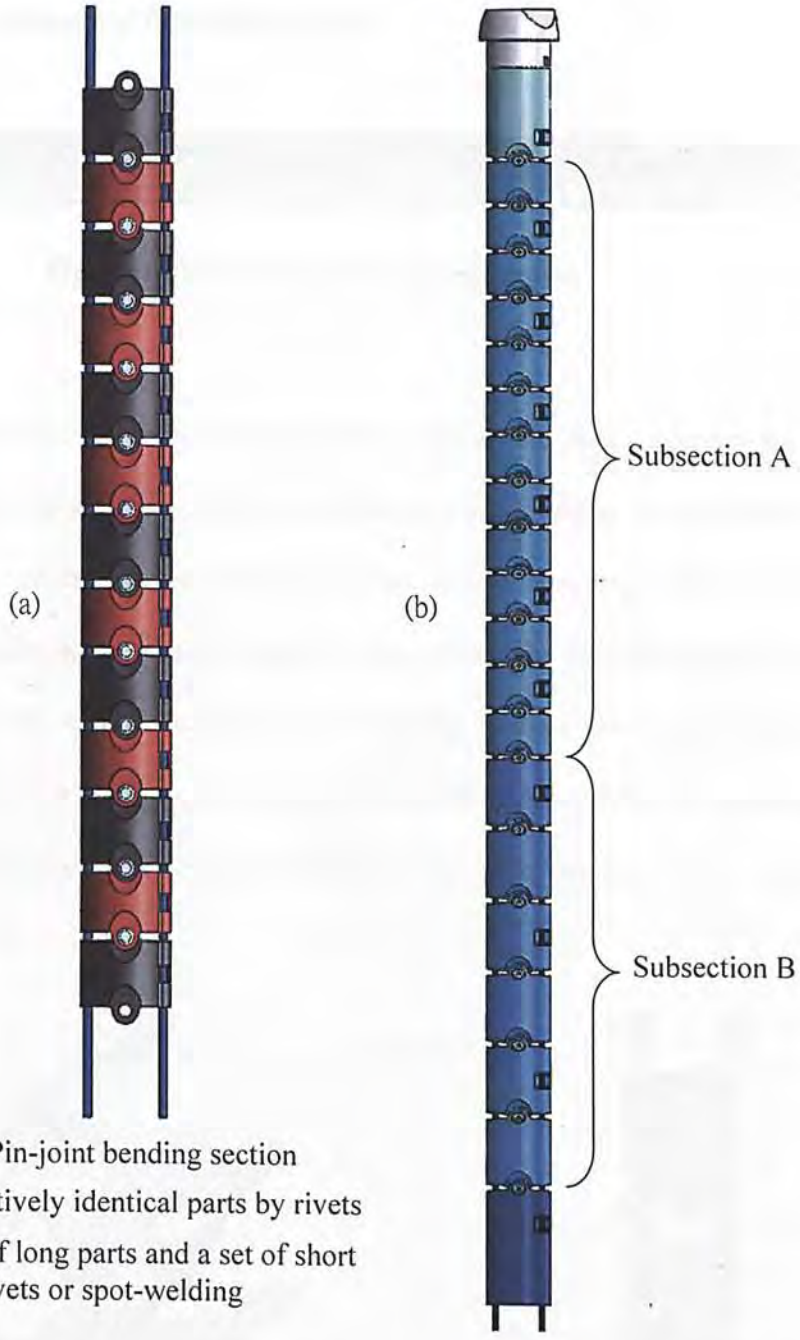

Figure 9: Pin-joint bending section
(a) Alternatively identical parts by rivets
(b) A set of long parts and a set of short parts by rivets or spot-welding

has longer length than Part A but both of them have the same diameter. This bending section can be regarded as a combination of two subsections which are formed by identical parts. The first subsection comprises Part B while the other comprises Part A called. For convenience, here the two subsections are called as subsection B and subsection A respectively. Subsection A can deflect 180° while subsection B can deflect 90°. All the parts are linked by rivets or spot-welding.

2.4.2 Wire-connected bending section

Figure 10: Wire-connected bending section

Fig. 10 illustrates the entire bending section with all the parts connected by a pair of wires. The bending section in the second design is formed by identical parts. The characteristics of this design attributes to the wire-connecting design which means all the parts are stringed up by a pair of wires. Since the connecting wires are always falling on the middle surface of the bending section, the length of the connecting wires will not change even though it is deflecting. Then it can be assumed that the connecting wires can always sustain the minimum bending stress under maximum deflection.

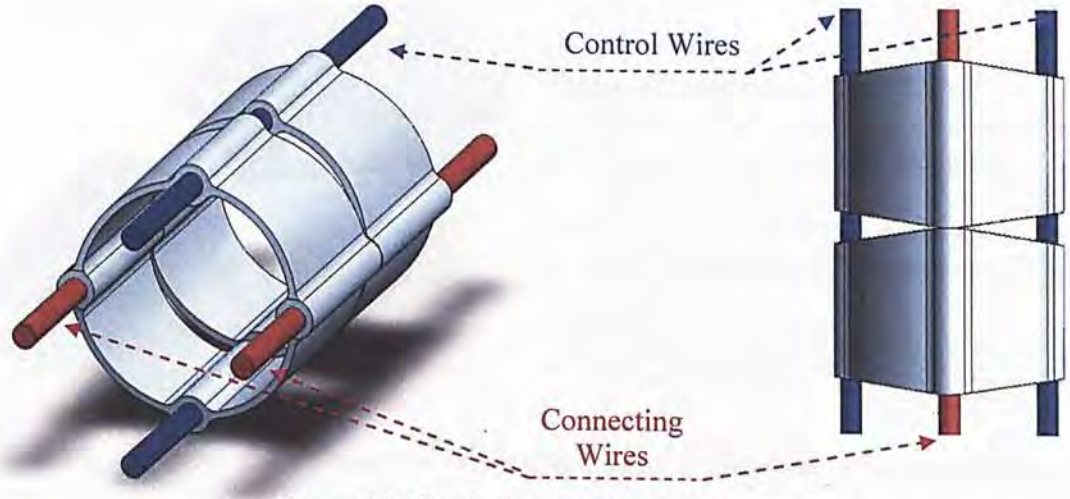

Figure 11: Identical parts by connecting wires

Fig. 11 illustrates how the parts are linked in which the control wires pierce through the parts. In addition, the holes for the wires to pass through can be reduced in length. This will reduce the friction between the part and the wire. However, it is

also important to notice that if stamping is used to manufacture the part with shortened holes, then there should be no problem. Otherwise, it is considerably difficult to make by machining.

2.5 CAD modeling of the bending section

2.5.1 Different designs of components

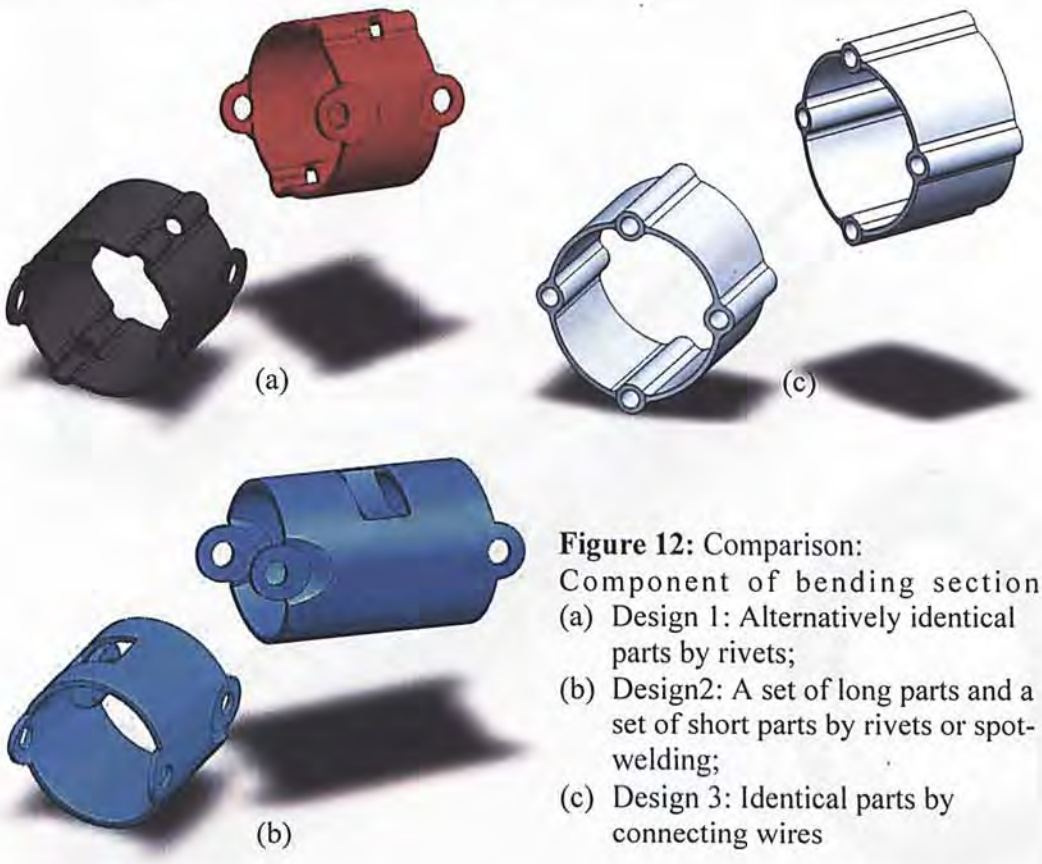

Figure 12: Comparison: Component of bending section
(a) Design 1: Alternatively identical parts by rivets;
(b) Design2: A set of long parts and a set of short parts by rivets or spot-welding;
(c) Design 3: Identical parts by connecting wires

Fig. 12 gives the comparison of the parts using in the three aforementioned designs. Usually the diameters of all bending sections remain the same. Therefore, the length of a part is the only dimension to be determined. Here two types of parts of different lengths are used in Designs 1 and 2 in Fig. 12 while the parts used in Design 3 are all identical. The length, the diameter and the gap distance between two

sections determine the radius and angle of the deflection. Detail of which will be given in the subsequent sections.

2.5.2 Configuration of the bending section

Taking the wire-connected bending section as an example, there are two more parts added at the distal end to form the whole bending section. In Fig. 13, it is clearly illustrated the exits for image bundle, light guides and working channel.

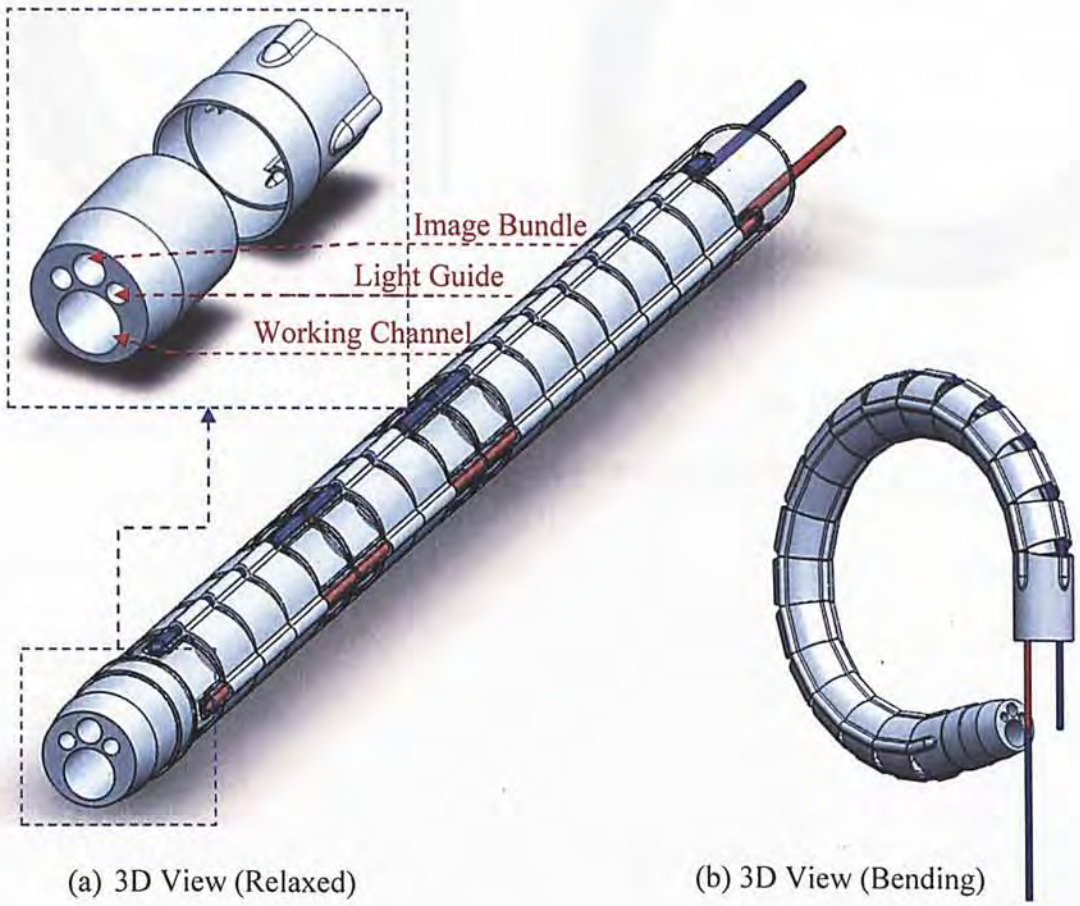

(a) 3D View (Relaxed)

(b) 3D View (Bending)

Figure 13: Different views of design2

Fig. 14 gives the 2D views of the design 2 and 3 when the bending section is fully deflected. One thing worth to mention is that the contact of two adjacent parts of design 3 is obvious a point contact. However the wire-connected design can achieve a face contact while full deflection occurs.

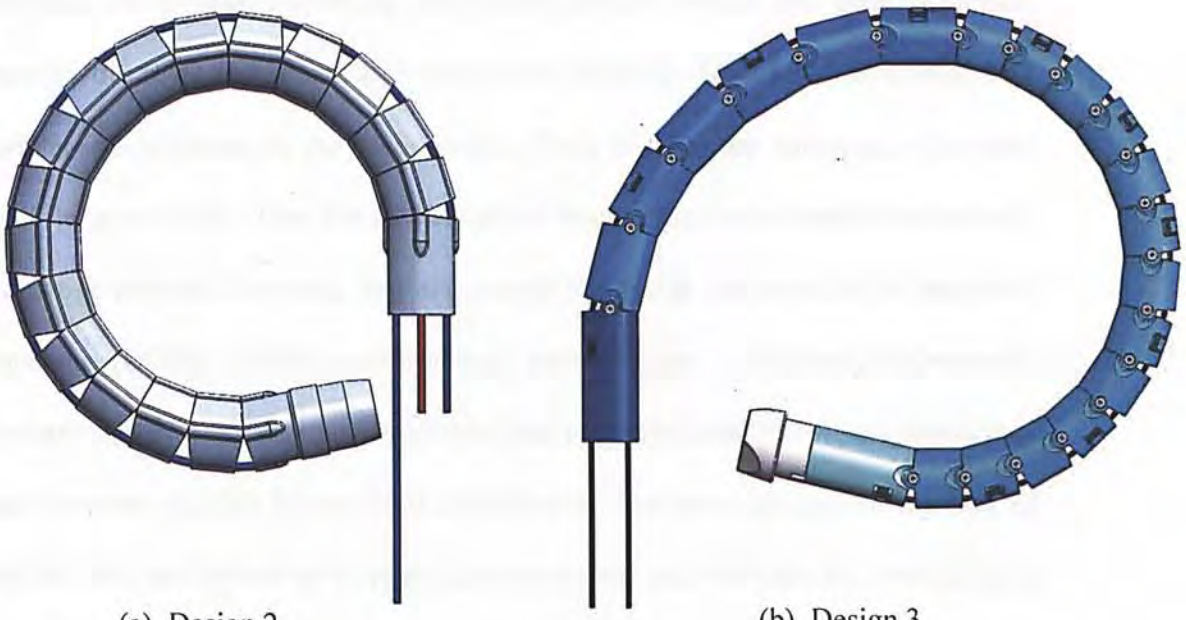

(a). Design 2 (b). Design 3

Figure 14: 2D views for full deflection

3. Wire-Driven Deflection Mechanism

3.1 Literature review

Nowadays, robot arms or manipulators are increasingly used both in industry and daily life. Generally speaking, robot arms could be divided into three categories, namely, discrete, serpentine and continuum [14][15]. Traditional sequential and parallel robots belong to the discrete type. Both of them are composed of several rigid links and joints. They are capable of reaching to the desired position accurately with large payload. However, they are usually big in size and have limited degree of freedoms (DOFs), which constrain their performance in confined environment. Continuum robots are compact and theoretically have infinite DOFs. As a result, they may be more suitable for confined environment. However, because of the lack of rigidity, they are limited by its position accuracy and payload capacity. According to literatures, existing continuum robots are mainly in the development stage with few practical applications [16]. Serpentine robots have higher rigidity than continuum robots and are more flexible than discrete robots. It has found many applications, such as endoscope in minimally invasive surgery [17].The ureteroscope mentioned in this thesis is particularly used in the urological surgery.

It is commonly known that traditional snake robots are driven by servo motors assembled at each joint; however nature works in a different way. For example, a human finger is made of rigid bones and flexible muscles and tendons [18]. As muscles can only yield tension to realize reciprocate motion, a group of

muscles should work together. While one extends, the other contracts. In the nature, such a motion is widely found. Other than human fingers and snakes, human spines and fishes also apply.

Various artificial muscles have been developed for deflectable robots, continuum or serpentine. There are mainly four types of artificial muscles: SMA (Shape Memory Alloy) wires [19], EAP (Electro Active Polymer) [20][21], PAM (Pneumatic Artificial Muscle) [22], and PZT (Piezoelectric Ceramic) [23]. For SMA artificial muscles, as heating and cooling process is necessary, the response time is quite long. Besides, high temperature makes it unsuitable for bio-related applications. For EAP artificial muscles, due to the low rigidity of the polymer their payload capacity is limited. PAM artificial muscles, typically McKibben actuator, can produce large force and are easy to control. However, they cannot survive without high pressure air compressor, which is usually complex and expensive. For PZT artificial muscles, the required voltage is generally high, and the working range is small. However, wire or cable can also function as human muscle [24]. They are inexpensive, flexible, and can bear large tension with small diameter. Practically, they can also transmit forces and motion. This application can easy be found on endoscopes. The study of deflection mechanism in this research is based on the method of wire-driven.

In this chapter, the geometry modeling will firstly be introduced in section 3.2. In which the relationship between the dimensions of the parts and the radius of deflection will be gone through. Based on the geometry modeling in section 3.2, simulations of the deflection for different configurations of bending sections will be

demonstrated in section 3.3.It follows by the trajectory analysis of the distal end in section 3.4. Last but not least, the statics analysis of the deflection mechanism will be provided in section 3.5

3.2 Geometry modeling of the bending section

3.2.1 Description of formulation

In this study, the deflection of the bending section is assumed to be a plane motion. In other words, the locations of the parts composing the bending section can be defined in a global x-y coordinate frame. The formulation is reasonable because the ureteroscope is able to perform a plane motion only. If the urologist wishes to change the orientation of the ureteroscope, he has to rotate the entire uretoscope to the desired angle and it is totally irrelevant to the deflection mechanism within the ureteroscope. Then the assumption can be made as follows

3.2.2 Assumption

A bending section can be formed by several sub-sections. In the following geometry analysis, the parts forming a sub-section are assumed to be identical. Then the analysis of the deflection can be reduced to consider a small section forming by two parts as shown in Fig. 15. Such assumption is effective since most existing models in the market use this design for the ease of manufacturing.

3.2.3 Notation

To study the bending, it is very important to clarify the key parameters in advance. The better way to do so is to denote some significant notations first:

- r : radius of the bending section
- l : length of the bending section
- g : half the distance of the gap between 2 parts when they are in relaxed state
- β : bending angle of a part
- R_N : neutral radius of the bending
- R_{in} : inner radius of the bending
- R_{out}: outer radius of the bending

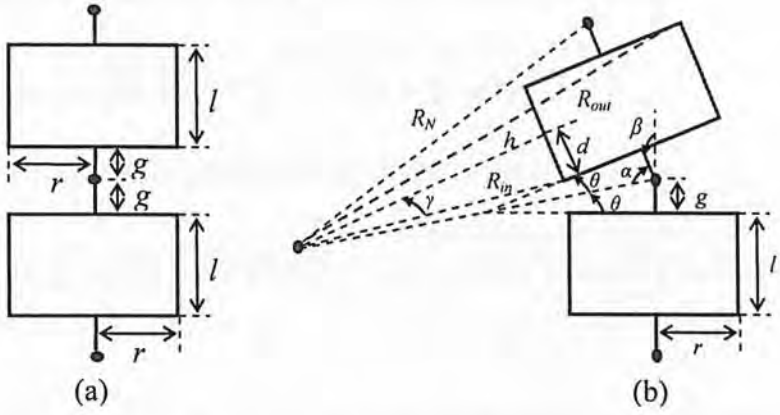

Figure 15: Schematic diagram of the 2-part subsection:

(a) Relaxed; (b) Deflecting

3.2.4 Geometry analysis

Fig. 15 contains two states of the 2-part subsection of the bending section. Fig.15(a) illustrates the relaxed state which means no force is applied to the wire. Fig.15(b) shows the counterclockwise deflection of the bending section at a certain moment while the left wire is pulled downwards. Fig. 16 demonstrates the geometry

of the bending section when full deflection occurs. From Fig. 15(b), the geometry of the bending section while deflecting can be concluded by equations (3.1) to (3.7).

$$\beta = 2\theta \tag{3.1}$$

$$\alpha = \frac{\pi}{2} - \theta = \frac{\pi-\beta}{2} \tag{3.2}$$

$$R_N = \frac{(d+g)}{\cos\alpha} = \frac{(d+g)}{\sin(\beta/2)} \tag{3.3}$$

Let $d = l/2$, then

$$h + r = (d+g)\tan\alpha = (d+g)\cot(\beta/2)$$

$$\Rightarrow \quad h = (d+g)\cot(\beta/2) - r \tag{3.4}$$

$$\tan\gamma = d/h$$

$$\Rightarrow \quad \gamma = \tan^{-1}(d/h) \tag{3.5}$$

The inner bending radius of the whole bending section is

$$R_{in} = \sqrt{d^2 + h^2} = \sqrt{d^2 + \left[(d+g)\cot\left(\frac{\beta}{2}\right) - r\right]^2} \tag{3.6}$$

The outer bending radius of the whole bending section is

$$R_{out} = \sqrt{d^2 + (h+2r)^2} = \sqrt{d^2 + \left[(d+g)\cot\left(\frac{\beta}{2}\right) + r\right]^2} \tag{3.7}$$

In most of the cases, we are more interested in the minimum radii of the bending section. Among which, R_{in} is the most concerned item by the doctors and the manufacturers of the medical devices. The minimum value of R_{in} can be given by:

$\frac{dR_{in}}{d\beta} = 0$: $\beta^* = 2\tan^{-1}\frac{g}{r}$ (3.8) => $R_{in_{min}}$ occurs and,

$$R_{in_{min}} = \sqrt{d^2 + \left[(d+g)\cot\left(\frac{\beta}{2}\right) - r\right]^2}\Bigg|_{\beta^*}$$

$$= \sqrt{d^2 + \left[(d+g)\cot\left(\tan^{-1}\frac{g}{r}\right) - r\right]^2}$$

$$= d\csc\frac{\beta}{2}$$

$$\therefore \quad R_{in_{min}} = \left(\frac{l}{2}\right)/sin\left(\frac{\beta}{2}\right) \tag{3.9}$$

Equation (3.9) can also be verified by considering the full deflection case which is shown on Fig. 16.

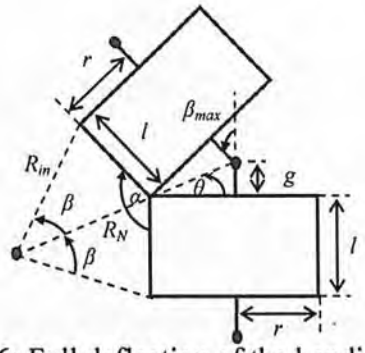

Figure 16: Full deflection of the bending section

By using the sine law,

$$\because \beta = 2\theta = 2\,tan^{-1}\frac{g}{r} \tag{3.10}$$

$$\therefore R_{in} = l\frac{\sin(\frac{\pi}{2}-\theta)}{\sin\beta} = l\frac{\cos\theta}{\sin 2\theta} = l\frac{\cos\theta}{2\sin\theta\cos\theta} = \frac{l}{2sin(\frac{\beta}{2})} \tag{3.11}$$

Obviously equation (3.9) and (3.11) are equivalent. At this moment, β reaches its maximum value and it can be denoted as β_{max}. Then we can obtain the total angle of bending,

$$\beta_{total} = N\beta_{max} \tag{3.12}$$

where N is the number of the parts forming the bending section.

As a result, given the dimensions of the bending section, N can be determined by the required maximum bending angle. The following example shown in Table 2 considers two models which have different specification on the bending section parts. Under different β_{total}, different number of sections is required.

Model	I		II	
l (mm)	1.6002		1.7780	
g (mm)	0.2032		0.1143	
r (mm)	1.2319		1.2319	
R_{min} *(mm)*	0.8109		0.8928	
β_{total}	180°	270°	180°	270°
N	10	16	17	25

Table 2: Different *N* for different models.

Fig. 17 shows the case of Model I when the bending is 270°. This is the primary active bending.

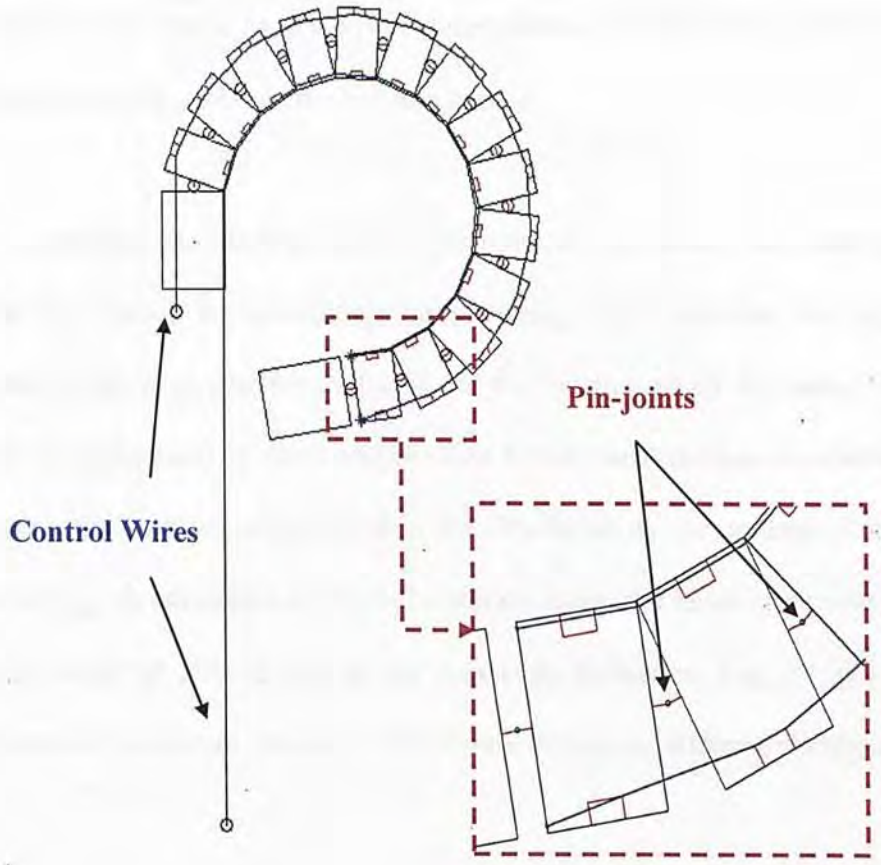

Figure 17: Illustration of Model I bending 270°

3.3 Simulations of the motion of the deflection mechanism

With the information from the previous section, simulations are made to provide a better observation or an easier way to study the motion of the deflection of the bending section. Because the urologist controls the ureteroscope to deflect very slowly, I assume that it is a static system. Also for simplicity, the deflecting angles between the parts are the same at any instant at this stage of study.

3.3.1 Construction of the simulation

Fig. 18 illustrates the flowchart of the simulation. It mainly consists of two stages. The first one is initialization in which some constant parameters will be defined and be calculated by the given dimensions of the bending section. The second stage is configuration of the bending section.

To configure the bending section, it is important to know where each part is located at that instant. By calculating the deflecting angles between two adjacent parts at an instant, it is possible to figure out the location of all the parts. Then it follows to orient the parts at their own positions. Since planar motion is considered at this moment, the parts are represented in the simulation by the contour of it cross section. As β_{max} is calculated in the initialization stage, the bending section in the simulation should be able to stop at the maximum deflection. Fig. 19 to Fig. 22 demonstrates the maximum deflection of different designs or different situations.

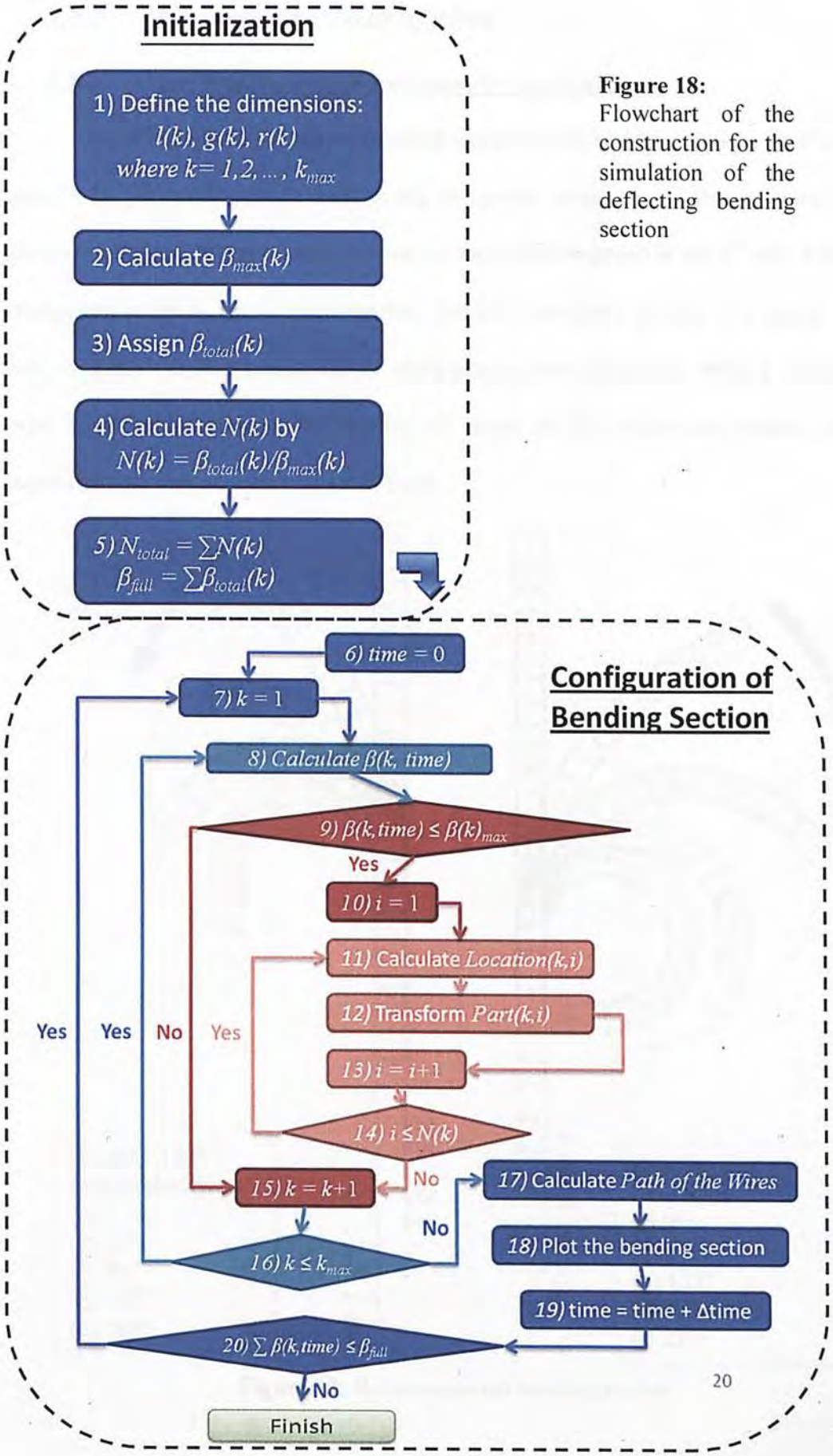

Figure 18:
Flowchart of the construction for the simulation of the deflecting bending section

3.3.2 Controlled by a pair of wires

3.3.2.1 For bending section composed by identical parts

Fig. 19 displays the wire-connected design of the bending section. Both (a) and (b) are performing the primary active deflection. However, the first six parts in (a) do not deflect. It is because there are two coil pipes mounted at the 6th part. Such design can easily be found in the market. The coil pipe plays the role as a spring. It can constrain the first part of the bending section from deflecting while a control wire is pulled. Therefore, the number of stages of the deflection requires the equivalent number of pairs of the coil pipes.

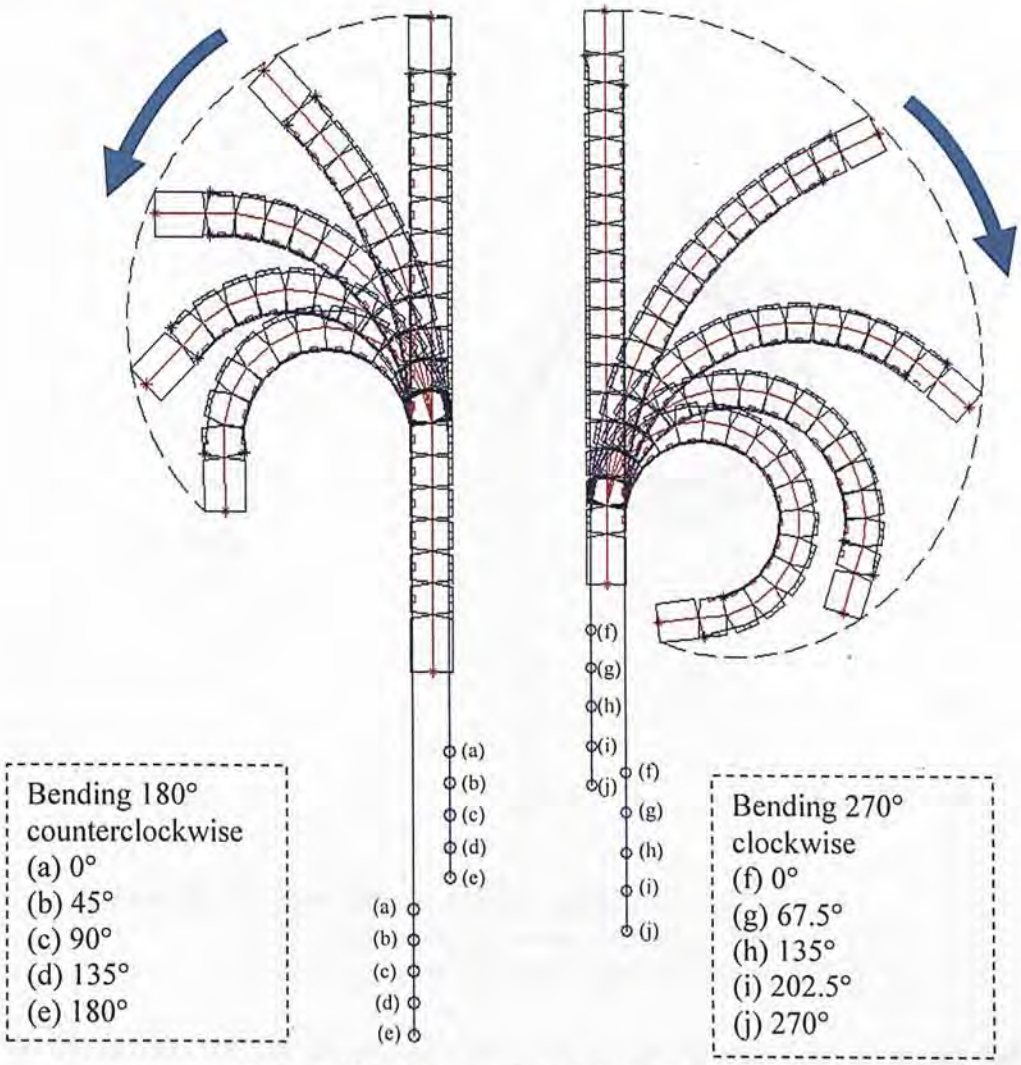

Figure 19: Wire-connected bending section

3.3.2.2 For bending section composed by two sub-sections

In Fig. 20(a), the left control wire is mounted at the end of the 12th part. Therefore, if the left wire is pulled, only the twelve parts which the wire pierces through deflect. It is an active deflection as the deflection is controlled by the wire.

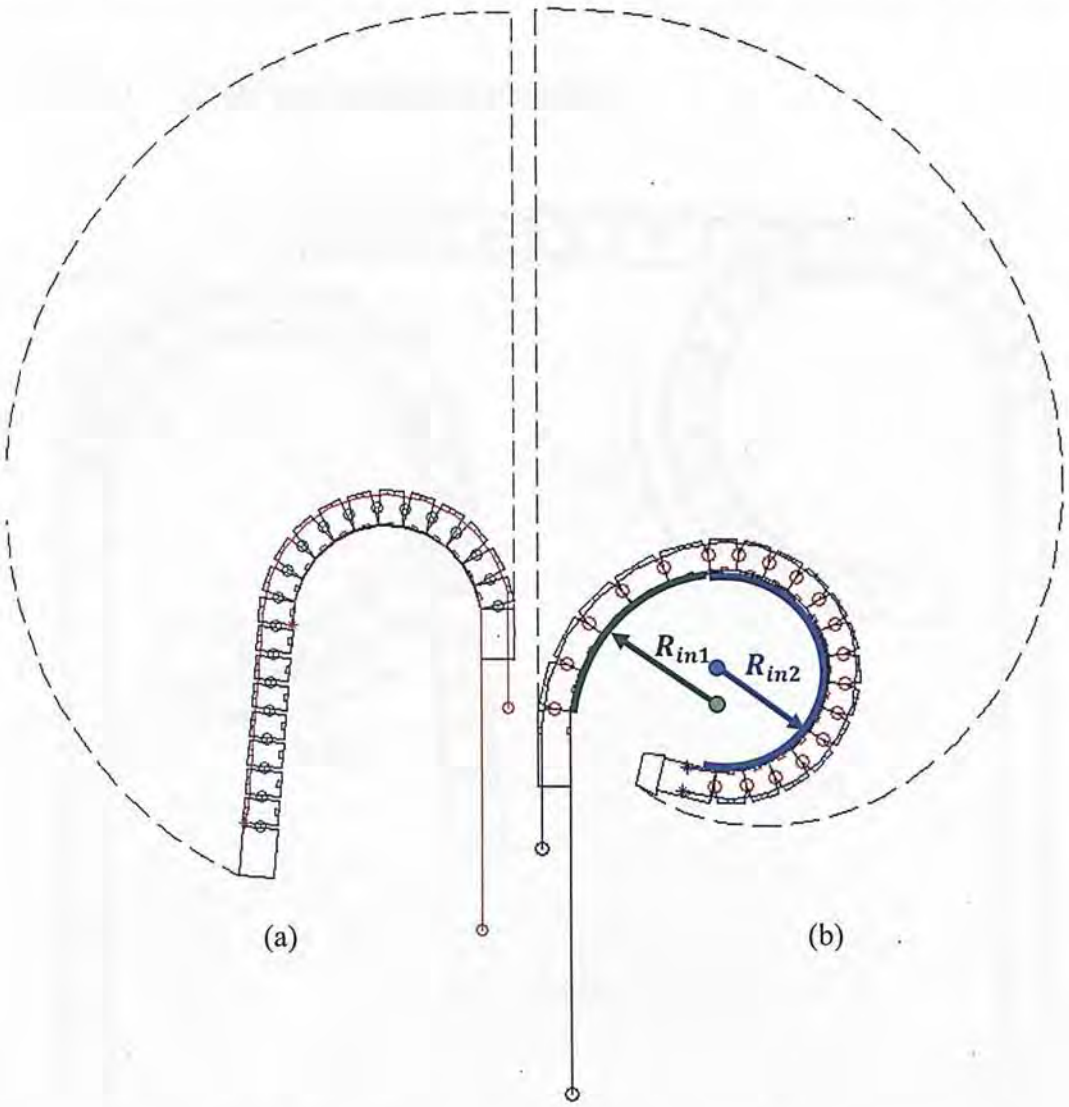

Figure 20: Pin-joint (Rivets or Spot-welding) design
(a) Identical parts: Secondary active deflection (-180°)
(b) 2 sets of parts: Primary active deflection (275°)

On the other hand, in Fig. 20(b), the control wires all the way pierce through the parts and mounted at the distal end of the bending section. Hence the whole bending

section deflects if either control wire is being pulled. It is interesting to point out that there are two inner radii, R_{in1} and R_{in2}, appears at full deflection. We can also observe $R_{in1}>R_{in2}$.

3.3.3 Controlled by two pairs of wires

3.3.3.1 Deflecting in the same direction

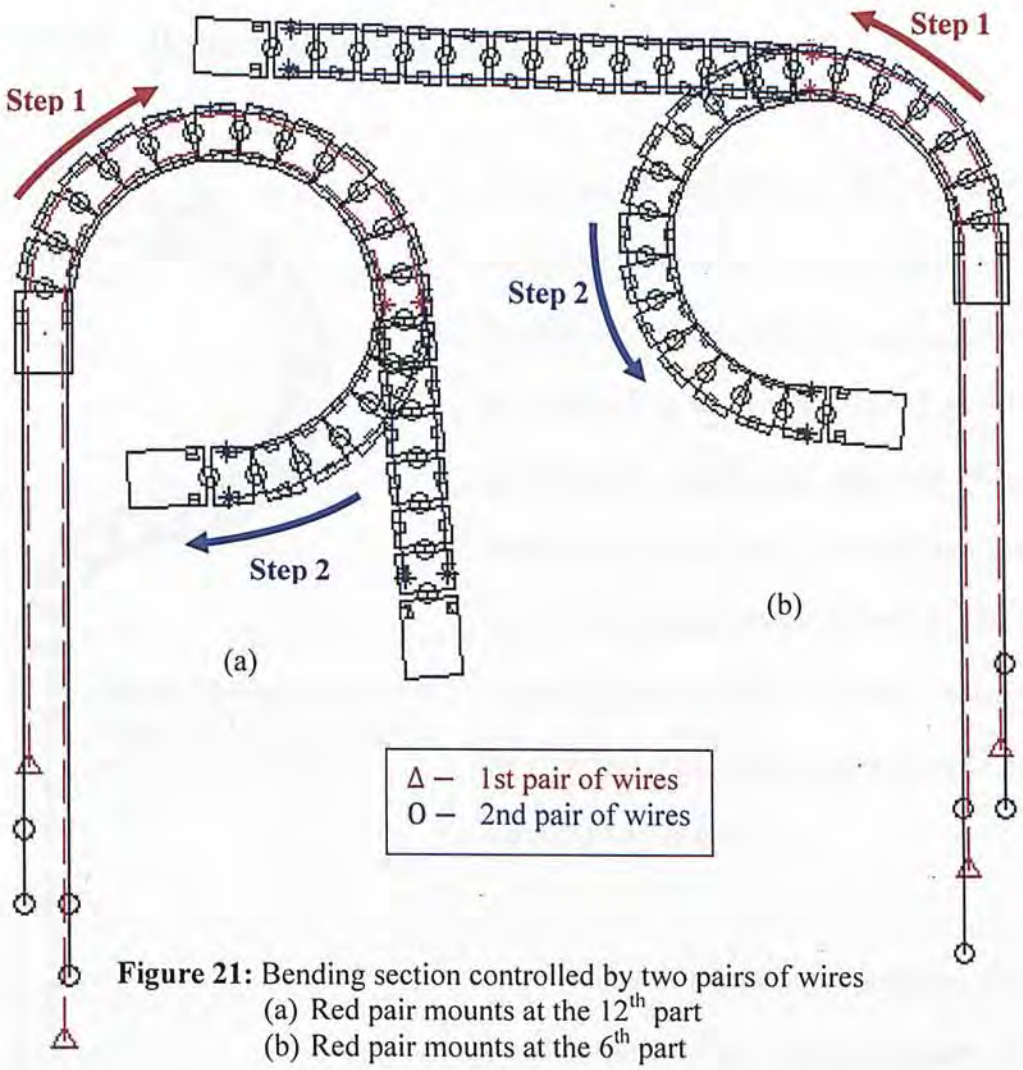

Figure 21: Bending section controlled by two pairs of wires
(a) Red pair mounts at the 12th part
(b) Red pair mounts at the 6th part

In Fig. 21, two pairs of wires are used to control the bending section. Which means the bending section can be able to perform two stages of active deflections.

Referring to Fig. 21(a), the pair of red wires is mounted at the 12th part of the bending section, thus it can control the first twelve parts to deflect to 180° clockwise. Meanwhile, the pair of blue wires is mounted at the distal end of the bending section. It enables one to pull one of the blue wires to make the rest of the bending section deflect to the extra 90°. On the contrary, in Fig. 21(b), the red wire is firstly pulled to control the first six parts deflecting to 90° and then the blue wire controls the rest to deflect to the extra 180°.

3.3.3.2 Deflecting in opposite direction

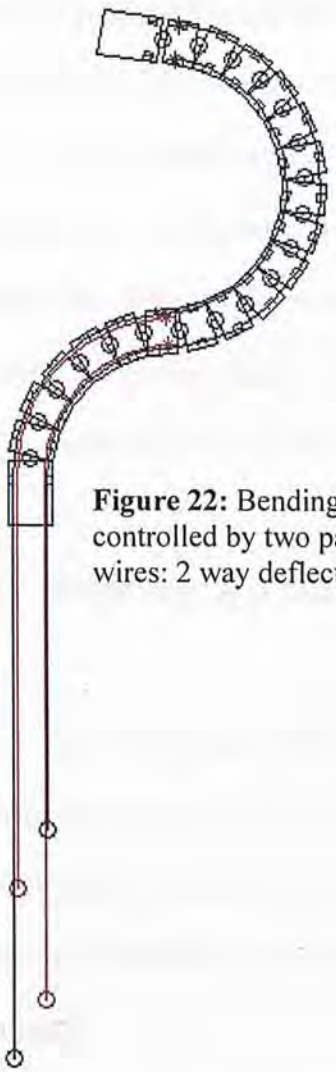

Figure 22: Bending section controlled by two pairs of wires: 2 way deflection

Thanks to this simulation, a special case of motion performed by this mechanism can be observed. At first, the lower sub-section of the bending section can deflect to 90° clockwise by pulling the right red wire. Next, the left blue wire is pulled until the rest of the bending section deflects to 180 ° counterclockwise. Fig. 22 shows exactly the case that the bending section reaches its maximum deflection.

With this simulation program, it is possible to change the parameters or dimensions of the bending section so that the corresponding performance can be

observed. It is also compatible for an input of a bending angle function $\beta(t)$ solved from the dynamic equations in future study.

3.4 Trajectory of the distal end

The study of trajectory is important because the urologists need to know how the distal end of the ureteroscope can reach the destination as well as where it will pass by while it is approaching to the destination. Not mentioning devices as specific as ureteroscope, there are a few studies about the continuum robots which are similar to the configuration of the bending section in this research. Most of them intend to treat the configuration of the bending section as a circular curve, thus the study would become much easier because of the simplification. It may be acceptable to treat it as an arc if precision requirement is not that serious. However, for the bending section of an ureteroscope, it is necessary to adopt the most realistic geometric features and dimensional values in order to obtain the most accurate outcome of calculations. In this section, difference between the circular curve assumption and realistic calculation will be provided for comparison as well.

3.4.1 Trajectory of a bending section composing by identical parts

Since the radius of the bending section is way shorter than the total length of it, here the trajectory of the bending section is considered as the trajectory of its neutral axis as illustrated on Fig. 23. Before carrying out the calculation, some notations are necessary to declare first. Meanwhile the notations denote in section 3.2 also apply.

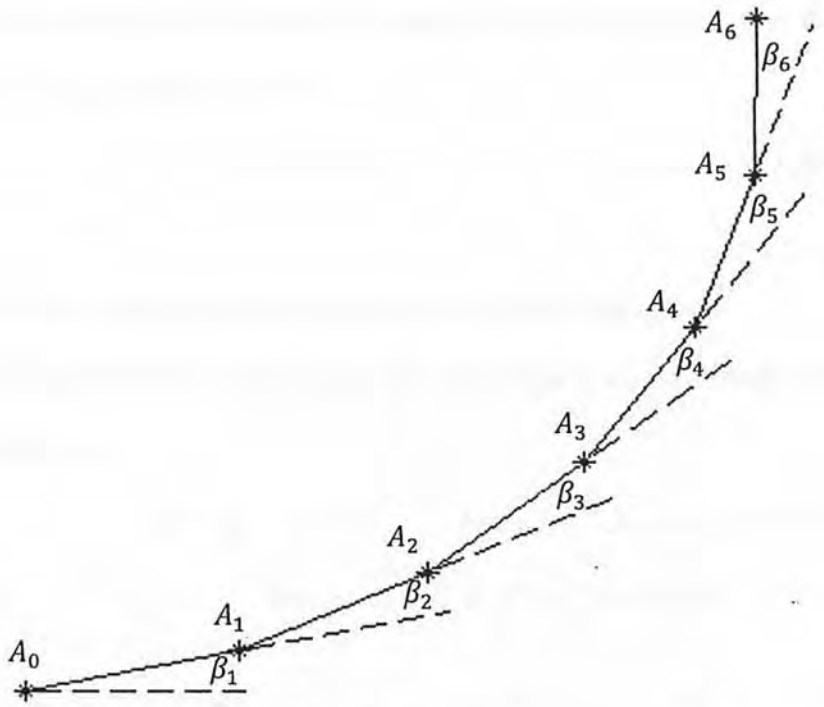

Figure 23: Neutral axis of bending section composed by identical parts

- m : number of parts composing the bending section
- L_i : length of the i th part of the bending section
- β_i : bending angle of the i th part relevant to the i-1th part
- R_N : neutral radius of the bending
- A_{i-1} , A_i : denotes the start and end points of the i th part

Then the coordinate of A_i , (x_i , y_i), can be easily calculated as:

$$x_i = L_i \cos\left(\sum_{k=1}^{i} \beta_k\right) + x_{i-1}$$

$$y_i = L_i \sin\left(\sum_{k=1}^{i} \beta_k\right) + y_{i-1}$$

where i = 1, 2, 3, … , m

(3.13)

Besides, the limits of deflection are calculated from section 3.2, thus the range of the deflection angle of each part is:

$$-\beta_i^* \leq \beta_i \leq \beta_i^*, \qquad where\ \beta_i^* = 2\tan^{-1}(g_i/r_i)$$

Meanwhile, some assumptions are made for further calculation.

1) The gap distances between any two adjunct parts within a bending section are the same. i.e.

$$g_i = g_j\,,\ r_i = r_j\,, \qquad for\ i,j = 1,2,\dots,m,\ and\ i \neq j$$

$$\text{Then} \qquad \beta_i^* = \beta^* = 2\tan^{-1}(g/r)$$

2) The neutral radii of all the parts within the bending section are equivalent.

Referring to section 3.2, the neutral radius related to the adjunct two parts is

$$R_N = \sqrt{(d+g)^2 + (h+r)^2} = \sqrt{(d+g)^2\,cot^2\left(\frac{\beta}{2}\right) + (d+g)^2}$$

$$= (d+g)csc\left(\frac{\beta}{2}\right) \tag{3.14}$$

3) The curvature along the bending section remains constant simultaneously while the bending section is under deflection.

∴ The curvature is the inverse of the neutral radius, i.e.

$$\kappa = \frac{1}{R_N} = \frac{1}{(d+g)}sin\left(\frac{\beta}{2}\right) \tag{3.15}$$

Aggregating the above assumptions, it is possible to figure out the relationships among the bending angles of different parts. For any two sets of adjunct parts, they should have the same curvature according to the third assumption. It can

be expressed mathematically as follows:

Suppose a, b denote any two sets of adjunct two parts within a sub-section of a bending section, then

$$\kappa_a = \kappa_b$$

$$\frac{1}{(d+g)} sin\left(\frac{\beta_a}{2}\right) = \frac{1}{(d+g)} sin\left(\frac{\beta_b}{2}\right)$$

$$\therefore \beta_a = \beta_b \tag{3.16}$$

In other words, the bending angles of a bending section composed by identical parts are the same instantly. Then equation (3.13) becomes:

$$x_i = L\,cos(i\beta) + x_{i-1}$$

$$y_i = L\,sin(i\beta) + y_{i-1} \tag{3.17}$$

From equation (3.17), it is easy to calculate the location of the last part, i.e., A_m , as well as the trajectory of it. Here A_0 can be assumed to be (0, 0) for the ease of calculation.

$$x_m = L\,cos(m\beta) + x_{m-1} = L\sum_{k=1}^{m} cos(k\beta) = LC$$

$$y_m = L\,sin(m\beta) + y_{m-1} = L\sum_{k=1}^{m} sin(k\beta) = LS$$

$$where\ C = \sum_{k=1}^{m} cos(k\beta) = \frac{1}{2}\left\{\frac{\sin[(m+\frac{1}{2})\beta]}{\sin(\frac{\beta}{2})} - 1\right\}$$

$$S = \sum_{k=1}^{m} sin(k\beta) = \frac{\sin(\frac{m}{2}\beta)\sin[(\frac{m+1}{2})\beta]}{\sin(\frac{\beta}{2})} \tag{3.18}$$

Example 1. For a bending section composed by 6 identical parts, the dimensions of each part are: $L = 3.3274mm,\ g = 0.1392mm,\ r = 1.0668mm.$

The trajectory of the distal end can be expressed as parametric functions of β:

$$x_6 = 3.3274 \times \frac{1}{2}\left(\frac{\sin[(6+\frac{1}{2})\beta]}{\sin(\frac{\beta}{2})} - 1\right) = 1.6637\left[\frac{\sin\left(\frac{13}{2}\beta\right)}{\sin\left(\frac{\beta}{2}\right)} - 1\right]$$

$$y_6 = 3.3274\frac{\sin(\frac{6}{2}\beta)\sin[(\frac{6+1}{2})\beta]}{\sin(\frac{\beta}{2})} = 3.3274\frac{\sin(3\beta)\sin\left(\frac{7}{2}\beta\right)}{\sin(\frac{\beta}{2})}$$

The maximum bending angle is:

$$\beta_{max} = 2\tan^{-1}(0.1392/1.0668) = 14.8683°$$

Then the range of bending angle is:

$$-14.8683° \leq \beta \leq 14.8683°$$

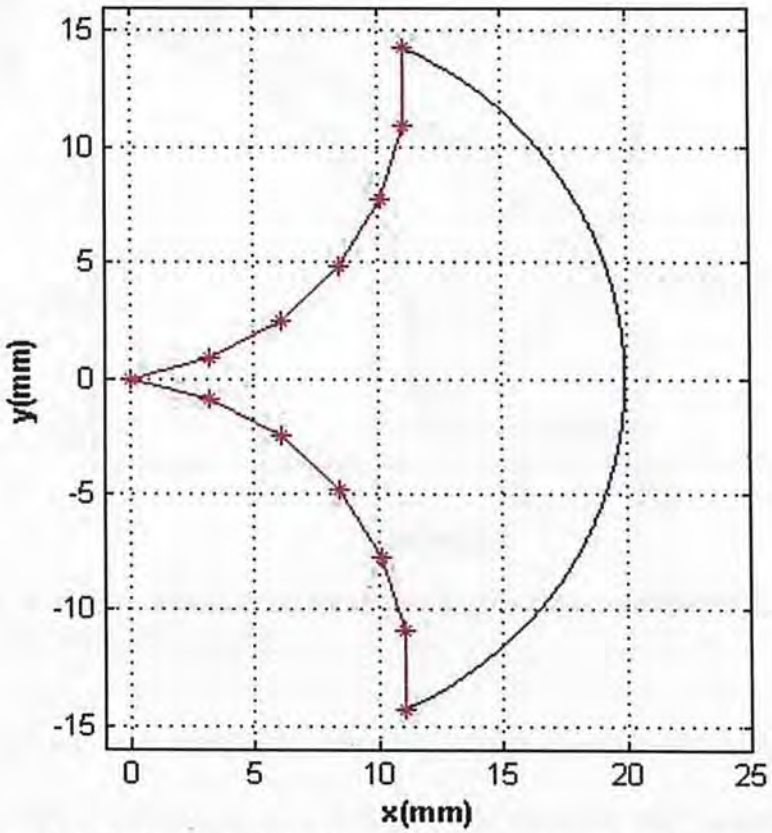

Figure 24: Trajectory of the distal end of the bending section composed by identical parts (blue) and the boundaries of deflection in both directions for the entire bending section (red).

Fig. 24 shows the trajectory of the distal end of this bending section for the above range of β. The blue curve is the trajectory while the red curves are the boundaries of deflection in both directions. The area bounded by three curves is the swept area of the entire bending section. Fig.25 demonstrates the locations of the entire bending section under different values of the partdeflection angle β.

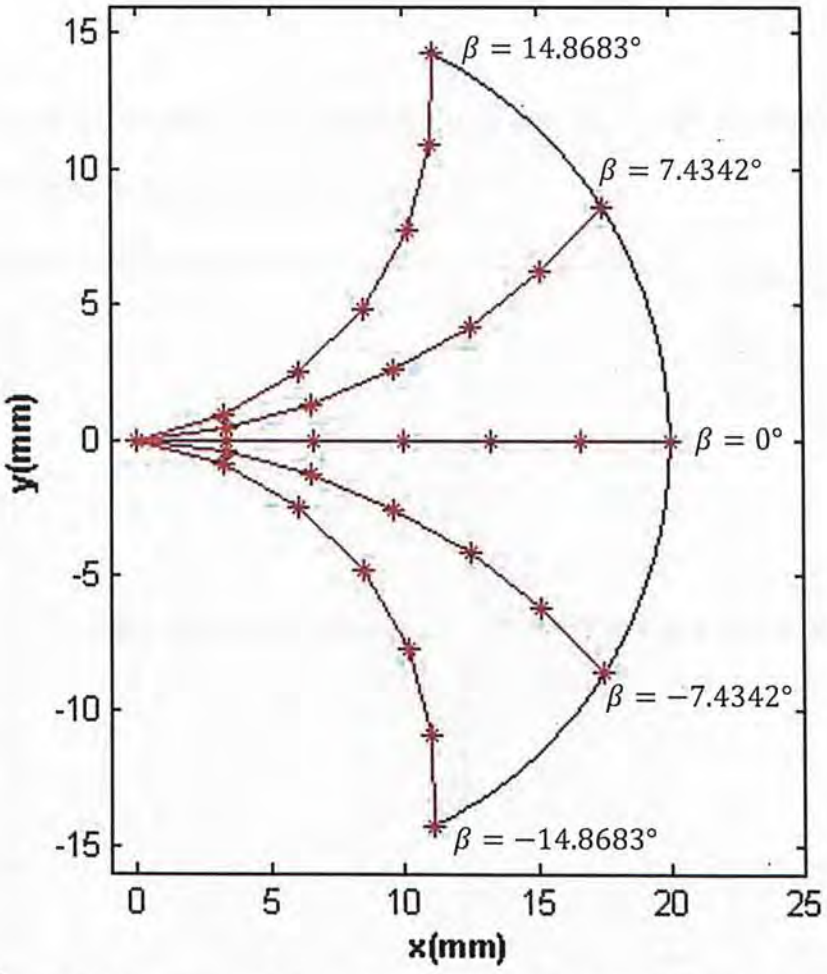

Figure 25: Locations of the entire bending section for different values of the part deflection angle β.

Referring to equation (3.12), a bending section composed by m identical parts should be able to deflect $\beta_{total} = m\beta_{max}$. For example, the bending section in example 1 can deflects up to $\pm 14.8683°$.

However, if the bending section is considered as a continuum robot arm, it can be treated as a circular curve as a whole. Because the neutral axis of the bending section will not extend or shorten no matter how it deflects, its length is constant. In other words, the circular curve should be a constant and can be expressed by:

$$L_{arc} = R_{arc}\beta_{total} \qquad \text{where } L_{arc} = mL = m(2g + 2d)$$

$$=> \quad R_{arc} = \frac{2m(d+g)}{\beta_{total}} = \frac{2m(d+g)}{m\beta} = \frac{2(d+g)}{\beta} \tag{3.19}$$

In order to compare R_N in equation (3.14) and R_{arc}, Fig. 26 shows the both radii with respect to the part deflection angle β.

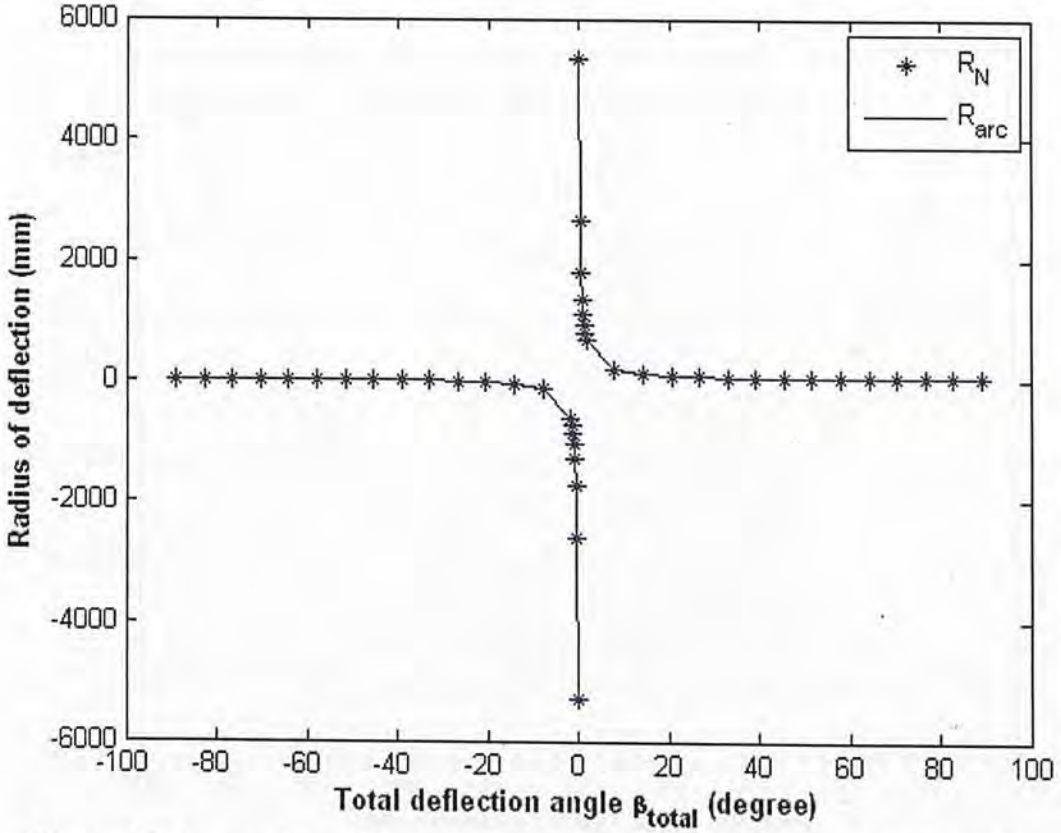

Figure 26: Comparison of R_N and R_{arc} with respect to the total deflection angle.

From Fig. 26, both radii are very large when the deflection angle is very small. It is because the bending section is nearly straight which means the curvature is

almost zero. In other words, the radius of deflection approaches to infinity. Meanwhile, it is very difficult to observe the difference between R_N and R_{arc}, therefore a parameter ε is introduced to be the ratio between these two radii. It can be simplifies in the following expression:

$$\varepsilon = \frac{R_N}{R_{arc}} = \frac{(d+g)csc\left(\frac{\beta}{2}\right)}{2(d+g)/\beta} = \frac{(\beta/2)}{sin(\beta/2)} \tag{3.20}$$

The curve in Fig. 27 represents the variation of the ratio when different total deflection angles of the bending section occur.

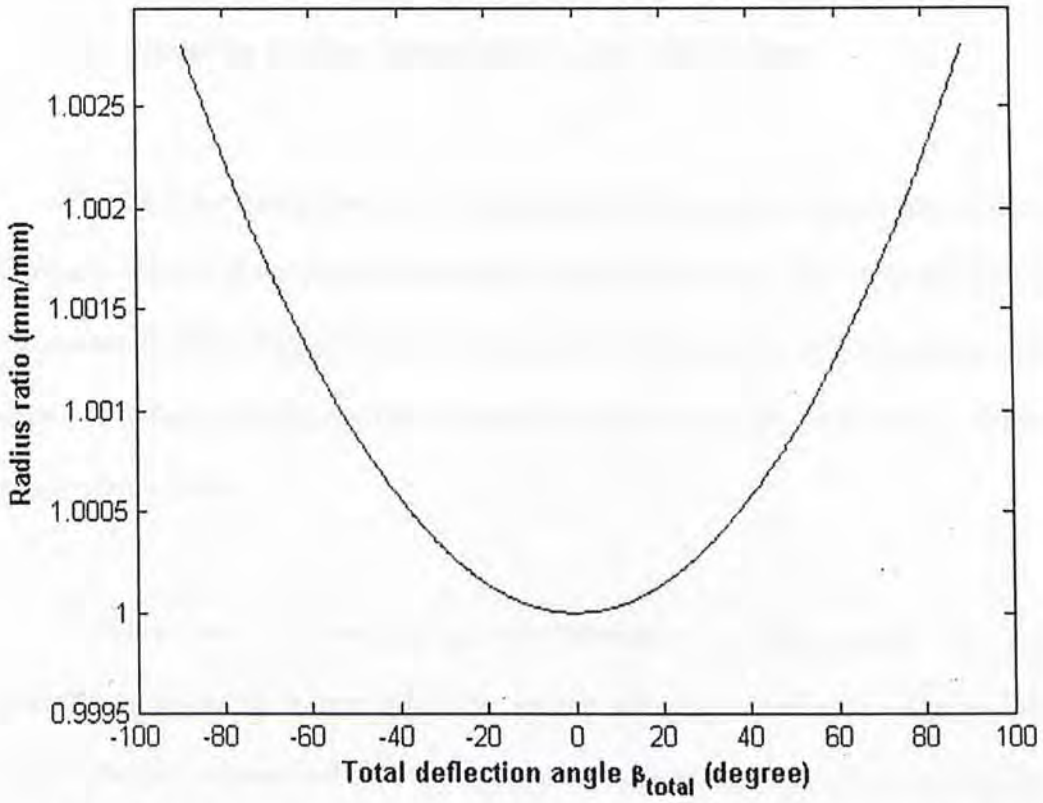

Figure 27: Variation of ratio ε with respect to different total deflection angle.

It can be easily observed that when the total deflection angle is very small, the radius about the neutral axis is most likely equal to the radius of the circular curve. It can be analyzed mathematically from equation (3.20).

For very small $\beta/2$, $sin(\beta/2) \approx \beta/2$ => $\varepsilon \approx 1$

In other words, the deflected bending section can be regarded as a continuum robot arm when the bending angle of one linkage is sufficiently small. For a desired result of deflection, increasing the number of linkages can also enhance the similarity of the two patterns.

3.4.2 Bending section composed by two sub-sections

Fig. 28 is the configuration of a bending section composed by two sub-sections. Similar to the one in the previous section, the trajectory of the entire bending section is considered as the trajectory of its neutral axis. All the parts in a sub-section are identical. Before carrying out the mathematical study, it is also sufficient to define the annotations first.

Suppose there are two sub-sections forming a bending section, the first subsection consists of m parts while the second subsection consists of n parts. The parts in the first sub-section distinguish themselves from the parts in the second sub-section by the length. The details of the notations are shown as follows:

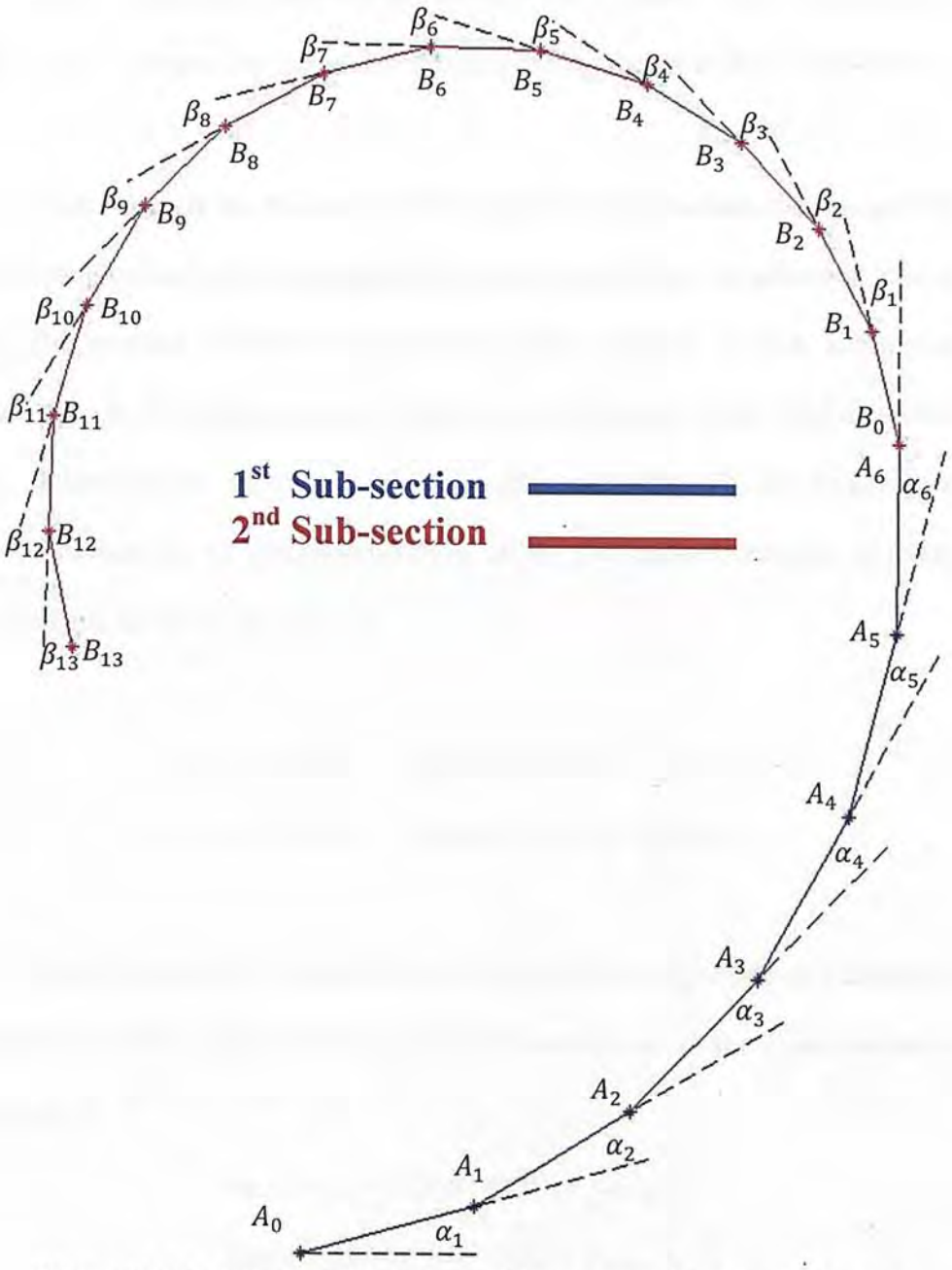

Figure 28: Neutral axis of bending section composed by identical parts

- m : number of parts composing the 1st sub-section
- n : number of parts composing the 2nd sub-section
- L_k : length of the part within the k-th sub-section, where k = 1, 2
- α_i : bending angle of the i-th part relevant to the i-1th part
- β_j : bending angle of the j-th part relevant to the j-1th part
- R_k : neutral radius of the k-th sub-section, where k = 1, 2

- A_{i-1}, A_i : denotes the start and end points of the i th part of the 1st sub-section
- B_{j-1}, B_j : denotes the start and end points of the j th part of the 2nd sub-section

In order to study the trajectory of this type of bending section, the assumptions made in the previous section also apply. But there is just a little modification have to make. The constant curvature assumption is made relevant to each sub-section instead of the entire bending section. Therefore, the deflection of the bending section in Fig. 28 involves two curvatures. It has also demonstrated on Fig. 20. As proved in previous section, due to constant curvature, all the part deflection angles of a sub-section should be the same, such that,

$$-\alpha^* \leq \alpha \leq \alpha^*, \qquad where\ \alpha^* = 2\tan^{-1}(g_1/r_1)$$
$$-\beta^* \leq \beta \leq \beta^*, \qquad where\ \beta^* = 2\tan^{-1}(g_2/r_2)$$

Again, the trajectory of the distal end is what we mostly concern. Referring to the equations define in the previous section, the coordinates of the distal end can be expressed by:

$$x_{m+n} = L_2\, cos(m\alpha + n\beta) + x_{m+n-1}$$
$$y_{m+n} = L_2\, sin(m\alpha + n\beta) + y_{m+n-1} \qquad (3.21)$$

For simplicity, here the gap distance between adjunct parts and the radius along the whole bending section are assumed to be to same, i.e.,

$$g_1 = g_2,\ r_1 = r_2,\ \ here\ 1,2\ denotes\ the\ 1st\ and\ 2nd\ subsection$$

It can also be easily proved that α^* is equal to β^*.

3.4.2.1 Controlled by a single pair of wires

If there is only a single pair of wires being used to control the whole bending section, then α can be regarded as equal to β because the rate of pulling the wire should be same along the whole wire. Hence, equations (3.21) can be rewritten as:

$$x_{m+n} = L_2\, cos[(m+n)\beta] + x_m = L_2 \sum_{k=1}^{m+n} cos(k\beta) + L_1 \sum_{k=1}^{m} cos(k\beta)$$

$$=> \quad x_{m+n} = \frac{L_1}{2}\left\{\frac{\sin\left[\left(m+\frac{1}{2}\right)\beta\right]}{\sin\left(\frac{\beta}{2}\right)} - 1\right\} + \frac{L_2}{2}\left\{\frac{\sin\left[\left(m+n+\frac{1}{2}\right)\beta\right]}{\sin\left(\frac{\beta}{2}\right)} - 1\right\}$$

$$=> \quad x_{m+n} = \frac{L_1 \sin\left[\left(m+\frac{1}{2}\right)\beta\right] + L_2 \sin\left[\left(m+n+\frac{1}{2}\right)\beta\right]}{2\sin(\beta/2)} - \frac{L_1+L_2}{2} \tag{3.22}$$

$$y_{m+n} = L_2\, sin[(m+n)\beta] + y_m = L_2 \sum_{k=1}^{m+n} sin(k\beta) + L_1 \sum_{k=1}^{m} sin(k\beta)$$

$$=> \quad y_{m+n} = \frac{L_1 \sin\left(\frac{m}{2}\beta\right) \sin\left[\left(\frac{m+1}{2}\right)\beta\right] + L_2 \sin\left[\left(\frac{m+n}{2}\right)\beta\right] \sin\left[\left(\frac{m+n+1}{2}\right)\beta\right]}{\sin\left(\frac{\beta}{2}\right)} \tag{3.23}$$

Example 2. For a bending section composed by two sub-sections, the first one consists of 6 identical parts while the second one has 13 identical parts. The dimensions are given as:

$$L_1 = 3.3274mm,\ L_2 = 2.1590mm,\ g = 0.1392mm,\ r = 1.0668mm.$$

The trajectory of the distal end can be expressed as parametric functions of β:

$$x_{m+n} = \frac{1.6637\sin(6.5\beta) + 1.0795\sin(19.5\beta)}{\sin(\beta/2)} - 2.7432$$

$$y_{m+n} = \frac{3.3274\sin(3\beta)\sin(3.5\beta) + 2.1590\sin(9.5\beta)\sin(10\beta)}{\sin(\beta/2)}$$

The maximum bending angle is:

$$\beta_{max} = 2\tan^{-1}(0.1392/1.0668) = 14.8683°$$

Then the range of bending angle is:

$$-14.8683° \leq \beta \leq 14.8683°$$

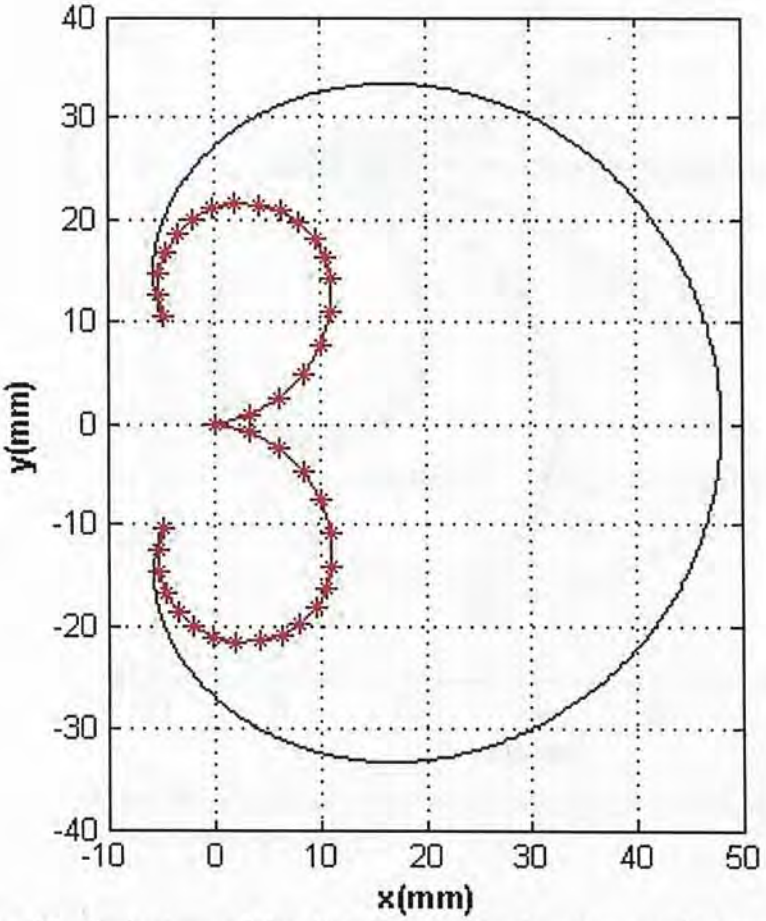

Figure 29: Trajectory of the distal end of the bending section composed by two sub-sections (blue) and the boundaries of deflection in both directions for the entire bending section (red).

Fig. 29 shows the trajectory of the distal end of this bending section for the above range of β. The blue curve is the trajectory while the red curves are the boundaries of deflection in both directions. The red stars, '*' are the joints of the

bending section. The area bounded by the three curves is the swept area of the entire bending section.

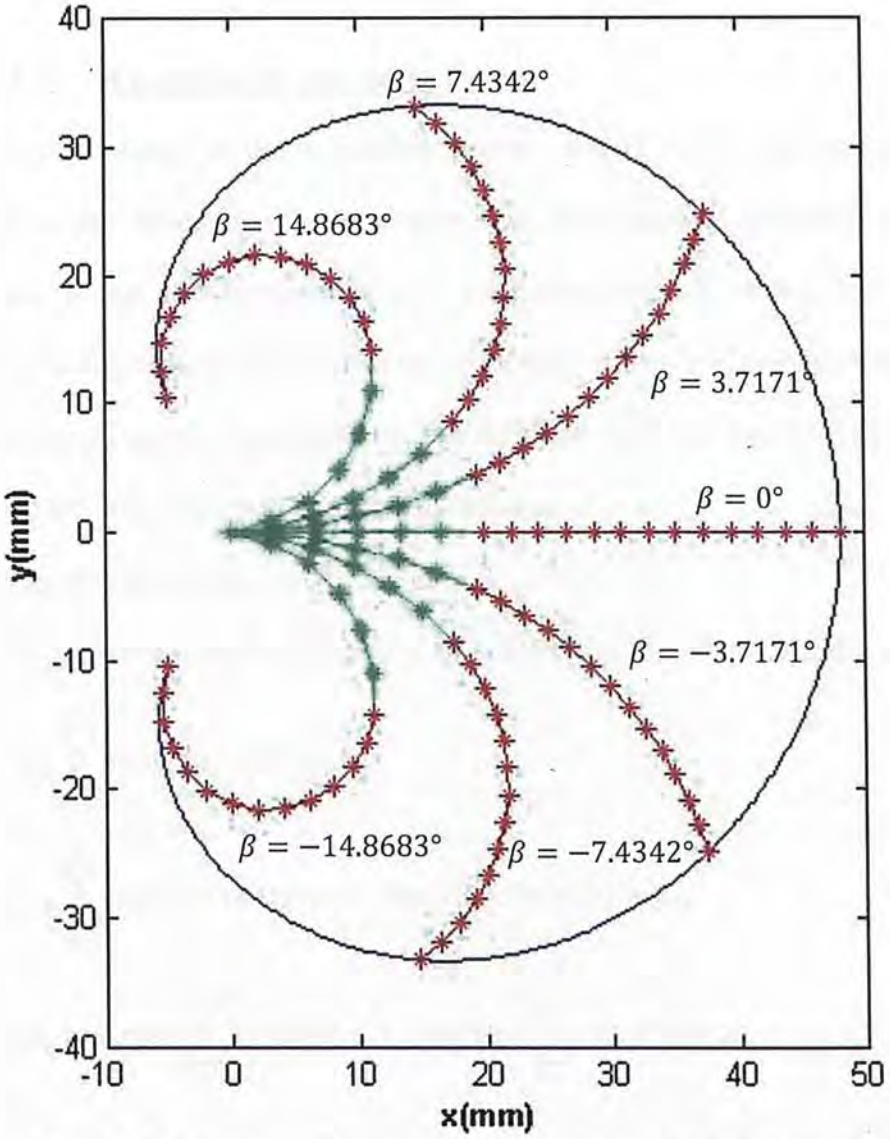

Figure 30: Locations of the entire bending section for different values of the part deflection angle β.

Since there is only one pair of control wires, all the parts deflect at the same time regardless of which sub-section it belongs while the wire is being pulled. The picture shown on Fig. 30 demonstrates the locations of the entire bending section under different values of the part deflection angle β. The green parts linked together to form the first sub-section while the red parts are forming the second sub-section. Referring to equation (3.12), the first subsection is able to deflect maximally to 89.2°

and the second sub-section is can reach 193.2879°. Therefore this bending section is possible to deflect to 282.4977°

3.4.2.2 Controlled by two pairs of wires

For the bending section controlled by two pairs of wires, each pair should mount at a part different with the others. Thus two stages of deflection can be performed. It can also be regarded as a mechanism consists of two degrees of freedom. For this reason, the formulas of the location of the distal end defined in the previous section cannot be applied here. The definition for it can start from equations (3.21) and the procedures will be shown as follows:

$$x_{m+n} = L_2\, cos(m\alpha + n\beta) + x_{m+n-1}$$

$$= L_2[cos(m\alpha + n\beta) + cos(m\alpha + (n-1)\beta) + \cdots + cos(m\alpha + \beta)] + x_m$$

$$= L_2 \sum_{k=1}^{n} cos(m\alpha + k\beta) + x_m$$

$$= L_2 \sum_{k=1}^{n} [cos(m\alpha)\, cos(k\beta) - sin(m\alpha)\, sin(k\beta)] + x_m$$

$$= L_2\, cos(m\alpha) \sum_{k=1}^{n} cos(k\beta) - L_2\, sin(m\alpha) \sum_{k=1}^{n} sin(k\beta) + x_m$$

$$= \frac{L_2\, cos(m\alpha)}{2} \left\{ \frac{\sin[(n+\frac{1}{2})\beta]}{\sin(\beta/2)} - 1 \right\} - \frac{L_2\, sin(m\alpha)\, \sin(\frac{n}{2}\beta) \sin[(\frac{n+1}{2})\beta]}{\sin(\beta/2)}$$

$$+ \frac{L_1}{2} \left\{ \frac{\sin\left[\left(m+\frac{1}{2}\right)\alpha\right]}{\sin(\alpha/2)} - 1 \right\}$$

$$y_{m+n} = L_2\, sin(m\alpha + n\beta) + y_{m+n-1}$$

$$= L_2[sin(m\alpha + n\beta) + sin(m\alpha + (n-1)\beta) + \cdots + sin(m\alpha + \beta)] + y_m$$

$$= L_2 \sum_{k=1}^{n} sin(m\alpha + k\beta) + y_m$$

$$= L_2 \sum_{k=1}^{n} [sin(m\alpha)\, cos(k\beta) + cos(m\alpha)\, sin(k\beta)] + y_m$$

$$= L_2\, sin(m\alpha) \sum_{k=1}^{n} cos(k\beta) + L_2\, cos(m\alpha) \sum_{k=1}^{n} sin(k\beta) + y_m$$

$$= \frac{L_2\, sin(m\alpha)}{2} \left\{ \frac{\sin[\frac{(n+1)\beta}{2}]}{\sin(\beta/2)} - 1 \right\} + \frac{L_2\, cos(m\alpha)\, \sin(\frac{n\beta}{2}) \sin[(\frac{n+1}{2})\beta]}{\sin(\beta/2)}$$

$$+ \frac{L_1 \sin(\frac{m\alpha}{2}) \sin[(\frac{m+1}{2})\alpha]}{\sin(\alpha/2)}$$

Therefore, the trajectory of the distal end of a bending section can be expressed as parametric functions of α *and* β:

$$x_{m+n} = \frac{L_2\, cos(m\alpha)}{2} \left\{ \frac{\sin[(n+\frac{1}{2})\beta]}{\sin(\beta/2)} - 1 \right\} - \frac{L_2\, sin(m\alpha)\, \sin(\frac{n}{2}\beta) \sin[(\frac{n+1}{2})\beta]}{\sin(\beta/2)}$$

$$+ \frac{L_1}{2} \left\{ \frac{\sin\left[\left(m+\frac{1}{2}\right)\alpha\right]}{\sin(\alpha/2)} - 1 \right\}$$

(3.24)

$$y_{m+n} = \frac{L_2\, sin(m\alpha)}{2} \left\{ \frac{\sin[(n+1)\beta/2]}{\sin(\beta/2)} - 1 \right\} + \frac{L_2\, cos(m\alpha)\, \sin(\frac{n\beta}{2}) \sin[(\frac{n+1}{2})\beta]}{\sin(\beta/2)}$$

$$+ \frac{L_1 \sin(\frac{m\alpha}{2}) \sin[(\frac{m+1}{2})\alpha]}{\sin(\alpha/2)}$$

(3.25)

Taking a look on equations (3.22) and (3.24), (3.23) and (3.25), it is not difficult to observe that the trajectory becomes much more complicated when the

number of pairs of control wires increases to two from one. According to different input of α and β, the trajectories of the distal end may varies correspondingly. The following cases list on Table 3 are considered to be the most common ones.

Case		Operations
I	Deflect in the same direction	1. The lower sub-section fully deflects. 2. The upper sub-section fully deflects
II		1. The upper sub-section fully deflects. 2. The lower sub-section fully deflects.
III		1. The lower sub-section reaches half of its full deflection. 2. The upper sub-section fully deflects. 3. The lower sub-section deflects until it reaches the limit.
IV	Deflect in opposite direction	1. The lower sub-section fully deflects counterclockwise. 2. The upper sub-section fully deflects clockwise.
V		1. The upper sub-section fully deflects clockwise. 2. The lower sub-section fully deflects counterclockwise.

Table 3: Case study of the bending section controlled by 2 pairs of wires.

In which the first three cases are to control the sub-sections to deflect to the same side. The first case is to make the lower sub-section fully deflect and the second sub-section follows. The second one is opposite the order compared with the first case. The third case includes three stages, namely, making the lower sub-section to reach half of its full deflection, controlling the upper sub-section to fully deflect and continuing the deflection of the lower sub-section until it reaches the limit. In these case studies, α and β are treated as the input and the trajectory of the distal end is the output.

Case 1:

Operations: 1. The lower sub-section fully deflects.

2. The upper sub-section fully deflects.

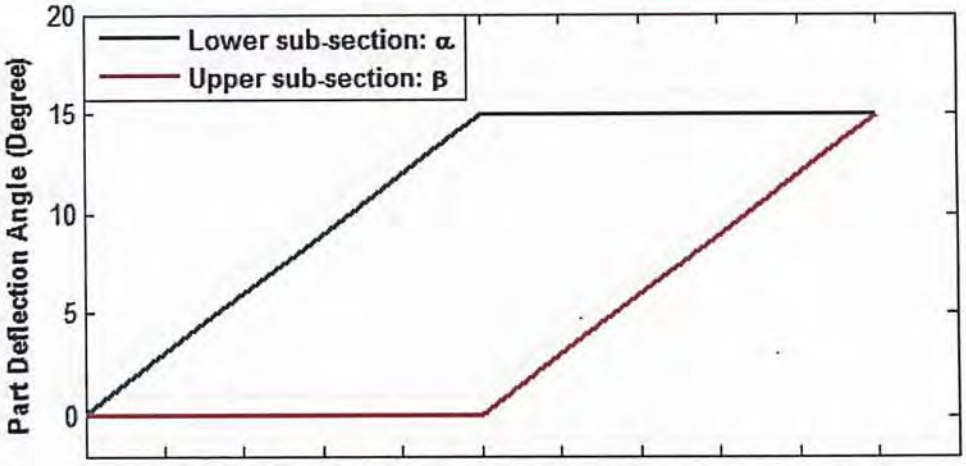

Figure 31: Input values of α and β for the first case study

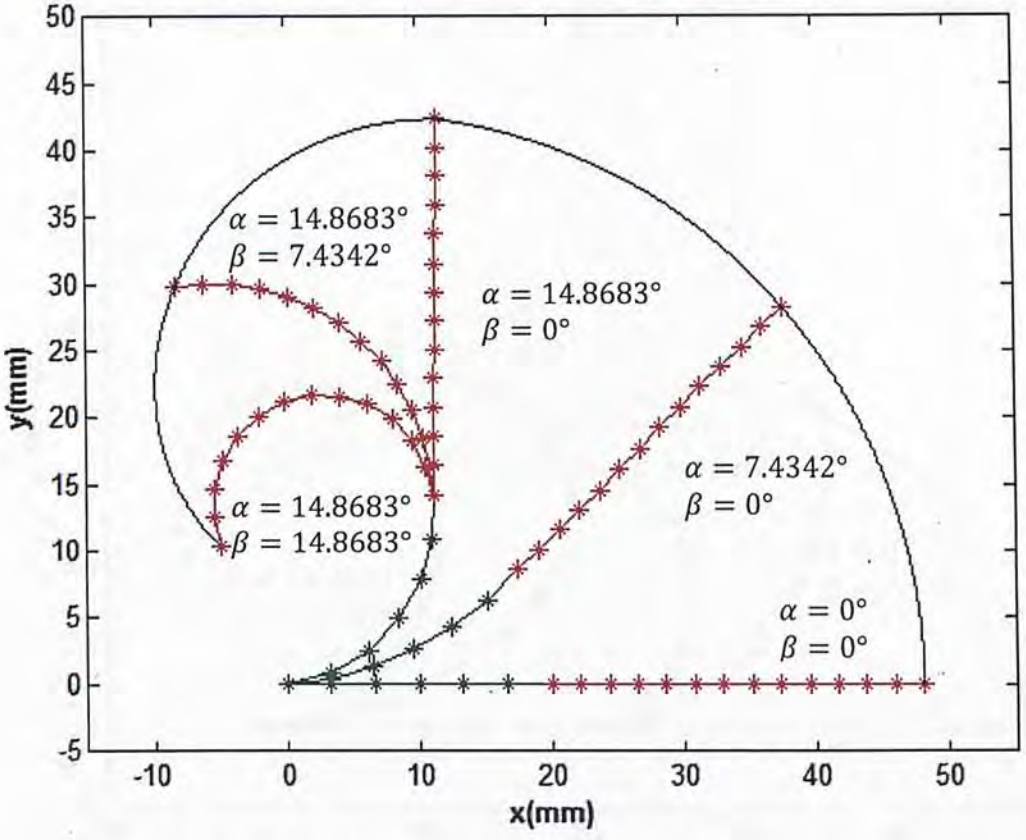

Figure 32: (Case 1) Trajectory of the distal end (blue) and locations of the entire bending section for different values of the part deflection angle α and β. The red part represents the upper sub-section while the green part represents the lower sub-section.

Case 2:

Operations: 1. The upper sub-section fully deflects.

2. The lower sub-section fully deflects.

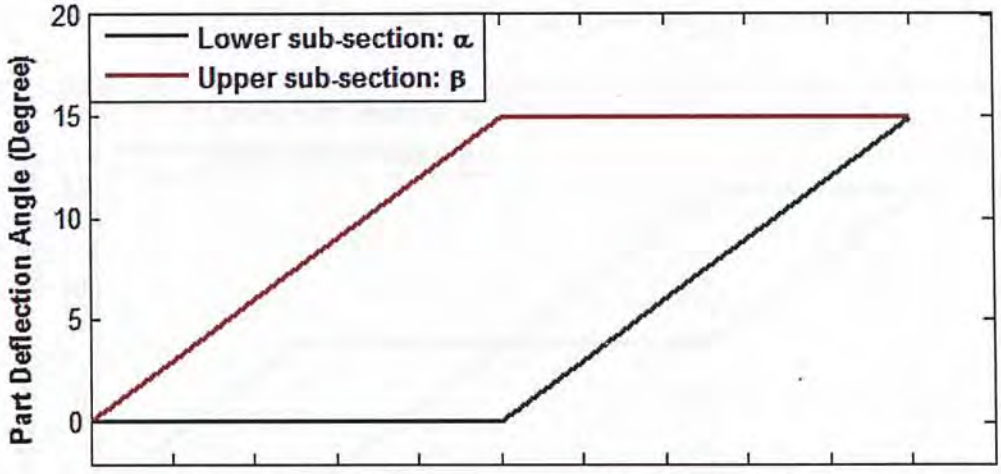

Figure 33: Input values of α and β for the second case study

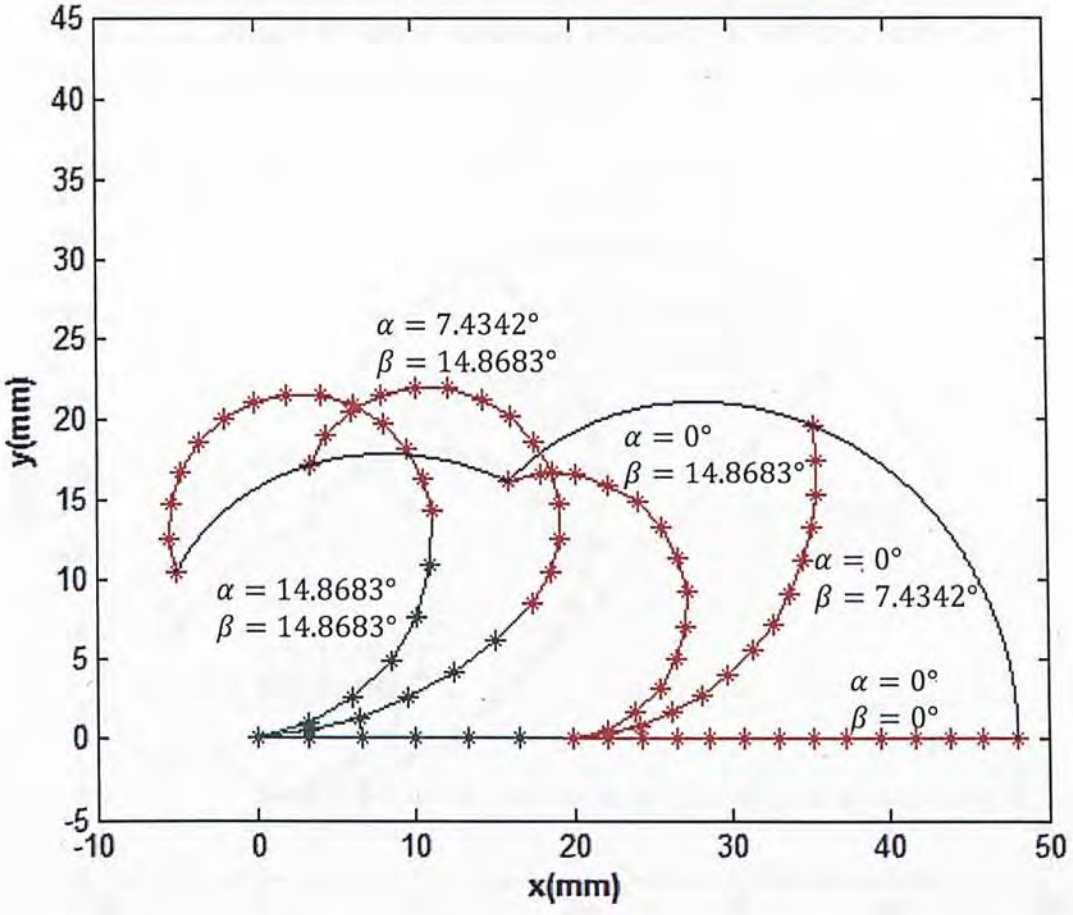

Figure 34: (Case2) Trajectory of the distal end (blue) and locations of the entire bending section for different values of the part deflection angle α and β.

Case 3:

Operations: 1. The lower sub-section reaches half of its full deflection.

2. The upper sub-section fully deflects.

3. The lower sub-section deflects until it reaches the limit.

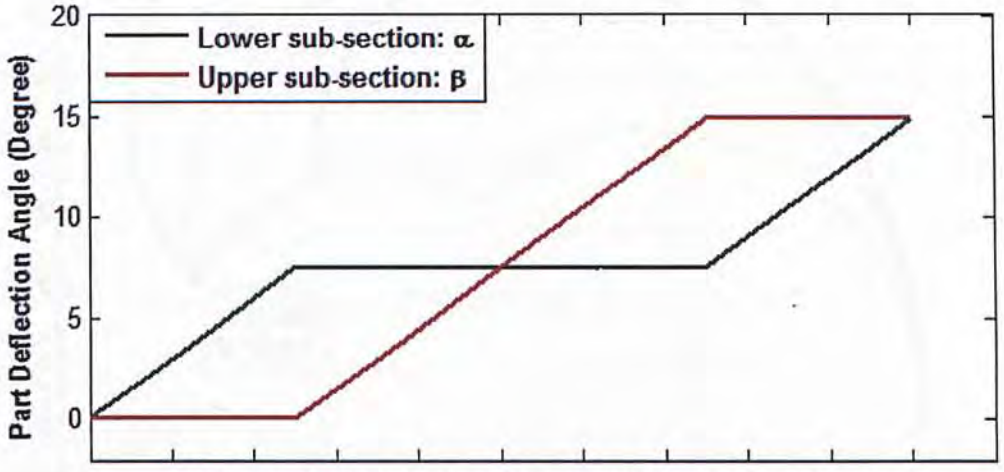

Figure 35: Input values of α and β for the third case study

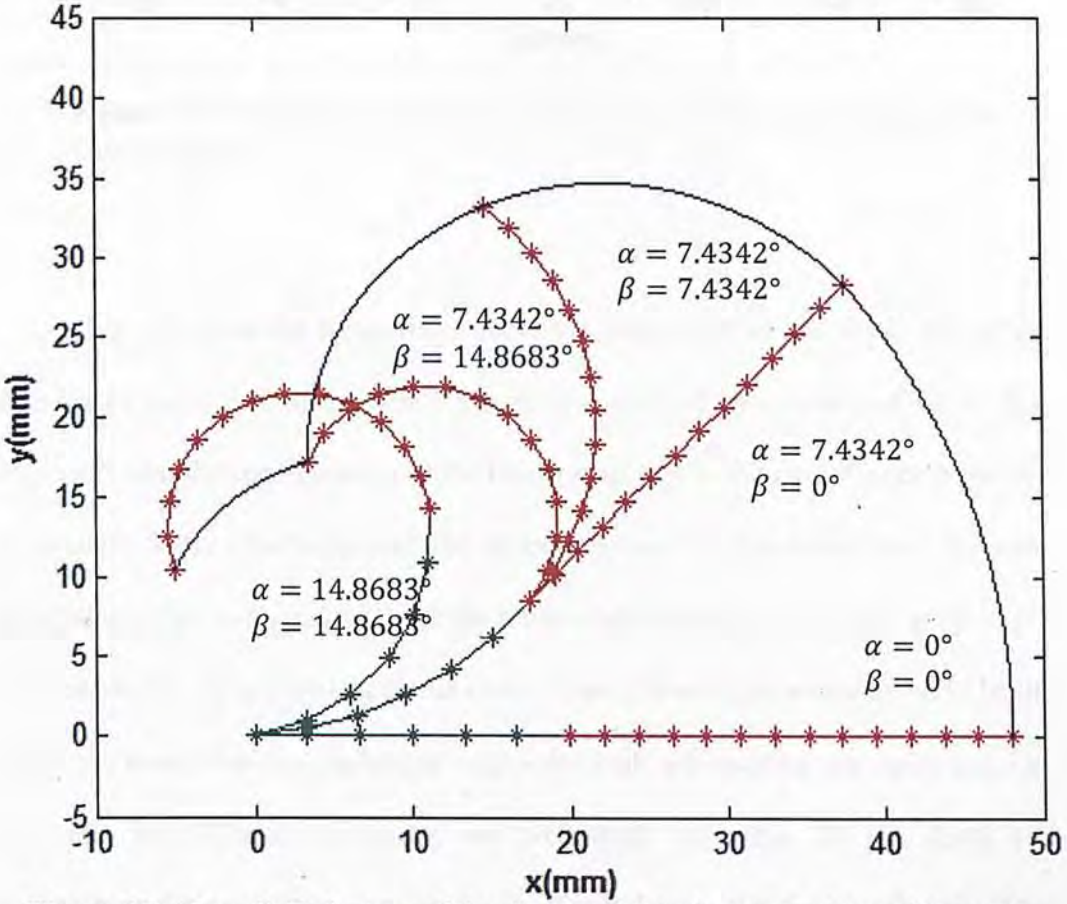

Figure 36: (Case 3) Trajectory of the distal end (blue) and locations of the entire bending section for different values of the part deflection angle α and β.

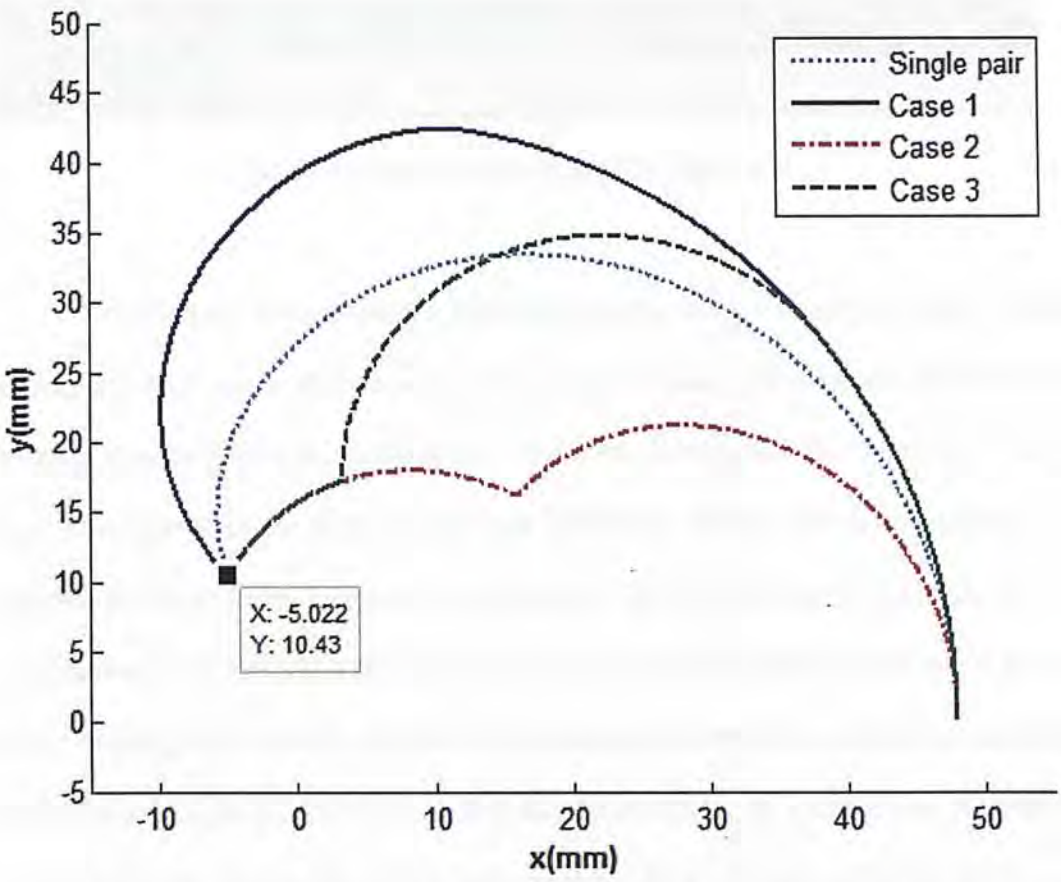

Figure 37: Trajectory of the distal end under different operations of the control wires.

Fig. 37 gives the comparison about the trajectories of the distal end of the three cases above and of the bending section controlled by one pair of wires. It is noticeable that the configuration of the bending section in the case studies is the one in Example 2. By observation, all the operations lead the distal end reach the same point because the sub-sections reach the limits of deflection, i.e., $\alpha = \alpha^*$ and $\beta = \beta^*$. Besides, due to the gap distances and radii of two sub-sections are assumed to be the same, the maximum part deflection angles for both sub-sections are equal too, i.e., $\alpha^* = \beta^*$. As different operations are performed, the paths for the distal end approaching the destination vary obviously. Table 4 gives the distance that the distal end travelled from the origin to the destination for cases on Fig. 37.

Case	1	2	3	Single Pair
Distance (mm)	106.7137	69.6567	87.5417	87.4145

Table 4: Travelled distance of the distal end

To reach the destination, the bending section in case 1 swept the largest area among the four cases. It is because the longer sub-section – upper sub-section remains straight during the deflection of the lower sub-section. It results in a long bending radius while the bending section is deflecting. In other words, the distal end follows the longest way to reach the destination. On the contrary, if the lower sub-section starts to deflect after the upper sub-section has fully deflected, the swept area of the bending section is the smallest. The distal end can reach the destination via the shortest path. In addition, for the bending section controlled by a single pair of wires, it does not show obvious advantage compared by using two pairs of wires. But it is believed that using a single pair of control wires is easier according to the feedbacks from the urologists.

Besides, two pairs of control wires allow the two sub-sections of a bending section to deflect in opposite ways. Case 4 and Case 5 below present the trajectory of the distal end under such operations. The former has the lower sub-section fully deflect counterclockwise and the upper sub-section deflects clockwise. Case 5 reverses the order of deflection for the two sub-sections. In fact, these two kinds of motions can also be expressed by equations (3.25). Just like the above case studies, Fig. 38 and Fig. 40 are the inputs of the part deflection angles α and β for the two cases respectively. Fig. 39 and Fig. 41 are the corresponding responses which are the trajectories of the distal end.

Case 4:

Operations: 1. The lower sub-section fully deflects counterclockwise.

2. The upper sub-section fully deflects clockwise.

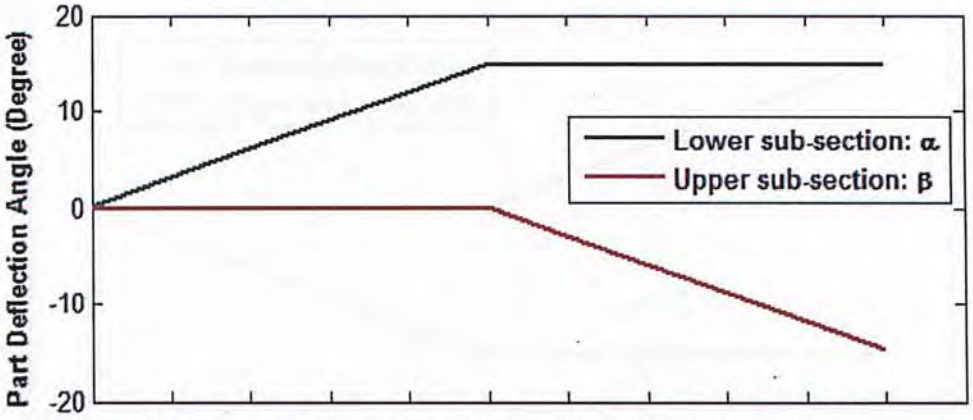

Figure 38: Input values of α and β for the forth case study

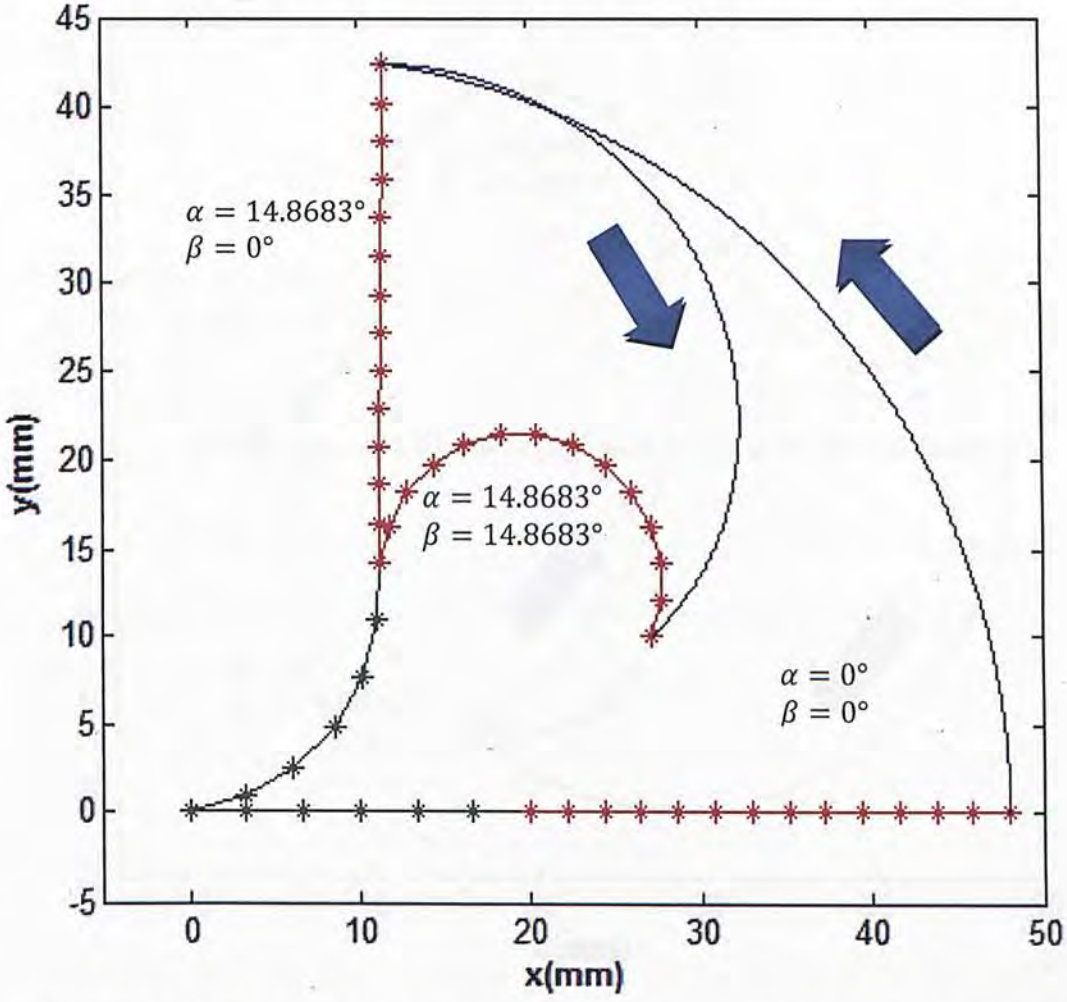

Figure 39: (Case 4) Trajectory of the distal end (blue) and locations of the entire bending section for different values of the part deflection angle α and β.

Case 5:

Operations: 1. The upper sub-section fully deflects clockwise.

2. The lower sub-section fully deflects counterclockwise.

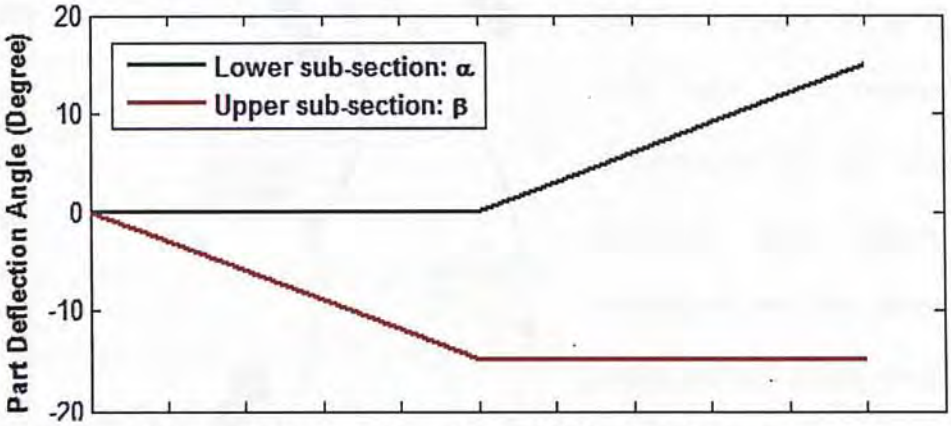

Figure 40: Input values of α and β for the fifth case study

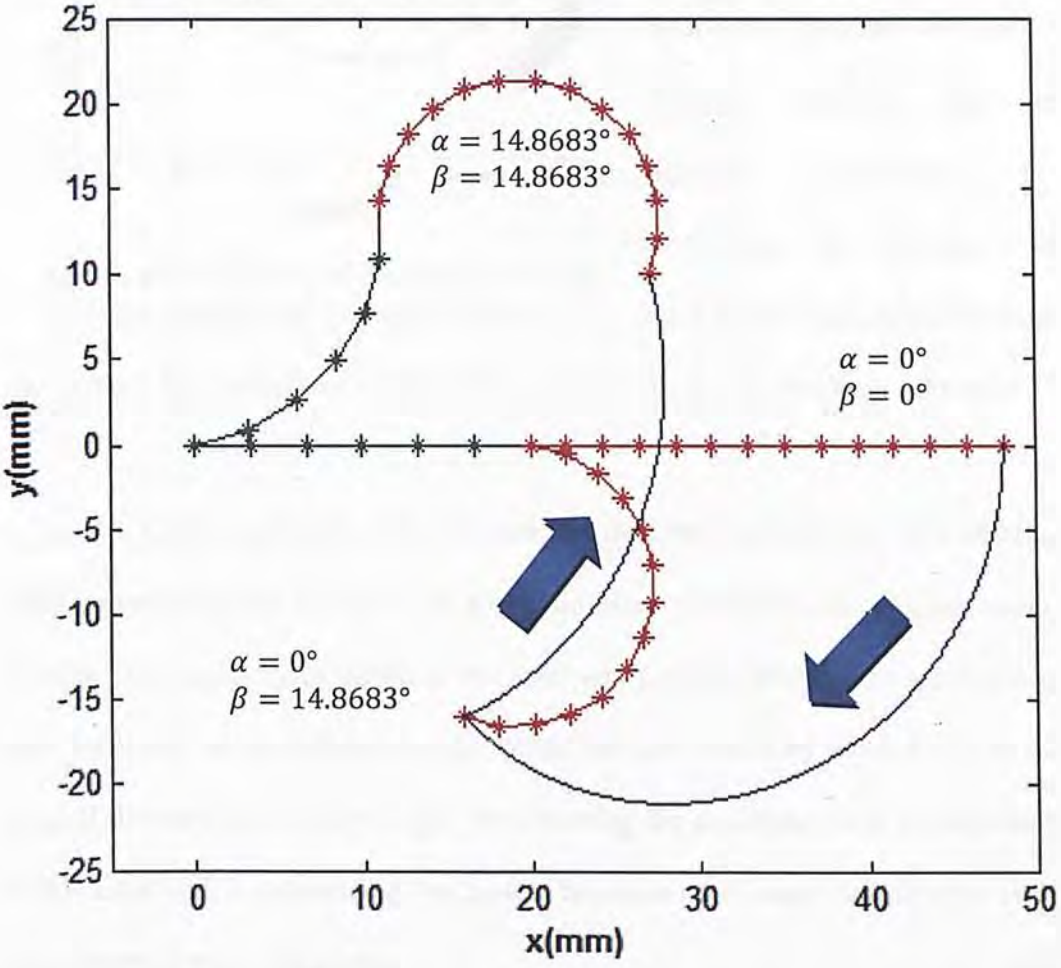

Figure 41: (Case 5) Trajectory of the distal end (blue) and locations of the entire bending section for different values of the part deflection angle α and β.

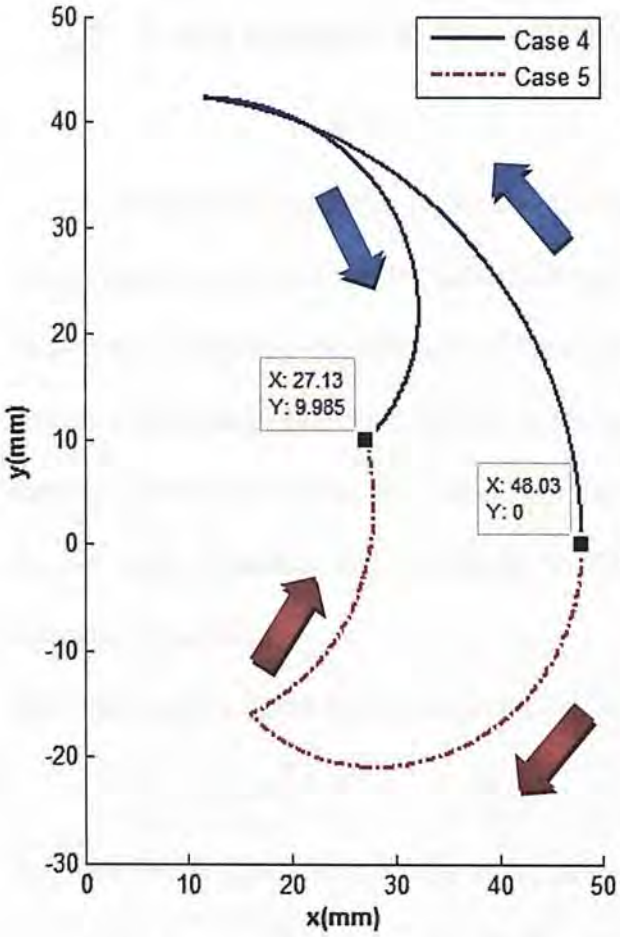

Figure 42: Trajectory of the distal end under different operations of the control wires.

For the ease of comparison, the trajectories of the distal end in Case4 and Case5 are plotted on Fig. 42. For both cases, their origins and destinations are the identical. However, even though the operations are the same, the order shifting would result in a completely different trajectory. Similar to the studies on Case1-3, different methods lead to different outcomes. By performing the operations in Case 4, the distance for the distal end to reach the destination is 106.7137mm while it is only 76.4613mm for Case 5.

As a short summary of this section, for the same configuration of a bending section controlling by two pairs of wires, different order and extent of operations influence the trajectory of the distal end sufficiently. Going through the shortest way may not always be the optimal choice. Hence, the user should lay down a plan on the basis of the particular circumstance. By observing the equations about the trajectory of the distal end, it appears that the system becomes much more complex for every pair of control wires embedded.

3.5 Static analysis of the deflection mechanism

The geometry modeling in this chapter concludes some sufficient parameters that people concern most. In this section, the tension within the controlled wires is studied by considering the variation of the strain and the stress while the bending section is deflecting. More specifically speaking, the change in length of the wire directly affects the strain, the stress and the tension. Such deduction can be proved in the following equations.

The inner bending radius of the wire in the gap is

$$R_1 = g\cot\frac{\beta}{2} - r \qquad (3.26)$$

The outer bending radius of the wire in the gap is

$$R_2 = g\cot\frac{\beta}{2} + r \qquad (3.27)$$

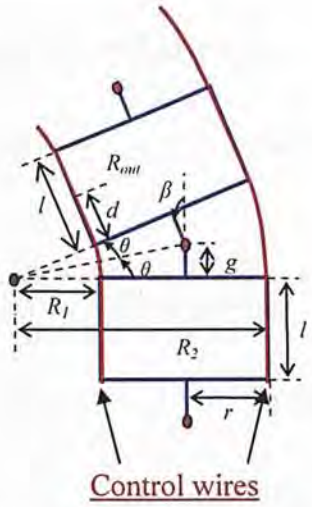

Figure 43: Configuration of the wires in 2-part subsection

As shown in Fig. 43, the left wire is considered to be pulled in order to make the bending section to deflect counterclockwise. Thus the left wire is associated with the R_{in} while the right wire is associated with R_{out}. However, the lengths of the wires on both sides are irrelevant to R_{in} and R_{out}. Instead, they are directly related to R_1 and R_2 respectively. The lengths are annotated as L_{in} and L_{out} and can be given by equations (3.28) and (3.29).

$$L_{in} = Nl + NR_1(2\theta) = N\left[l + \left(g\cot\frac{\beta}{2} - r\right)\beta\right] \qquad (3.28)$$

$$L_{out} = Nl + NR_2(2\theta) = N\left[l + \left(g\cot\frac{\beta}{2} + r\right)\beta\right] \qquad (3.29)$$

where N is the number of the parts forming the bending section.

According to the configuration of the deflection mechanism, the proximal ends of the left wire and the right wire are fixed on the lever or the rotator independently. Therefore, it is better to calculate the changes in length for both wires. At the relaxed state, the lengths of wires on both sides within the bending section are L_o which is given by equation (3.30). Also, the pulling length of the wire can be given by equation (3.31) where a is the radius of the rotor and $\varphi$is the rotated angle of the rotor.

$$L_o = N(l + 2g) \tag{3.30}$$

$$L_r = a\varphi \tag{3.31}$$

$$\Delta L_{in} = L_{in} - L_o + L_r = N\left[l + \left(g\cot\frac{\beta}{2} - r\right)\beta\right] - N(l + 2g) + a\varphi$$

$$\Rightarrow \quad \Delta L_{in} = N\left[\left(g\cot\frac{\beta}{2} - r\right)\beta - 2g\right] + a\varphi \tag{3.32}$$

$$\Delta L_{out} = L_{out} - L_o - L_r = N\left[l + \left(g\cot\frac{\beta}{2} + r\right)\beta\right] - N(l + 2g) - a\varphi$$

$$\Rightarrow \quad \Delta L_{out} = N\left[\left(g\cot\frac{\beta}{2} + r\right)\beta - 2g\right] - a\varphi \tag{3.33}$$

Compared ΔL_{in} and ΔL_{out}, the difference between them is

$$\Delta L_{diff} = \Delta L_{out} - \Delta L_{in} = 2(Nr\beta - a\varphi) \tag{3.34}$$

The total change in length for both wires is

$$\Delta L_{total} = \Delta L_{in} + \Delta L_{out} = 2Ng\left(\beta\cot\frac{\beta}{2} - 2\right) \tag{3.35}$$

$$\text{or} \quad = 4Ng\left(\frac{\beta}{2}\cot\frac{\beta}{2} - 1\right)$$

Assuming that the wire being pulled is purely moving along the hole within

According to the configuration of the deflection mechanism, the proximal ends of the left wire and the right wire are fixed on the lever or the rotator independently. Therefore, it is better to calculate the changes in length for both wires. At the relaxed state, the lengths of wires on both sides within the bending section are L_o which is given by equation (3.30). Also, the pulling length of the wire can be given by equation (3.31) where a is the radius of the rotor and $\varphi$is the rotated angle of the rotor.

$$L_o = N(l + 2g) \tag{3.30}$$

$$L_r = a\varphi \tag{3.31}$$

$$\Delta L_{in} = L_{in} - L_o + L_r = N\left[l + \left(g\cot\frac{\beta}{2} - r\right)\beta\right] - N(l + 2g) + a\varphi$$

$$\Rightarrow \quad \Delta L_{in} = N\left[\left(g\cot\frac{\beta}{2} - r\right)\beta - 2g\right] + a\varphi \tag{3.32}$$

$$\Delta L_{out} = L_{out} - L_o - L_r = N\left[l + \left(g\cot\frac{\beta}{2} + r\right)\beta\right] - N(l + 2g) - a\varphi$$

$$\Rightarrow \quad \Delta L_{out} = N\left[\left(g\cot\frac{\beta}{2} + r\right)\beta - 2g\right] - a\varphi \tag{3.33}$$

Compared ΔL_{in} and ΔL_{out}, the difference between them is

$$\Delta L_{diff} = \Delta L_{out} - \Delta L_{in} = 2(Nr\beta - a\varphi) \tag{3.34}$$

The total change in length for both wires is

$$\Delta L_{total} = \Delta L_{in} + \Delta L_{out} = 2Ng\left(\beta\cot\frac{\beta}{2} - 2\right) \tag{3.35}$$

$$\text{or} \quad = 4Ng\left(\frac{\beta}{2}\cot\frac{\beta}{2} - 1\right)$$

Assuming that the wire being pulled is purely moving along the hole within

the bending section, ΔL_{in} should be equal to zero during the deflection of the bending section, i.e. $\Delta L_{in} = 0$. Hence, the required angle for deflection can be obtained by

$$N\left[\left(g\cot\frac{\beta}{2}-r\right)\beta-2g\right]+a\varphi=0$$

$$\Rightarrow \quad \varphi=\frac{Ng\left[2-\left(\cot\frac{\beta}{2}-r\right)\beta\right]}{a} \tag{3.36}$$

By substituting equation (3.36) into (3.33),

$$\Delta L_{out}=N\left[\left(g\cot\frac{\beta}{2}+r\right)\beta-2g\right]+N\left[\left(g\cot\frac{\beta}{2}-r\right)\beta-2g\right]$$

$$\Rightarrow \quad \Delta L_{out}=2Ng(\beta\cot\frac{\beta}{2}-2) \quad \text{or} \quad 4Ng\left(\frac{\beta}{2}\cot\frac{\beta}{2}-1\right) \tag{3.37}$$

Hence, the mechanical strain and stress of the wire can be calculated by

$$\varepsilon=\frac{\Delta L_{total}}{2(L_o+L_c)} \tag{3.38}$$

$$\sigma=E\varepsilon=E\frac{\Delta L_{total}}{2(L_o+L_c)} \tag{3.39}$$

Where L_c is the length of the coil pipe

Since the length of the wire within the insertion tube is way longer than the portion within the bending section, the cross section area of the tube can be regarded as constant during deflection and is denoted as A_o. Besides, there is also pre-loaded tension, T_p, added in the system. Thus the result tension exerted along the wire is

$$T=T_p+\sigma A_o=T_p+EA_o\frac{\Delta L_{total}}{2(L_o+L_c)}$$

$$\Rightarrow \quad T=T_p+\frac{4NgEA_o}{2(L_o+L_c)}\left(\frac{\beta}{2}\cot\frac{\beta}{2}-1\right) \tag{3.40}$$

Consider the maximum deflection or full deflection, i.e. $\beta_{max} = 2\,tan^{-1}\frac{g}{r}$

$$\varphi_{max} = \frac{N\left[2g-\left(g\cot\frac{\beta}{2}-r\right)\beta\right]}{a}\Bigg|_{\beta_{max}} = \frac{2Ng}{a} \tag{3.41}$$

From equation (3.37), it can be observed that the required rotating angle for fully deflecting the bending section is directly proportional to the total length of the gaps between the parts.

Also, the change in length of the right wire at full deflection is

$$\Delta L_{out}{}^{*} = 2Ng(\beta\cot\frac{\beta}{2}-2)\Big|_{\beta_{max}} = 4Ng\left(\frac{r}{g}tan^{-1}\frac{g}{r}-1\right) \tag{3.42}$$

Hence,

$$\Delta L_{total}{}^{*} = 4Ng\left(\frac{r}{g}tan^{-1}\frac{g}{r}-1\right) \tag{3.43}$$

The tension at full deflection is

$$T^{*} = T_p + \frac{4NgEA_o}{2(L_o+L_c)}\left(\frac{r}{g}tan^{-1}\frac{g}{r}-1\right) \tag{3.44}$$

In order to prevent the wire from compression, the pre-loaded tension must be larger than the tension due to stress from pulling the wire. Therefore,

$$T^{*} \geq 0$$

$$\Rightarrow \quad T_p \geq \frac{4NgEA_o}{2(L_o+L_c)}\left(1-\frac{r}{g}tan^{-1}\frac{g}{r}\right) \tag{3.45}$$

Example 3 (Model I in Table 3):

$$l = 1.6002mm, g = 0.2032mm, r = 1.2319mm,$$

$$r_w = 0.09525mm, A = \pi {r_w}^2 = 0.028502mm^2, L_c = 1m, E = 200GPa$$

$For\ \beta_{total} = 180°, then\ N = 10, L_o = 20.066mm,$ the minimum pre-loaded tension,

$$T_{p_{min}} = \frac{4NgEA_o}{2(L_o + L_c)}\left(1 - \frac{r}{g}tan^{-1}\frac{g}{r}\right) = 0.2027N$$

$For\ \beta_{total} = 270°, then\ N = 16, L_o = 32.1056mm,$ the minimum pre-loaded tension,

$$T_{p_{min}} = \frac{4NgEA_o}{2(L_o + L_c)}\left(1 - \frac{r}{g}tan^{-1}\frac{g}{r}\right) = 0.2815N$$

Example 4 (Model II in Table 3):

$$l = 1.7780mm, g = 0.1143mm, r = 1.2319mm,$$

$$r_w = 0.09525mm, A = \pi {r_w}^2 = 0.028502mm^2, L_c = 1m, E = 200GPa$$

$For\ \beta_{total} = 180°, then\ N = 17, L_o = 34.1122mm,$ the minimum pre-loaded tension,

$$T_{p_{min}} = \frac{4NgEA_o}{2(L_o + L_c)}\left(1 - \frac{r}{g}tan^{-1}\frac{g}{r}\right) = 0.0612N$$

$For\ \beta_{total} = 270°, then\ N = 25, L_o = 50.1650mm,$ the minimum pre-loaded tension,

$$T_{p_{min}} = \frac{4NgEA_o}{2(L_o + L_c)}\left(1 - \frac{r}{g}tan^{-1}\frac{g}{r}\right) = 0.0886N$$

Fig. 44 shows the relationship between the required minimum pre-loaded tension and the total deflection angle of Model I and II. Obviously the larger the bending angle is, the larger pre-loaded tension is required. It helps to determine the length of the coil pipe as well as the insertion tube of the ureteroscope.

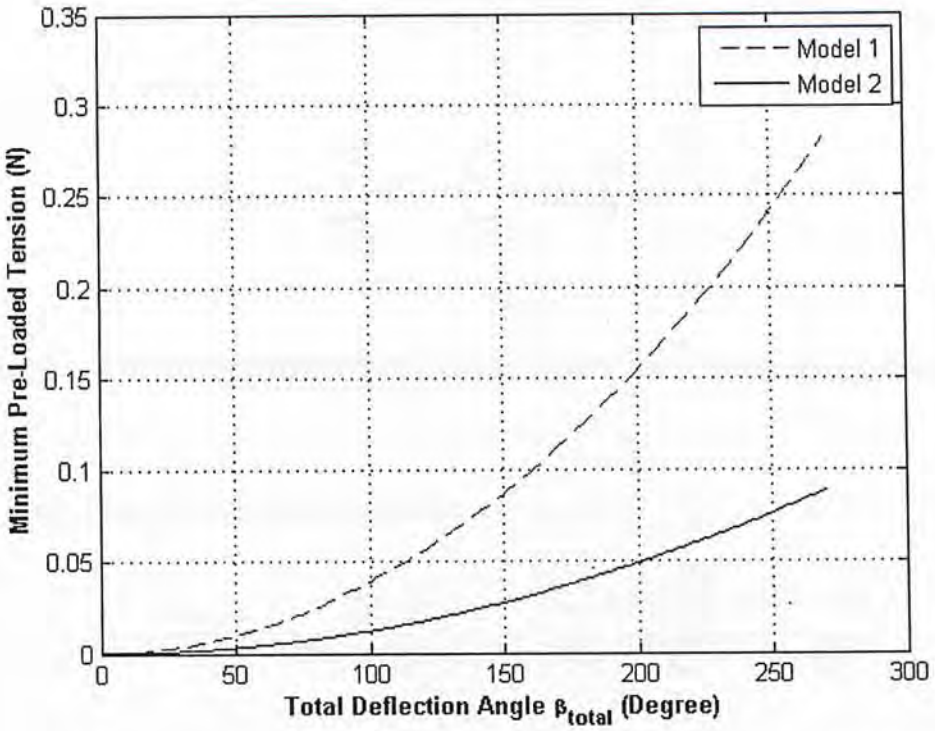

Figure 44: Minimum pre-loaded tension vs. Total deflection angle

Besides, different materials of the wires would be able to sustain different amount of tension. By considering the elasticity of the material, the yield stress is adopted to evaluate the maximum tension. For the stress exerted on the wire larger than the yield stress that it can sustain, the wire is unable to return to its original length or it only partially returns when it is unloaded. The most commonly used materials of the wires are stainless steel and Nitinol. The former has yield stress at around 520 MPa while the latter has its at about 340 MPa. Table 5 lists out the maximum and minimum tension of the wires made of stainless steel and Nitinol associated with the dimensions of Model I and II.

Material	Model I		Model II	
	Min. Tension	Max. Tension	Min. Tension	Max. Tension
Stainless Steel	0.2815N	14.8210N	0.0886N	14.8210N
Nitinol	0.0394N	9.6907N	0.0124N	9.6907N

Table 5: Tension of wire made from different materials

Furthermore, for the bending section formed by m sets of parts, equation (3.13) can be revised as

$$\Delta L_{total} = \sum_{i=1}^{m} \Delta L_i = \sum_{i=1}^{m} 4N_i g_i \left(\frac{\beta_i}{2}\cot\frac{\beta_i}{2} - 1\right) \tag{3.21}$$

where ΔL_i is the length difference of the wire in the i^{th} set of parts during deflection.

In this case, the strain of the wire is

$$\varepsilon = \frac{\Delta L_{total}}{L_o} = \frac{\sum_{i=1}^{m} \Delta L_i}{2(L_c + \sum_{i=1}^{m} L_o)} = \frac{\sum_{i=1}^{m} 2N_i g_i \left(\frac{\beta_i}{2}\cot\frac{\beta_i}{2} - 1\right)}{2(L_c + \sum_{i=1}^{m} N_i(l_i + g_i))} \tag{3.22}$$

The corresponding stress and tension can be calculated as above.

4. Application: Design of Ureteroscope

Having studied the deflection mechanism in the previous chapters, it is more practical to work on the design of a ureteroscope by using this information. The purpose of this project was to design a brand new flexible ureteroscope with some special features. For the sake of achieving the goal of this project, communication with relevant company in the USA was done from time to time. We shared our understandings and opinions about the design to each other. The work of maintenance by the technicians in the company was observed in order to know what they mostly concerned and what troubles that they encountered during the repair of the ureteroscopes. In this chapter, the design of the bending section and control body will be presented in two sections accordingly.

4.1 Design of the bending section

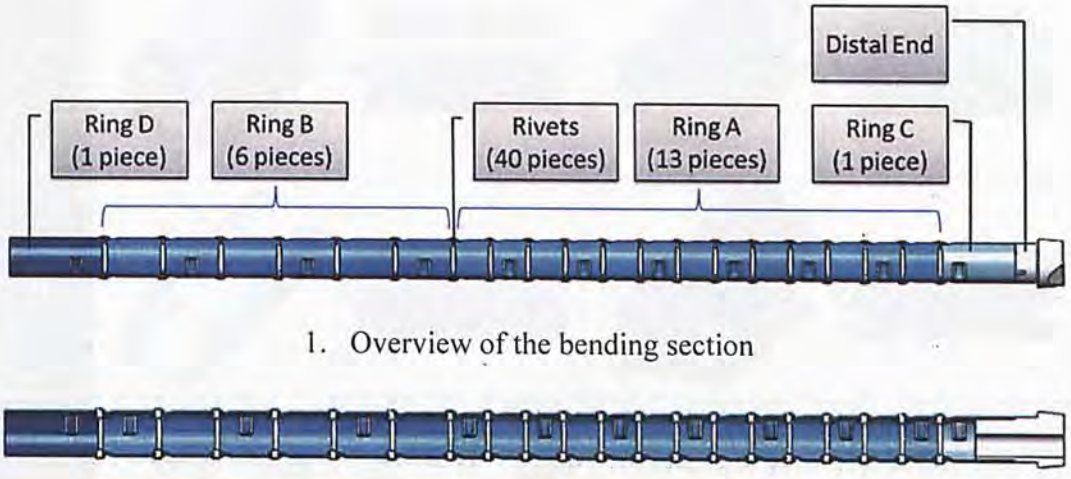

1. Overview of the bending section

2. Cross-sectional view (from top)

Figure 45: Bending section design for MedServ

This bending section consists of two sub-sections and is connected by rivets. The overview of it is shown on Fig. 45. It mainly consists of 22 parts which can be divided into 4 groups. The first group actually is the upper sub-section. This sub-section is composed by 13 pieces of Ring A. The second group is the lower sub-section which comprises 6 pieces of Ring B. Next group is the distal end and Ring C. Finally Ring D is used to connect the bending section and the insertion tube. Different views of the parts involved are shown in Table 6.

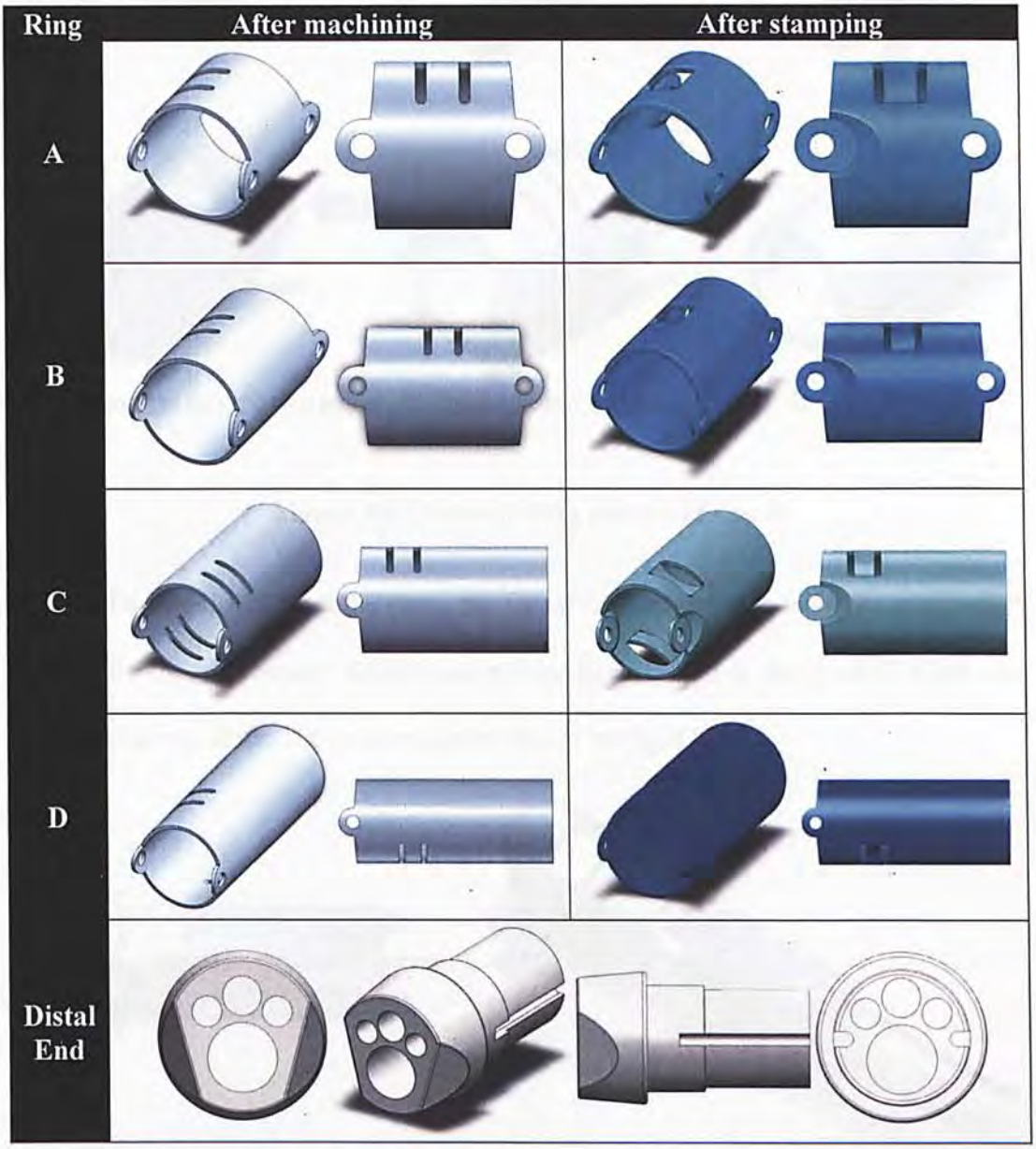

Table 6: Parts introduction – After machining to after stamping

To make the rings, it basically includes two processes – machining and stamping. The manufacturing processes of the rings are similar. Here taking ring B as an example, the machining process of it is given in Fig. 46.

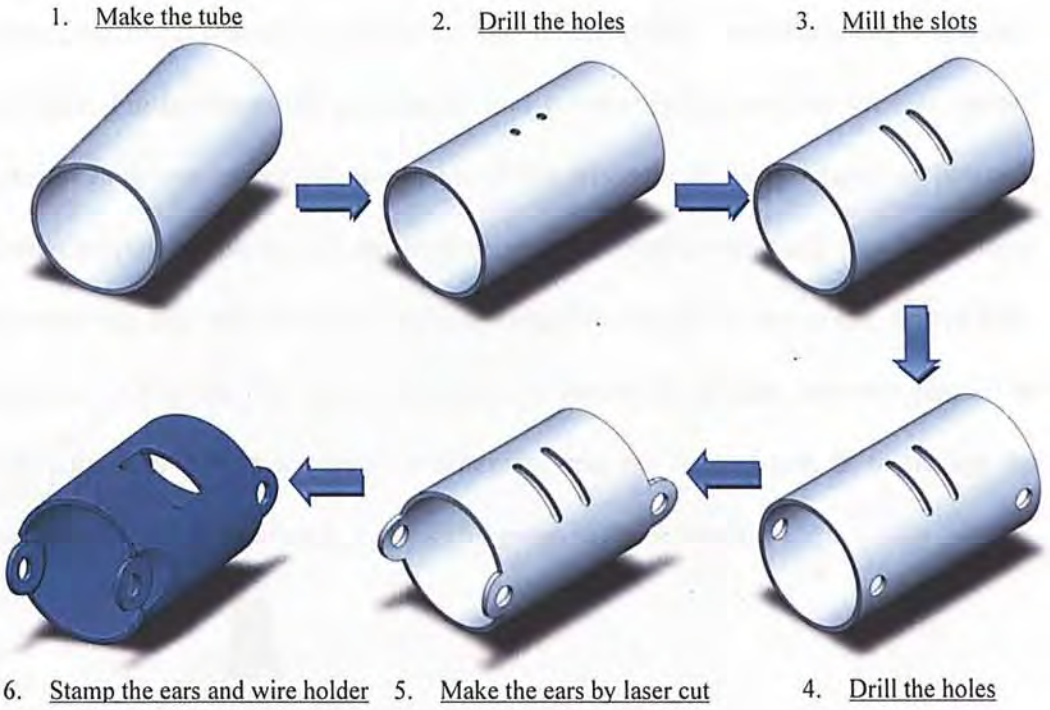

Figure 46: The machining process of ring B

Distinguished from the rings, the Distal End can only be made by machining due to its special contour. Before assembling Ring C into it, the control wires are mounted at two slots. The process can be shown in Fig. 47.

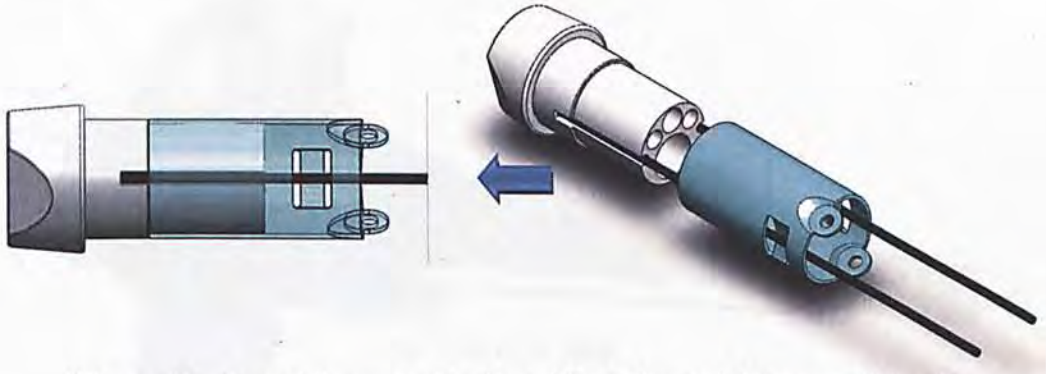

Figure 47: Assembly among the Distal End, Control Wires and Ring C

4.2 Design of the control body

There are some major considerations while designing an ureteroscope: safety, maneuvability, durability, assembility and diassembility, manufacturing feasibility and cost. Furthermore, the appearance and comfortability are also vital as people sometimes do not investigate the inside of the products. If the products can function similarly well, people would rather to choose the most comfortable one or the most eye-catching one. Balancing the above criteria, the overall picture of the control body is shown in Fig. 48. The work of design can mainly be divided into two parts. The first part is to design a control mechanism and the second part is to design the housing of it. Details of each part will be given in the following.

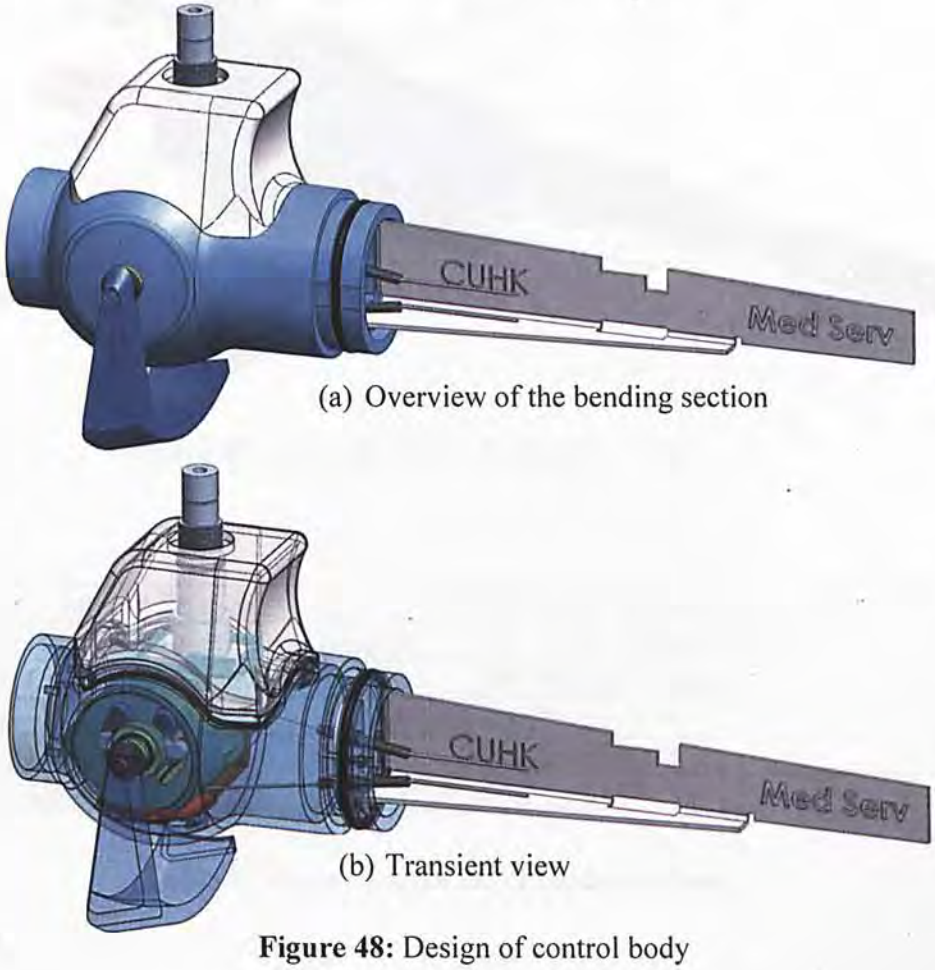

(a) Overview of the bending section

(b) Transient view

Figure 48: Design of control body

4.2.1 Parts introduction and major assembling

For the ease of observing the components within the design of the control body, exploded view is made and shown in Fig. 49. The names of major components are given in Table 7 as well. The detail of the control mechanism will be given later in this section.

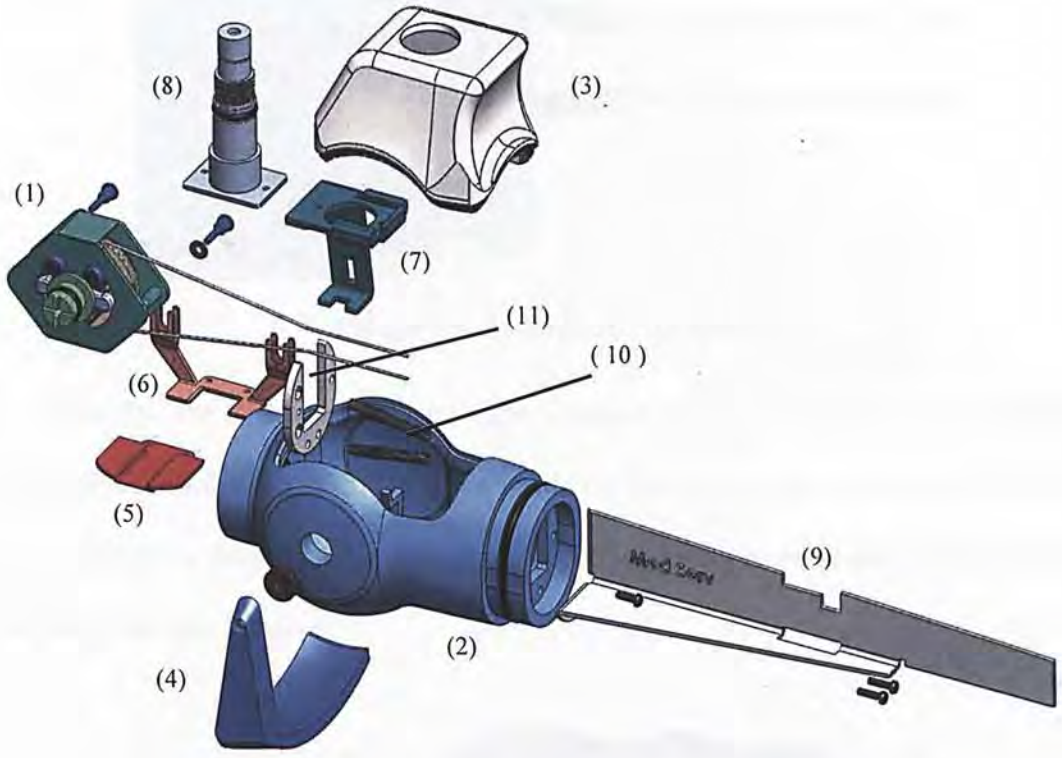

Figure 49: Exploded view of the control body

(1) Control mechanism	(7) Light guide support
(2) Housing of control mechanism	(8) Light guide tunnel
(3) Cover of housing	(9) Handle support
(4) Control lever	(10) Spring
(5) Lower support	(11) Spring lock
(6) Upper support	

Table 7: Major components of the control body

In order to assemble the control body, the housing (2) is considered as the base component. All the other components are installed into it. First the set of springs (10) should be installed and the spring lock (11) follows. Fig. 50 illustrates the successful assembly of the springs and the lock. Here one screw is used to fix it.

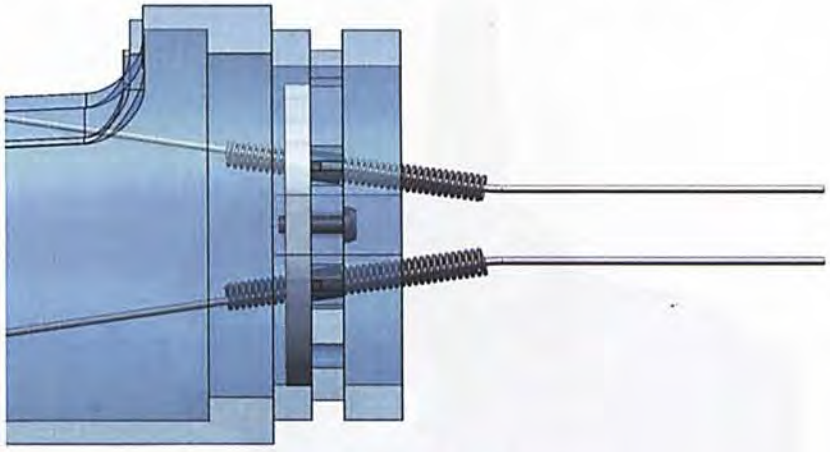

Figure 50: Assembly of the springs

Then the lower support (5) and upper support (6) are assembled accordingly before the control mechanism (1) is put inside the housing as shown on Fig. 51. The two blue screws are put on the slots of the upper support thus the control mechanism would not be able to move.

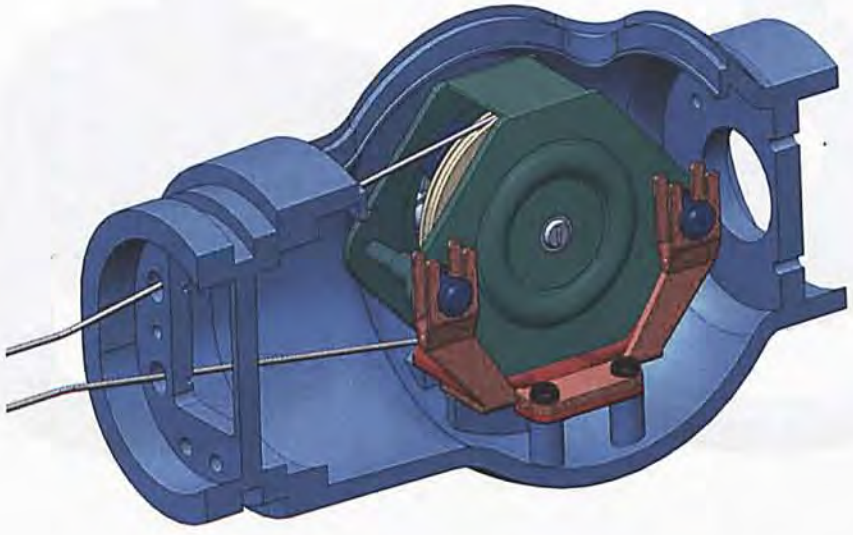

Figure 51: Assembly of the control mechanism

After successfully assembled the control mechanism, the light guide support (7) and the light guide tunnel should be mated first before install into the housing. A thin rubber is stuck on the light guide support as a cushion to reduce the stress on the control mechanism exerted by the light guide support.

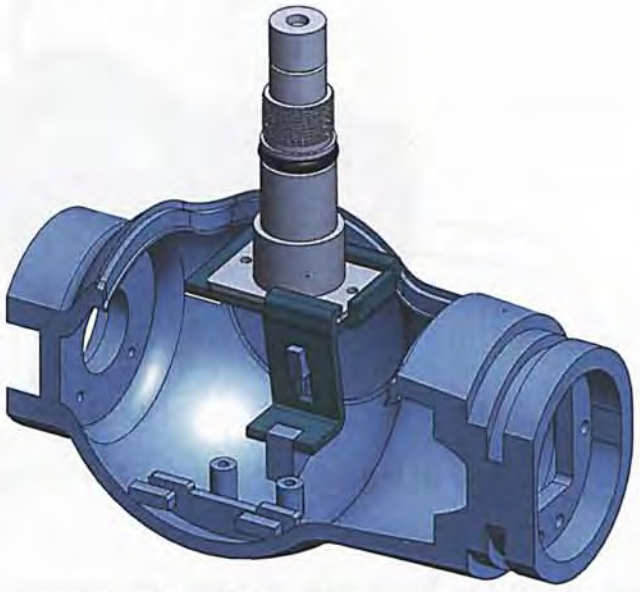

Figure 52: Assembly of the light guide tunnel and its

After fixed the control mechanism within the housing, the control lever (4) can also be assembled as shown on Fig. 53.

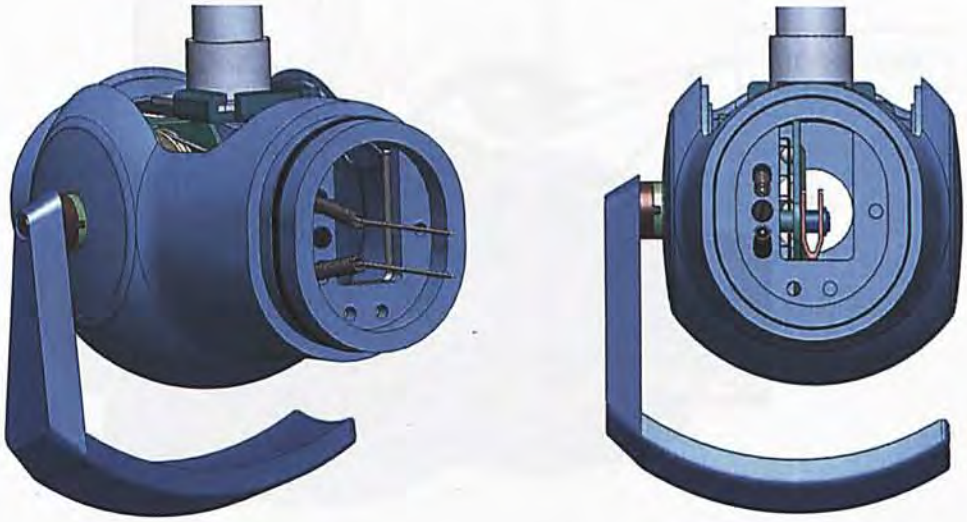

Figure 53: Assembly of the lever and the control mechanism

Last but not least, the cover of housing can be put on the housing passing through the light guide tunnel.

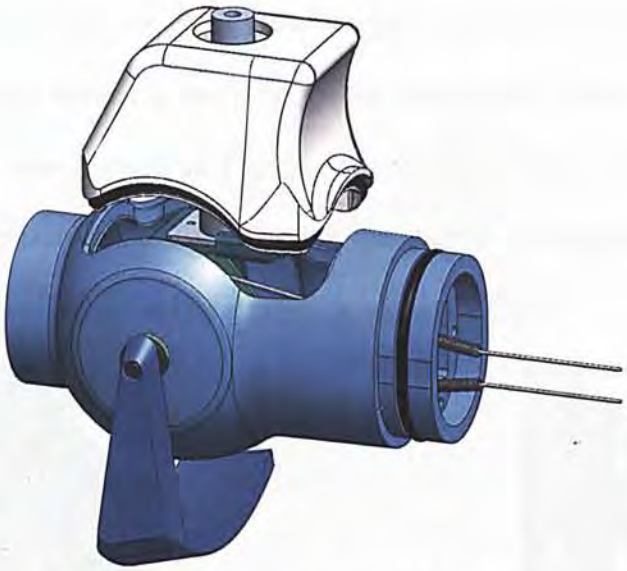

Figure 54: Mating the housing and its cover

Since the whole ureteroscope must be waterproof and totally sealed, here rubber rings are used to seal the gaps of the connections between different components. Fig. 55 demonstrated the case.

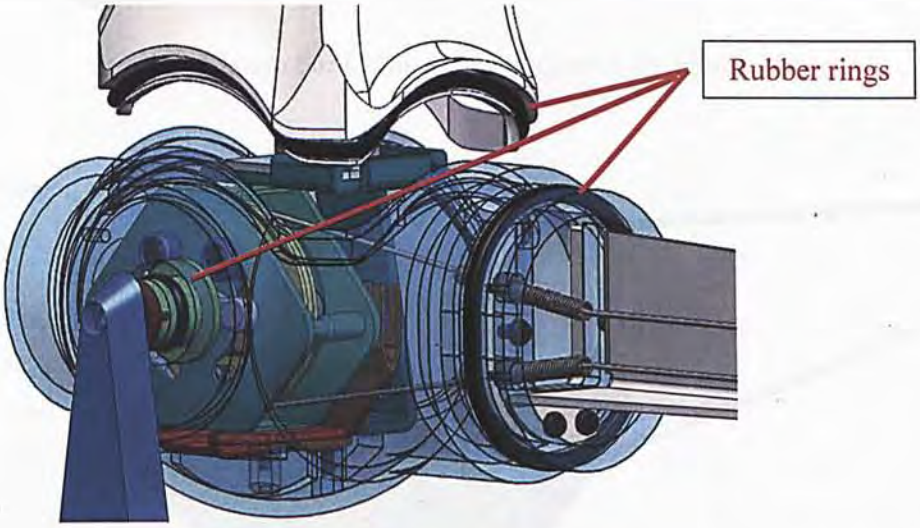

Figure 55: Rubber rings are used to seal the gaps of the connections

4.2.2 Control Mechanism

The control mechanism of an ureteroscope is expected to be able to control the bending section to deflect in two ways on the same plane. The overall picture of the mechanism is demonstrated in Fig. 56. The design of lever is for the ease of manipulating the ureteroscope. By removing the support components, springs and control lever, a core mechanism like a pulley is shown on Fig. 57.

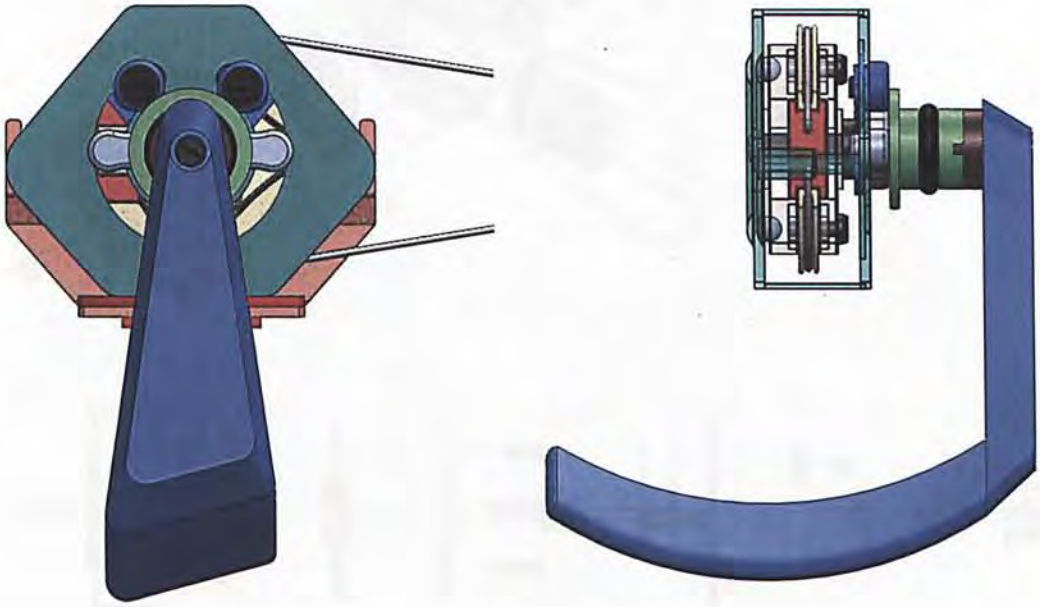

Figure 56: Control mechanism of the ureteroscope

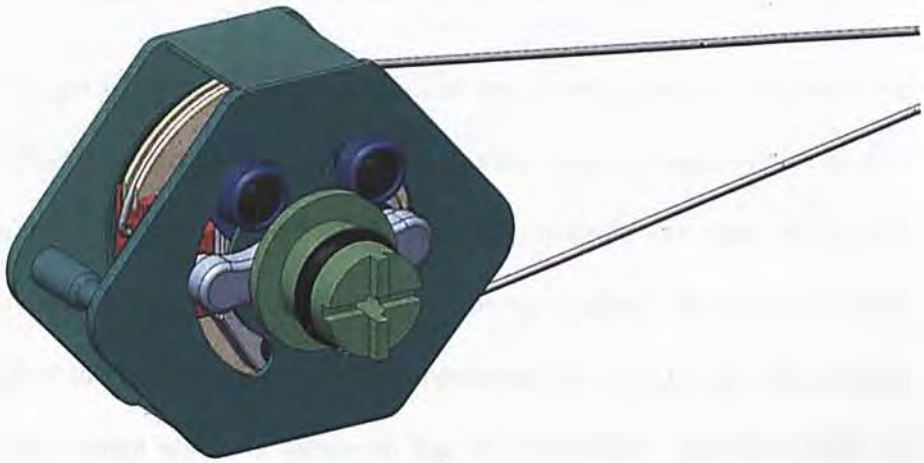

Figure 57: Wheel mechanism of the ureteroscope

The exploded views of the control mechanism are provided in Fig. 58 for the ease of observation.

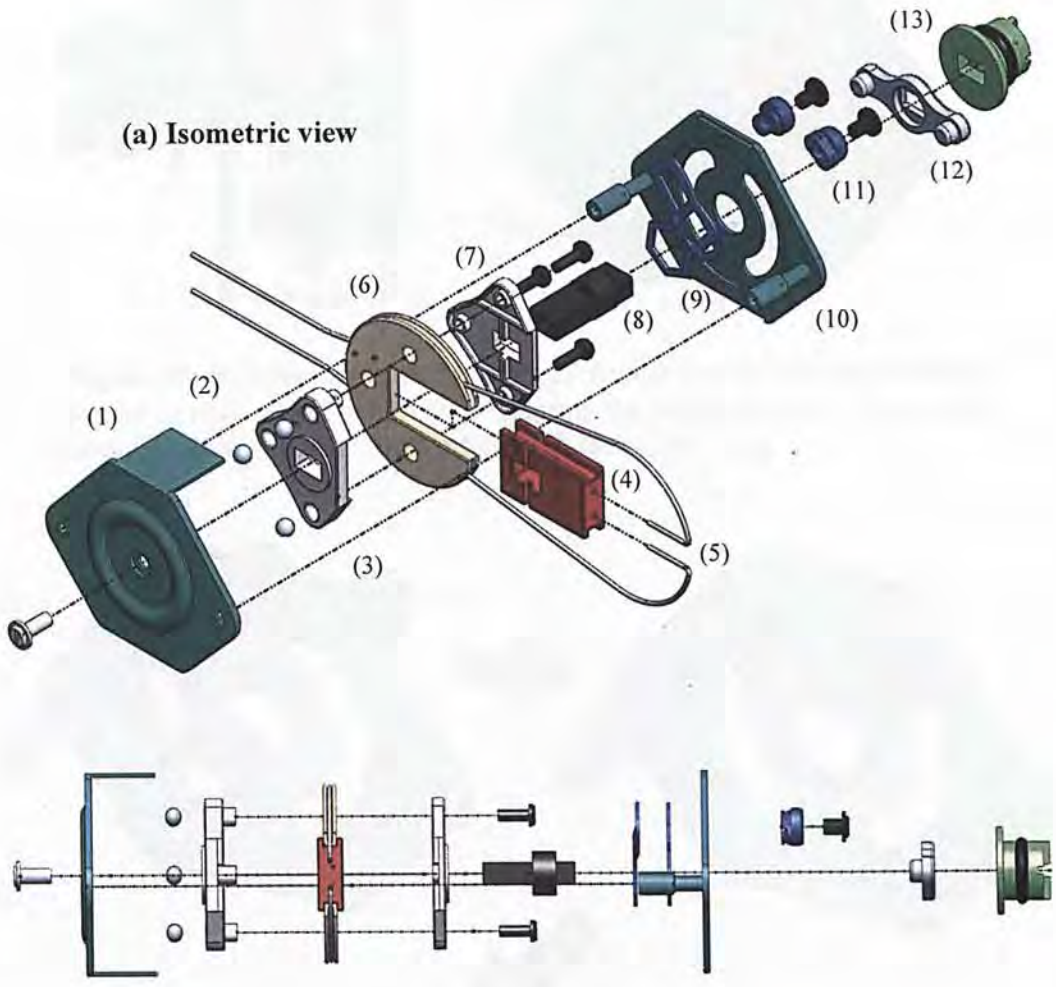

Figure 58: Exploded view of the wheel mechanism

This design of wheel mechanism indeed has some features to improve the manipulation for the ureteroscope. The first one is the ease of assembly. It can also be shown on the exploded view in Fig. 58. Secondly, in order to reduce the friction of steering, a ball bearing system is employed in the mechanism. Meanwhile, a screw is used to adjust the extent of looseness. Components (1) – (3) in Fig. 58 compose the ball bearing system which is shown on Fig. 59. In addition, specific design for tuning the angulation range can be seen on Fig. 60.

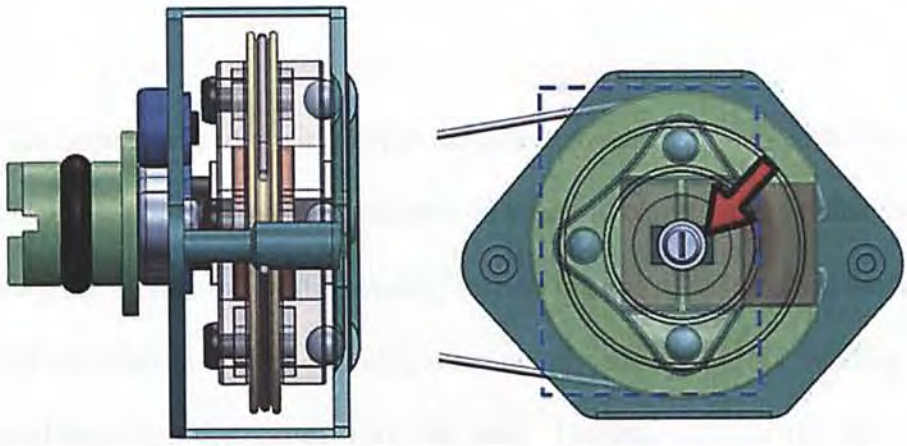

Figure 59: Ball bearing within the wheel mechanism design: Ball bearing is used to reduce the friction while steering the ureteroscope. A screw (red arrow) is used as a slack/tight adjuster of the ball bearing.

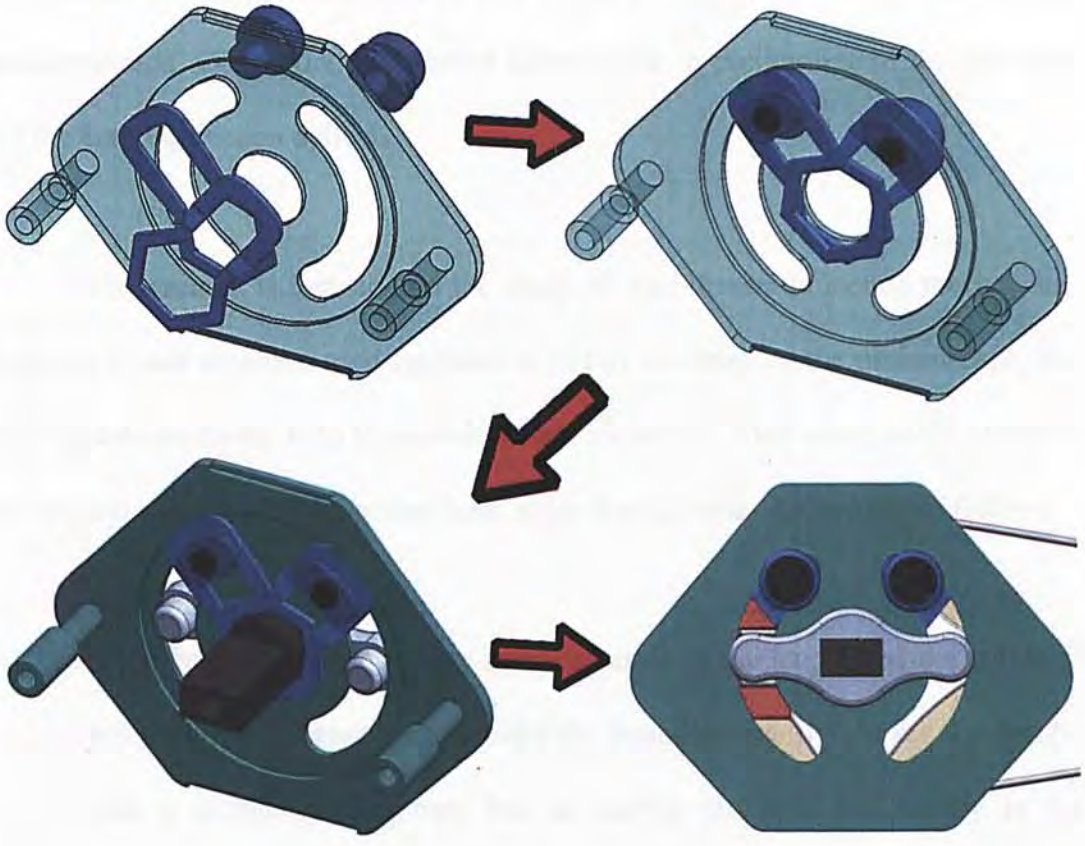

Figure 60: Assembly of the augulation block

5. Conclusion and Future Work

The appearance of a wire-driven deflection mechanism may look like a snake robot. Indeed, it has more advantages such as easier to control and smaller in size by assembling the motors out of the bending section instead of assembling them at each joint. The wire-driven deflection mechanism mainly consists of the bending section, the control wire and the control lever or rotor. The trajectory of the tip motion is constrained by the design of the parts forming the bending section as well as the locations of the wire-holders within the parts. The wires are connecting between the servo motor at the proximal end of the bending section and somewhere in the bending section. Controlling the control lever results in pulling one of the wire and thus the bending section deflects.

This research is focusing on the study of wire-driven deflection mechanism. Referring to one common used application of this mechanism, the ureteroscope, the CAD models are firstly built to provide a clear view of it. After doing some literature reviews and sharing with the technicians, some design issues are reveals as follows:

(a) As the bending section is very small in terms of the length and the radius of each part, it is necessary to consider the manufacturability during the design. Also, a simpler design may lead to saving the time and money in the manufacturing process;

(b) According to some surveys done, durability of the ureteroscopes seems to be hard to improve due to the material and the size of the bending section is

constrained. So far it is better to focus on improving the maintenance which can be achieved by lowering the cost and time. Hence, the ability of assembly should be considered;

From the geometry modeling, it is found that the maximum deflection angle only relates to the gap distance and radius of the bending section. Thus the number of parts involved can be determined by the desired deflection angle. Afterwards, based on the geometric information, some simulations are made to study the deflections of the bending section. Interaction between the control wires and the bending section is provided as well. The simulations can also verify the derived equations.

In this study, the number of sub-sections and the number of pairs of control wires used in a bending section are the most concerned factors. It is found that such configuration of the bending section can be treated as a continuum robot only if the part deflection angle is very small. By assuming that constant curvature applies along each sub-section of the bending section during it deflects, the deflection angle of each part can be treated as equivalent simultaneously. The trajectory of the distal end can then be expressed as a function of the part deflection angle. For one more pair of control wires involved, the trajectory would result in more complicated variation. It is also found that the travel distance for the distal end from origin to destination is the shortest if the bending section is controlled to deflect from the farthest sub-section to the closest sub-section.

As the deflection occurs slowly under the control of the urologist, it is better to study the statics rather than the dynamics of the system. The force analysis of the

wire-driven deflection mechanism is undergoing the derivation. A fundamental analysis is done by considering the statics only when all the bending angles between adjacent parts are assumed to be equivalent at an instant.

Last but not least, a bending section and the control body of a ureteroscope are designed. It concerns not only the knowledge from in or out of this study, but also the people who will actually use it. The bending section comprising two sub-sections are controlled by a single pair of wires. The design of control body has been considered the ease of manufacturing and assembly for the technicians as well as the comfortability for the urologists. It will be great if the prototype can be made soon.

In the future, the work about the deflection mechanism of endoscopic devices should be focused on the force analysis. A successful force analysis can be a solid foundation for the development of automatic endoscopic surgery. The approach can be using the Lagragian method and the principle of least action by considering the minimum potential energy under some constraints such as the control wires must be fixed on the certain parts. Herein all the bending angles are treated as generalized coordinates. It is expected that solving a set of Lagrange's equations will give the solutions of bending angles and the input force which can be the applied moment to wheel mechanism. By plugging in the angles in the simulation, the motion of the deflection mechanism can be observed. Hence, the derivation of the mathematical model can be verified.

Other than application like ureteroscope, there are other possible applications for this wire-driven mechanism. Instead of a single system, two or more systems may

be combined to form an integrating system. The integrated system maybe use in the biology inspired robots such as octopus robot. Besides, there is an innovative design of continuum robot which is called concentric tube continuum robot or also known as active cannulas is invented for the potential medical applications [15]. The special feature of it attributes to the bending actuation method. This operation is done by controlling the pre-curved elastic tubes at the "backbone" of the design to twist in order to transmit the rotation and translation to one another. More work should be carried out on the optimization of this design and it is expected a revolution of the deflection mechanism.

6. Bibliography

[1]. Abdel-Razzak OM, Bagley DH: Clinical experience with flexible ureteropyeloscopy. *J Urol* 1992; 148: 1788–1792.

[2]. Bagley DH: Intrarenal access with the flexible ureteropyeloscope: effects of active and passive tip deflection. *J Endourol* 1993; 7: 221–224.

[3]. Johnson DE, Cromeens DM, Price RE: Use of the holmium:YAG laser in urology. *Lasers Surg Med* 1992; 12: 353–363.

[4]. Sayer J, Johnson DE, Price RE, Cromeens DM: Ureteral lithotripsy with the holmium: YAG laser. *J Clin Laser Med Surg* 1993; 11: 61–65.

[5]. Albert P: The holmium:YAG laser: applications in urology. *Clin Laser Mon* 1993; 11: 39–41.

[6]. Bagley D, Erhard M: Use of the holmium laser in the upper urinary tract. *Tech Urol* 1995; 1: 25–30.

[7]. Marshall VF: Fiberoptics in urology. *J Urol* 1964; 91: 110.

[8]. Takagi T, Go T, Takayasu H, Aso Y: Fiberoptic pyeloureteroscope. *Surgery* 1971; 70: 661–663.

[9]. Bush IM, Goldberg E, Javadpour N, Chakrobortty H, Morelli F: Ureteroscopy and renoscopy: a preliminary report. *Chic Med Sch Q* 1970; 30: 46–49.

[10]. Conlin MJ, Marberger M, Bagley DH: Ureteroscopy. Development and instrumentation. *Urol Clin North Am* 1997; 24: 25–42.

[11]. Buscarini M, Conlin M. Update on flexible ureteroscopy. *Urol Int.* 2008;80(1):1-7

[12]. Hudson RG, Conlin MJ, Bagley DH: Ureteric access with flexible ureteroscopes: effect of the size of the ureteroscope. *BJU Int* 2005; 95: 1043–1044

[13]. Bratslavsky G, Moran ME: Current trends in ureteroscopy. *Urol Clin North Am* 2004; 31: 181–187, xi.

[14]. G. Robinson and J. B. C. Davies, "Continuum Robots – a State of the Art," *Proceedings of the 1999 IEEE International Conference on Robotics and Automation*, pp. 2849-2854, May, 1999..

[15]. R. J. Webster III and B. A. Jones. "Design and Kinematic Modeling of Constant Continuum Robots: A Review," *Int.J.of Robotics Research*, vol.29, pp.1661-1683, 2010

[16]. P. E. Dupont, J. Lock, B. Itkowitz and E. Butler. "Design and Control of Concentric-Tube Robots", *IEEE Transactions on Robotics*. vol. 26, No. 2, p.209-225, 2010.

[17]. W.J. Yoon, P.G. Reinhall and E.J. Seibel, "Analysis of Electro-active Polymer Bending: A Component in a Low Cost Ultrathin Scanning Endoscope", *Sensors and Actuators A: Phys,* 133 pp.506-517, 2007.

[18]. D.L. Nelson, "Patient Anatomy Education Page", http://www.davidlnelson.md/anatomy13%20Extensor%20Mechanism.htm

[19]. V.D. Sars, S. Hyliyo and J. Szewczyk. "A practical approach to the design and control of active endoscopes", *Mechatronics*. vol. 20, pp.251-264, 2010.

[20]. C. Laschi, B. Mazzolai, V. Mattoli, etc. "Design of a biomimetic robotic octopus arm" , *Bioinspiration & Biomimetic,* doi: 10.1088/1748-3182/4/1/015006, 2009

[21]. C. Laschi, B. Mazzolai, V. Mattoli, etc. "Design and Development of A Soft Actuator for a Robot Inspired By the Octopus Arm" *Experi. Robotics: The 11th Intern. Sympo. STAR* 54, pp 25-33, 2009

[22]. B. A. Jones, I. D. Walker, "Kinematics for Multisection Continuum Robots," *IEEE Transactions on Robotics*, vol. 22, No.1, pp.43-57, Feb. 2006.

[23]. Takaharu Idogaki, Takayuki Tominaga, Kouji Senda, etc. "Bending and expanding motion actuators," *Sensors and Actuators A: Phys,* 54, pp.760-764, 1996.

[24]. Michael W. Hannan, Ian D. Walker, "Kinematics and the Implementation of an Elephant's Trunk Manipulator and other Continuum Style Robots", *Journal of Robotics Systems*,vol.20, Issue 2, pp 45-63, Feb, 2003

Appendix A: List of Publication

Journal

Publication Name	International Journal of Mechanical Sciences
Page numbers	10.1016
Date published	August 2010
Title of paper	Kinematic analysis of an auto-winding system with the pawl-lever mechanism and its application in energy harvesting
Full author list	Man Cheong Lei, Longhan Xie, Ruxu Du
ISSN	0020-7403

Conference

Publication Name	Proceedings of the ASME 2011 International Mechanical Engineering Congress & Exposition
Title of paper	Design and analysis of a biomimetic wire-driven robot arm
Full author list	Zheng Li, Ruxu Du, Man Cheong Lei, S. Yuan
Title of conference	International ASME 2011 International Mechanical Engineering Congress & Exposition
Date & location	11-17 Nov. 2011, Denver, Colorado, USA

Publication Name	Proceedings Book of the World Congress on Engineering and Computer Science 2011
Title of paper	Geometry Modeling and Simulation of the Wire-Driven Bending Section of a Flexible Ureteroscope
Full author list	Man Cheong Lei, Ruxu Du
Title of conference	International Conference on Modeling, Simulation and Control, WCECS 2011
Date & location	19-21 Oct, San Francisco, California, USA

Publication Name	International Conference on Control Automation and Systems, 2010
Page numbers	2019 - 2023
Date published	Nov 9, 2010
Title of paper	A study on the bending mechanism of the flexible ureteroscope
Full author list	Man Cheong Lei, Ruxu Du
ISBN	978-1-4244-7453-0
Title of conference	International Conference on Control Automation and Systems, 2010
Date & location	27-30 Oct. 2010, Gyeonggi-do, KOREA

Appendix B: MATLAB Programs

- **Simulations of Bending Section (BS)**

- **Trajectory study about the distal end**

- **Mathematical Functions**

B1. Wire-connected BS (Primary Active deflection 180°)

This program is to simulate the wire-connected bending section to perform a primary active deflection to the angle of 180°. The first six parts do not deflect. It is because there are two coil pipes mounted at the 6th part.

```
mov = avifile('wire180_traj.avi')

max_angle = 275/180*pi;

g = 0.2032;
l = 1.6002;
r = 1.3971;
dbeta = 0.0025;
t = 0.0762;

theta = atan(g/r);
alpha = pi-2*theta;
beta  = 2*theta;
R = sin(alpha/2)/sin(beta)*l;

hole_r = r-0.254;
hole_w = 0.4572;

N = floor(max_angle/beta);

rot_angle = 0:dbeta:beta;
rot_angle = -rot_angle;
req_angle = 180/180*pi;
N_need = round(pi/beta);

figure(1);

for k = 1:N+2 %% +2 because head and tail components

    if k == 1
        node(k).location = [0 0 1];
        node(k).body = ones(6,1)*node(k).location + [-r, -l, 0; -r, l+g,
```

```
0; 0, l+2*g, 0; r, l+g, 0; r, -l, 0; -r, -l, 0];
        node(k).axis = ones(2,1)*node(k).location + [0, -l, 1; 0, l+2*g,
1];
        node(k).hole = ones(12,1)*node(k).location;
    elseif k ~= N+2
        node(k).location = node(k-1).location + [0, l+2*g, 0];
        node(k).body = ones(7,1)*node(k).location + [0, 0, 0; -r, g, 0;
-r, g+l, 0; 0, l+2*g, 0; r, l+g, 0; r, g, 0; 0, 0, 0];
        node(k).axis = ones(2,1)*node(k).location + [ 0, 0, 0; 0, l+2*g,
0];
        node(k).hole = ones(12,1)*node(k).location + [-r, g+l/2-hole_w/2,
0; -hole_r, g+l/2-hole_w/2, 0; -hole_r, g+l/2+hole_w/2, 0; -r,
g+l/2+hole_w/2, 0; r, g+l/2-hole_w/2, 0; hole_r, g+l/2-hole_w/2, 0;
hole_r, g+l/2+hole_w/2, 0; r, g+l/2+hole_w/2, 0;  r-t, g, 0; r-t, g+l,
0; -r+t, g, 0; -r+t, g+l, 0];
    end;

    if k == N+2
        node(k).location = node(k-1).location + [0, l+2*g, 0];
        node(k).body = ones(6,1)*node(k).location + [0, 0, 0; -r, g, 0;
-r, g+2*l, 0; r, 2*l+g, 0; r, g, 0; 0, 0, 0];
        node(k).axis = ones(2,1)*node(k).location + [ 0, 0, 1;  0, g+2*l,
1];
        node(k).hole = ones(12,1)*node(k).location;
    end;

    axis equal;
    axis([-25 5 -30 40]);
    hold on;

end;

hold off;

F(1)=getframe;
mov = addframe(mov,F(1));

traj = [node(1).body(4,:)];
```

```
for n = 1:length(rot_angle)

   wire_L = [];
   wire_R = [];
   length_wire_L = 0;
   length_wire_R = 0;

   for k = 1:N+2

      plot(node(1).axis(1,1),node(1).axis(1,2),'r*');
      plot(node(1).axis(1:2,1),node(1).axis(1:2,2),'r-');

      if k ~= 1
         if k >= N+2-N_need
            node(k).location = node(k-1).location +
(Rot((k-(N+2-N_need))*rot_angle(n))*[0, l+2*g, 0]')';
         end;
         if k ~= N+2
            if k >= N+2-N_need-1
               node(k).body =
(Tran(node(k).location)*(Rot((k-(N+2-N_need)+1)*rot_angle(n))*[0, 0,
1; -r, g, 1; -r, g+l, 1; 0, l+2*g, 1; r, l+g, 1; r, g, 1; 0, 0, 1]'))';

               node(k).axis =
(Tran(node(k).location)*(Rot((k-(N+2-N_need)+1)*rot_angle(n))*[ 0, 0,
1; 0, l+2*g, 1]'))';

               node(k).hole =
(Tran(node(k).location)*(Rot((k-(N+2-N_need)+1)*rot_angle(n))*[-r,
g+l/2-hole_w/2, 1; -hole_r, g+l/2-hole_w/2, 1; -hole_r, g+l/2+hole_w/2,
1; -r, g+l/2+hole_w/2, 1; r, g+l/2-hole_w/2, 1; hole_r, g+l/2-hole_w/2,
1; hole_r, g+l/2+hole_w/2, 1; r, g+l/2+hole_w/2, 1; r-t, g, 1; r-t, g+l,
1; -r+t, g, 1; -r+t, g+l, 1]'))';
            end;

%% ========= For the control wires ==================
%% Judge the direction of the rotation
            wire_R = [wire_R; node(k).hole(6,:); node(k).hole(7,:)];
```

```
            if k == N+1
               wire_R(2*(k-1),:) = node(k).hole(10,:);
            end;

            if k <= N+1
               wire_L = [wire_L; node(k).hole(11,:);
node(k).hole(12,:)];
            end;

            if k == N+1
               wire_L(2*(k-1),:) = node(k).hole(12,:);
            end;

            length_wire_L = length_wire_L +
sqrt(sum((node(k-1).hole(3,:) - node(k).hole(2,:)).^2)) +
sqrt(sum((node(k).hole(2,:) - node(k).hole(3,:)).^2));
            length_wire_R = length_wire_R +
sqrt(sum((node(k-1).hole(10,:) - node(k).hole(9,:)).^2)) +
sqrt(sum((node(k).hole(9,:) - node(k).hole(10,:)).^2));

%% ============== End of control wires ================

         else   %% if k = N+2
            node(k).body =
(Tran(node(k).location)*(Rot((N_need)*rot_angle(n))*[0, 0, 1; -r, g, 1;
-r, g+2*l, 1; r, 2*l+g, 1; r, g, 1; 0, 0, 1]'))';

            node(k).axis =
(Tran(node(k).location)*(Rot((N_need)*rot_angle(n))*[ 0, 0, 1;  0,
g+2*l, 1]'))';

            node(k).hole = ones(12,1)*node(k).location;
            traj = [traj; node(k).body(4,:)];

            plot(node(k).axis(2,1),node(k).axis(2,2),'r*');
            plot(node(k).axis(1:2,1),node(k).axis(1:2,2),'r-');
         end;
      else   %% if k = 1
         node(k).hole = ones(12,1)*node(k).location;
```

```
        end;

        plot(node(k).axis(1:2,1),node(k).axis(1:2,2),'r-');
        plot(node(k).hole(1:4,1),
node(k).hole(1:4,2),'r-',node(k).hole(5:8,1),node(k).hole(5:8,2),'r-
');
        axis equal;
        axis([-25 5 -30 40]);
        hold on;
        plot(node(k).body(:,1),node(k).body(:,2),'k-');
    end;

    delta_wire = length_wire_L - length_wire_R;
    wire_L = [wire_L(1,:); wire_L];
    wire_L(1,2) = wire_L(1,2) - 18 + delta_wire;
    wire_R = [wire_R(1,:); wire_R];
    wire_R(1,2) = wire_R(1,2) - 18 - delta_wire;

    plot(wire_L(:,1),wire_L(:,2),'b-', wire_R(:,1),wire_R(:,2),'b-');

plot(wire_L(length(wire_L),1),wire_L(length(wire_L),2),'b*',wire_R(l
ength(wire_R),1),wire_R(length(wire_R),2),'b*');
    plot(wire_L(1,1),wire_L(1,2),'bo',wire_R(1,1),wire_R(1,2),'bo');
    plot(traj(:,1), traj(:,2), 'g--');

    drawnow;
    hold off;
    F(n)=getframe;
    mov = addframe(mov,F(n));
end;

movie(F,1);
mov = close(mov);
```

B2. Wire-connected BS (Primary Active deflection 270°)

This program is to simulate the wire-connected bending section to perform a primary active deflection to the angle of 270°. The two coil pipes mounted at the first part so that the whole bending section fully deflects.

```
mov = avifile('wire270_traj.avi')

max_angle = 275/180*pi;

g = 0.2032;
l = 1.6002;
r = 1.3971;
dbeta = 0.0025;
t = 0.0762;

theta = atan(g/r);
alpha = pi-2*theta;
beta  = 2*theta;
R = sin(alpha/2)/sin(beta)*l;

hole_r = r-0.254;
hole_w = 0.4572;
N = floor(max_angle/beta);
rot_angle = 0:dbeta:beta;
req_angle = 275/180*pi;

if (req_angle/beta) > N
   N_need = floor(req_angle/beta);
else
   N_need = round(req_angle/beta);
end;
figure(1);

for k = 1:N+2 %% +2 because head and tail components

   if k == 1
      node(k).location = [0 0 1];
```

```
        node(k).body = ones(6,1)*node(k).location + [-r, -l, 0; -r, l+g,
0; 0, l+2*g, 0; r, l+g, 0; r, -l, 0; -r, -l, 0];
        node(k).axis = ones(2,1)*node(k).location + [0, -l, 1; 0, l+2*g,
1];
        node(k).hole = ones(12,1)*node(k).location;
    elseif k ~= N+2
        node(k).location = node(k-1).location + [0, l+2*g, 0];
        node(k).body = ones(7,1)*node(k).location + [0, 0, 0; -r, g, 0;
-r, g+l, 0; 0, l+2*g, 0; r, l+g, 0; r, g, 0; 0, 0, 0];
        node(k).axis = ones(2,1)*node(k).location + [ 0, 0, 0; 0, l+2*g,
0];
        node(k).hole = ones(12,1)*node(k).location + [-r, g+l/2-hole_w/2,
0; -hole_r, g+l/2-hole_w/2, 0; -hole_r, g+l/2+hole_w/2, 0; -r,
g+l/2+hole_w/2, 0; r, g+l/2-hole_w/2, 0; hole_r, g+l/2-hole_w/2, 0;
hole_r, g+l/2+hole_w/2, 0; r, g+l/2+hole_w/2, 0;  r-t, g, 0; r-t, g+l,
0; -r+t, g, 0; -r+t, g+l, 0];
    end;

    if k == N+2
        node(k).location = node(k-1).location + [0, l+2*g, 0];
        node(k).body = ones(6,1)*node(k).location + [0, 0, 0; -r, g, 0;
-r, 2*l-g, 0; r, 2*l-g, 0; r, g, 0; 0, 0, 0];
        node(k).axis = ones(2,1)*node(k).location + [ 0, 0, 1;  0, 2*l-g,
1];
        node(k).hole = ones(12,1)*node(k).location;
    end;

    axis equal;
    axis([-5 30 -30 40]);
    hold on;

end;

hold off;

F(1)=getframe;
mov = addframe(mov,F(1));

traj = [node(1).body(2,:)];
```

```
for n = 1:length(rot_angle)

   wire_L = [];
   wire_R = [];
   length_wire_L = 0;
   length_wire_R = 0;

   for k = 1:N+2

      plot(node(1).axis(1,1),node(1).axis(1,2),'r*');
      plot(node(1).axis(1:2,1),node(1).axis(1:2,2),'r-');

      if k ~= 1

         if k >= N+2-N_need
            node(k).location = node(k-1).location +
(Rot((k-(N+2-N_need))*rot_angle(n))*[0, l+2*g, 0]')';
         end;

         if k ~= N+2
            if k >= N+2-N_need-1
               node(k).body =
(Tran(node(k).location)*(Rot((k-(N+2-N_need)+1)*rot_angle(n))*[0, 0,
1; -r, g, 1; -r, g+l, 1; 0, l+2*g, 1; r, l+g, 1; r, g, 1; 0, 0, 1]'))';

               node(k).axis =
(Tran(node(k).location)*(Rot((k-(N+2-N_need)+1)*rot_angle(n))*[ 0, 0,
1; 0, l+2*g, 1]'))';

               node(k).hole =
(Tran(node(k).location)*(Rot((k-(N+2-N_need)+1)*rot_angle(n))*[-r,
g+l/2-hole_w/2, 1; -hole_r, g+l/2-hole_w/2, 1; -hole_r, g+l/2+hole_w/2,
1; -r, g+l/2+hole_w/2, 1; r, g+l/2-hole_w/2, 1; hole_r, g+l/2-hole_w/2,
1; hole_r, g+l/2+hole_w/2, 1; r, g+l/2+hole_w/2, 1; r-t, g, 1; r-t, g+l,
1; -r+t, g, 1; -r+t, g+l, 1]'))';
            end;

%% ========= For the control wires ==================
```

```
            wire_L = [wire_L; node(k).hole(2,:); node(k).hole(3,:)];

            if k == N+1
               wire_L(2*(k-1),:) = node(k).hole(12,:);
            end;

            if k <= N_need+1
               wire_R = [wire_R; node(k).hole(9,:);
node(k).hole(10,:)];
            end;

            if k == N_need+1
               wire_R(2*(k-1),:) = node(k).hole(10,:);
            end;

            length_wire_L = length_wire_L +
sqrt(sum((node(k-1).hole(3,:) - node(k).hole(2,:)).^2)) +
sqrt(sum((node(k).hole(2,:) - node(k).hole(3,:)).^2));
            length_wire_R = length_wire_R +
sqrt(sum((node(k-1).hole(10,:) - node(k).hole(9,:)).^2)) +
sqrt(sum((node(k).hole(9,:) - node(k).hole(10,:)).^2));

%% ============== End of control wires ================
         else   %% if k = N+2
            node(k).body =
(Tran(node(k).location)*(Rot((N_need)*rot_angle(n))*[0, 0, 1; -r, g, 1;
-r, 2*l-g, 1; r, 2*l-g, 1; r, g, 1; 0, 0, 1]'))';

            node(k).axis =
(Tran(node(k).location)*(Rot((N_need)*rot_angle(n))*[ 0, 0, 1;  0,
2*l-g, 1]'))';

            node(k).hole = ones(12,1)*node(k).location;

            traj = [traj; node(k).body(3,:)];

            plot(node(k).axis(2,1),node(k).axis(2,2),'r*');
            plot(node(k).axis(1:2,1),node(k).axis(1:2,2),'r-');
         end;
```

```
        else   %% if k = 1
            node(k).hole = ones(12,1)*node(k).location;
        end;

        plot(node(k).axis(1:2,1),node(k).axis(1:2,2),'r-');
        plot(node(k).hole(1:4,1),
node(k).hole(1:4,2),'r-',node(k).hole(5:8,1),node(k).hole(5:8,2),'r-
');
        axis equal;
        axis([-5 30 -30 40]);
        hold on;
        plot(node(k).body(:,1),node(k).body(:,2),'k-');
    end;

    delta_wire = length_wire_L - length_wire_R;

    wire_L = [wire_L(1,:); wire_L];
    wire_L(1,2) = wire_L(1,2) - 18 + delta_wire;
    wire_R = [wire_R(1,:); wire_R];
    wire_R(1,2) = wire_R(1,2) - 18 - delta_wire;

    plot(wire_L(:,1),wire_L(:,2),'b-', wire_R(:,1),wire_R(:,2),'b-');

plot(wire_L(length(wire_L),1),wire_L(length(wire_L),2),'b*',wire_R(l
ength(wire_R),1),wire_R(length(wire_R),2),'b*');
    plot(wire_L(1,1),wire_L(1,2),'bo',wire_R(1,1),wire_R(1,2),'bo');
    plot(traj(:,1), traj(:,2), 'g--');

    drawnow;
    hold off;
    F(n)=getframe;
    mov = addframe(mov,F(n));
end;
movie(F,1);
mov = close(mov);
```

B3. Pin-joint BS composed by identical parts (Partial deflection: 180°)

This program is to simulate the pin-joint bending section to deflect to the angle of 180°. The left control wire is mounted at the end of the 12th part. If the left wire is pulled, only the twelve parts which the wire pierces through deflect. It is an active deflection as the deflection is controlled by the wire.

```
mov = avifile('rivet_1_180_traj.avi')

max_angle = 275/180*pi;

g = 0.00625;
l = 0.0665;
r = 0.0485;
dbeta = 0.0025;
t = 0.003;

theta = atan(g/r);
alpha = pi-2*theta;
beta  = 2*theta;
R = sin(alpha/2)/sin(beta)*l;

bias_angle = 25/180*pi;
hole_r = 0.084/2*cos(bias_angle);
hole_w = 0.018;

N = round(max_angle/beta);
rot_angle = 0:dbeta:beta;
rot_angle = -rot_angle;
req_angle = 180/180*pi;
N_need = round(pi/beta);

figure(1);

for k = 1:N+2

    if k == 1
        node(k).location = [0 0 1];
```

```
        node(k).body = ones(5,1)*node(k).location + [-r, -l, 0; -r, l+g,
0; r, l+g, 0; r, -l, 0; -r, -l, 0];
        node(k).axis = ones(4,1)*node(k).location + [ 0, 0, 0;  0, 0, 0  ;
0, l+g, 0; 0, l+2*g, 0];
        node(k).hole = ones(12,1)*node(k).location;
    elseif k ~= N+2
        node(k).location = node(k-1).location + [0, l+2*g, 0];
        node(k).body = ones(5,1)*node(k).location + [-r, g, 0; -r, g+l,
0; r, l+g, 0; r, g, 0; -r, g, 0];
        node(k).axis = ones(4,1)*node(k).location + [ 0, 0, 0;  0, g,   0;
0, l+g, 0; 0, l+2*g, 0];
        node(k).hole = ones(12,1)*node(k).location + [-r, g+l/2-hole_w/2,
0; -hole_r, g+l/2-hole_w/2, 0; -hole_r, g+l/2+hole_w/2, 0; -r,
g+l/2+hole_w/2, 0; r, g+l/2-hole_w/2, 0; hole_r, g+l/2-hole_w/2, 0;
hole_r, g+l/2+hole_w/2, 0; r, g+l/2+hole_w/2, 0;  r-t, g, 0; r-t, g+l,
0; -r+t, g, 0; -r+t, g+l, 0];
    end;

    if k == N+2
        node(k).location = node(k-1).location + [0, l+2*g, 0];
        node(k).body = ones(5,1)*node(k).location + [-r, g, 0; -r, g+2*l,
0; r, 2*l+g, 0; r, g, 0; -r, g, 0];
        node(k).axis = ones(4,1)*node(k).location + [ 0, 0, 1;  0, g, 1;
0, g, 1; 0, g, 1];
        node(k).hole = ones(12,1)*node(k).location;
    end;


plot(node(k).axis(1:2,1),node(k).axis(1:2,2),'g-',node(k).axis(3:4,1
),node(k).axis(3:4,2),'g-');
    plot(node(k).hole(1:4,1),
node(k).hole(1:4,2),'g-',node(k).hole(5:8,1),node(k).hole(5:8,2),'g-
');
    axis equal;
    axis([-1.4 1.4 -1 1.8]);
    hold on;
    plot(node(k).body(:,1),node(k).body(:,2),'b-');

end;
```

```
hold off;

traj = [node(1).body(4,:)];

for n = 1:length(rot_angle)

   wire_L = [];
   wire_R = [];
   length_wire_L = 0;
   length_wire_R = 0;

   for k = 1:N+2
      if k ~= 1
         if k ~= 2
            if k <= N_need+1
               node(k).location = node(k-1).location +
(Rot((k-2)*rot_angle(n))*[0, l+2*g, 0]')';
            else
               node(k).location = node(k-1).location +
(Rot((N_need)*rot_angle(n))*[0, l+2*g, 0]')';
            end;
         end;

         if k ~= N+2
            if k <= N_need+1
               node(k).body =
(Tran(node(k).location)*(Rot((k-1)*rot_angle(n))*[-r, g, 1; -r, g+l, 1;
r, l+g, 1; r, g, 1; -r, g, 1]'))';

               node(k).axis =
(Tran(node(k).location)*(Rot((k-1)*rot_angle(n))*[ 0, 0, 1;  0, g,   1;
0, l+g, 1; 0, l+2*g, 1]'))';

               node(k).hole =
(Tran(node(k).location)*(Rot((k-1)*rot_angle(n))*[-r, g+l/2-hole_w/2,
1; -hole_r, g+l/2-hole_w/2, 1; -hole_r, g+l/2+hole_w/2, 1; -r,
g+l/2+hole_w/2, 1; r, g+l/2-hole_w/2, 1; hole_r, g+l/2-hole_w/2, 1;
hole_r, g+l/2+hole_w/2, 1; r, g+l/2+hole_w/2, 1; r-t, g, 1; r-t, g+l,
1; -r+t, g, 1; -r+t, g+l, 1]'))';
```

```
            else
                node(k).body =
(Tran(node(k).location)*(Rot((N_need)*rot_angle(n))*[-r, g, 1; -r, g+l,
1; r, l+g, 1; r, g, 1; -r, g, 1]'))';

                node(k).axis =
(Tran(node(k).location)*(Rot((N_need)*rot_angle(n))*[ 0, 0, 1;  0, g,
1; 0, l+g, 1; 0, l+2*g, 1]'))';

                node(k).hole =
(Tran(node(k).location)*(Rot((N_need)*rot_angle(n))*[-r,
g+l/2-hole_w/2, 1; -hole_r, g+l/2-hole_w/2, 1; -hole_r, g+l/2+hole_w/2,
1; -r, g+l/2+hole_w/2, 1; r, g+l/2-hole_w/2, 1; hole_r, g+l/2-hole_w/2,
1; hole_r, g+l/2+hole_w/2, 1; r, g+l/2+hole_w/2, 1; r-t, g, 1; r-t, g+l,
1; -r+t, g, 1; -r+t, g+l, 1]'))';
            end;

            %% Judge the direction of the rotation
            if rot_angle(n) > 0

                wire_L = [wire_L; node(k).hole(2,:);
node(k).hole(3,:)];

                if k == N+1
                    wire_L(2*(k-1),:) = node(k).hole(12,:);
                end;

                if k <= N_need+1
                    wire_R = [wire_R; node(k).hole(9,:);
node(k).hole(10,:)];
                end;

                if k == N_need+1
                    wire_R(2*(k-1),:) = node(k).hole(10,:);
                end;

            elseif rot_angle(n) < 0

                wire_R = [wire_R; node(k).hole(6,:);
```

```
node(k).hole(7,:)];

                if k == N+1
                   wire_R(2*(k-1),:) = node(k).hole(10,:);
                end;

                if k <= N_need+1
                   wire_L = [wire_L; node(k).hole(11,:);
node(k).hole(12,:)];
                end;

                if k == N_need+1
                   wire_L(2*(k-1),:) = node(k).hole(12,:);
                end;

             else
                wire_L = [wire_L; node(k).hole(2,:);
node(k).hole(3,:)];
                wire_R = [wire_R; node(k).hole(6,:);
node(k).hole(7,:)];
                if k == N+1
                   wire_L(2*(k-1),:) = node(k).hole(12,:);
                   wire_R(2*(k-1),:) = node(k).hole(10,:);
                end;
             end;
             length_wire_L = length_wire_L +
sqrt(sum((node(k-1).hole(3,:) - node(k).hole(2,:)).^2)) +
sqrt(sum((node(k).hole(2,:) - node(k).hole(3,:)).^2));
             length_wire_R = length_wire_R +
sqrt(sum((node(k-1).hole(10,:) - node(k).hole(9,:)).^2)) +
sqrt(sum((node(k).hole(9,:) - node(k).hole(10,:)).^2));
          else
             node(k).body =
(Tran(node(k).location)*(Rot((N_need)*rot_angle(n))*[-r, g, 1; -r,
g+2*l, 1; r, 2*l+g, 1; r, g, 1; -r, g, 1]'))';
             node(k).axis =
(Tran(node(k).location)*(Rot((N_need)*rot_angle(n))*[ 0, 0, 1;  0, g,
1; 0, g, 1; 0, g, 1]'))';
```

```
            node(k).hole = ones(12,1)*node(k).location;
            traj = [traj; node(k).body(3,:)];
        end;
        plot(node(k).location(:,1),node(k).location(:,2),'go');
    else
        node(k).hole = ones(12,1)*node(k).location;
    end;

plot(node(k).axis(1:2,1),node(k).axis(1:2,2),'g-',node(k).axis(3:4,1
),node(k).axis(3:4,2),'g-');
    plot(node(k).hole(1:4,1),
node(k).hole(1:4,2),'g-',node(k).hole(5:8,1),node(k).hole(5:8,2),'g-
');
    axis equal;
    axis([-1.4 1.4 -1 1.8]);
    hold on;
    plot(node(k).body(:,1),node(k).body(:,2),'b-');
end;

delta_wire = length_wire_L - length_wire_R;
wire_L = [wire_L(1,:); wire_L];
wire_L(1,2) = wire_L(1,2) - 0.6 + delta_wire;
wire_R = [wire_R(1,:); wire_R];
wire_R(1,2) = wire_R(1,2) - 0.6 - delta_wire;
plot(wire_L(:,1),wire_L(:,2),'r-', wire_R(:,1),wire_R(:,2),'r-');

plot(wire_L(length(wire_L),1),wire_L(length(wire_L),2),'r*',wire_R(l
ength(wire_R),1),wire_R(length(wire_R),2),'r*');
plot(wire_L(1,1),wire_L(1,2),'ro',wire_R(1,1),wire_R(1,2),'ro');
plot(traj(:,1), traj(:,2), 'k--');

drawnow;
hold off;

F(n)=getframe;
mov = addframe(mov,F(n));
end;
movie(F,1);
mov = close(mov);
```

B4. Pin-joint BS composed by identical parts (Full deflection: 270°)

This program is to simulate the pin-joint bending section to deflect to the angle of 270°. The left control wire is mounted at the end of the final part. If the left wire is pulled, the whole bending section deflects. It is an active deflection as the deflection is controlled by the wire.

```
mov = avifile('rivet_1_270_traj.avi')

max_angle = 275/180*pi;

g = 0.00625;
l = 0.0665;
r = 0.0485;
dbeta = 0.0025;
t = 0.003;

theta = atan(g/r);
alpha = pi-2*theta;
beta  = 2*theta;
R = sin(alpha/2)/sin(beta)*l;

bias_angle = 25/180*pi;
hole_r = 0.084/2*cos(bias_angle);
hole_w = 0.018;

N = round(max_angle/beta);
rot_angle = 0:dbeta:beta;
req_angle = 275/180*pi;
N_need = round(req_angle/beta);

figure(1);

for k = 1:N+2
    if k == 1
        node(k).location = [0 0 1];
        node(k).body = ones(5,1)*node(k).location + [-r, -l, 0; -r, l+g,
0; r, l+g, 0; r, -l, 0; -r, -l, 0];
```

```
        node(k).axis = ones(4,1)*node(k).location + [ 0, 0, 0;  0, 0, 0  ;
0, l+g, 0; 0, l+2*g, 0];
        node(k).hole = ones(12,1)*node(k).location;
    elseif k ~= N+2
        node(k).location = node(k-1).location + [0, l+2*g, 0];
        node(k).body = ones(5,1)*node(k).location + [-r, g, 0; -r, g+l,
0; r, l+g, 0; r, g, 0; -r, g, 0];
        node(k).axis = ones(4,1)*node(k).location + [ 0, 0, 0;  0, g,   0;
0, l+g, 0; 0, l+2*g, 0];
        node(k).hole = ones(12,1)*node(k).location + [-r, g+l/2-hole_w/2,
0; -hole_r, g+l/2-hole_w/2, 0; -hole_r, g+l/2+hole_w/2, 0; -r,
g+l/2+hole_w/2, 0; r, g+l/2-hole_w/2, 0; hole_r, g+l/2-hole_w/2, 0;
hole_r, g+l/2+hole_w/2, 0; r, g+l/2+hole_w/2, 0;  r-t, g, 0; r-t, g+l,
0; -r+t, g, 0; -r+t, g+l, 0];
    end;

    if k == N+2
        node(k).location = node(k-1).location + [0, l+2*g, 0];
        node(k).body = ones(5,1)*node(k).location + [-r, g, 0; -r, g+2*l,
0; r, 2*l+g, 0; r, g, 0; -r, g, 0];
        node(k).axis = ones(4,1)*node(k).location + [ 0, 0, 1;  0, g, 1;
0, g, 1; 0, g, 1];
        node(k).hole = ones(12,1)*node(k).location;
    end;

plot(node(k).axis(1:2,1),node(k).axis(1:2,2),'g-',node(k).axis(3:4,1
),node(k).axis(3:4,2),'g-');
    plot(node(k).hole(1:4,1),
node(k).hole(1:4,2),'g-',node(k).hole(5:8,1),node(k).hole(5:8,2),'g-
');
    axis equal;
    axis([-1.4 1.4 -1 1.8]);
    hold on;
    plot(node(k).body(:,1),node(k).body(:,2),'b-');

end;

hold off;
traj = [node(1).body(1,:)];
```

```
for n = 1:length(rot_angle)

   wire_L = [];
   wire_R = [];
   length_wire_L = 0;
   length_wire_R = 0;

   for k = 1:N+2

      if k ~= 1

         if k ~= 2
            if k <= N_need+1
               node(k).location = node(k-1).location +
(Rot((k-2)*rot_angle(n))*[0, l+2*g, 0]')';
            else
               node(k).location = node(k-1).location +
(Rot((N_need)*rot_angle(n))*[0, l+2*g, 0]')';
            end;
         end;

         if k ~= N+2
            if k <= N_need+1
               node(k).body =
(Tran(node(k).location)*(Rot((k-1)*rot_angle(n))*[-r, g, 1; -r, g+l, 1;
r, l+g, 1; r, g, 1; -r, g, 1]'))';
               node(k).axis =
(Tran(node(k).location)*(Rot((k-1)*rot_angle(n))*[ 0, 0, 1;  0, g,   1;
0, l+g, 1; 0, l+2*g, 1]'))';
               node(k).hole =
(Tran(node(k).location)*(Rot((k-1)*rot_angle(n))*[-r, g+l/2-hole_w/2,
1; -hole_r, g+l/2-hole_w/2, 1; -hole_r, g+l/2+hole_w/2, 1; -r,
g+l/2+hole_w/2, 1; r, g+l/2-hole_w/2, 1; hole_r, g+l/2-hole_w/2, 1;
hole_r, g+l/2+hole_w/2, 1; r, g+l/2+hole_w/2, 1; r-t, g, 1; r-t, g+l,
1; -r+t, g, 1; -r+t, g+l, 1]'))';
            else
               node(k).body =
(Tran(node(k).location)*(Rot((N_need)*rot_angle(n))*[-r, g, 1; -r, g+l,
1; r, l+g, 1; r, g, 1; -r, g, 1]'))';
```

```
                node(k).axis =
(Tran(node(k).location)*(Rot((N_need)*rot_angle(n))*[ 0, 0, 1;  0, g,
1; 0, l+g, 1; 0, l+2*g, 1]'))';
                node(k).hole =
(Tran(node(k).location)*(Rot((N_need)*rot_angle(n))*[-r,
g+l/2-hole_w/2, 1; -hole_r, g+l/2-hole_w/2, 1; -hole_r, g+l/2+hole_w/2,
1; -r, g+l/2+hole_w/2, 1; r, g+l/2-hole_w/2, 1; hole_r, g+l/2-hole_w/2,
1; hole_r, g+l/2+hole_w/2, 1; r, g+l/2+hole_w/2, 1; r-t, g, 1; r-t, g+l,
1; -r+t, g, 1; -r+t, g+l, 1]'))';
            end;

                wire_R = [wire_R; node(k).hole(9,:);
node(k).hole(10,:)];

                if k == N+1
                    wire_R(2*(k-1),:) = node(k).hole(10,:);
                end;

                if k <= 12+1
                    wire_L = [wire_L; node(k).hole(2,:);
node(k).hole(3,:)];
                end;

                if k == 12+1
                    wire_L(2*(k-1),:) = node(k).hole(12,:);
                end;
            length_wire_L = length_wire_L +
sqrt(sum((node(k-1).hole(3,:) - node(k).hole(2,:)).^2)) +
sqrt(sum((node(k).hole(2,:) - node(k).hole(3,:)).^2));
            length_wire_R = length_wire_R +
sqrt(sum((node(k-1).hole(10,:) - node(k).hole(9,:)).^2)) +
sqrt(sum((node(k).hole(9,:) - node(k).hole(10,:)).^2));

        else
            node(k).body =
(Tran(node(k).location)*(Rot((N_need)*rot_angle(n))*[-r, g, 1; -r,
g+2*l, 1; r, 2*l+g, 1; r, g, 1; -r, g, 1]'))';

            node(k).axis =
```

```
(Tran(node(k).location)*(Rot((N_need)*rot_angle(n))*[ 0, 0, 1;  0, g,
1; 0, g, 1; 0, g, 1]'))';
                node(k).hole = ones(12,1)*node(k).location;
                traj = [traj; node(k).body(2,:)];
            end;
            plot(node(k).location(:,1),node(k).location(:,2),'go');
        else
            node(k).hole = ones(12,1)*node(k).location;
        end;
        ),node(k).axis(3:4,2),'g-');
        plot(node(k).hole(1:4,1),
node(k).hole(1:4,2),'g-',node(k).hole(5:8,1),node(k).hole(5:8,2),'g-
');
        axis equal;
        axis([-1.4 1.4 -1 1.8]);
        hold on;
        plot(node(k).body(:,1),node(k).body(:,2),'b-');
    end;

    delta_wire = length_wire_L - length_wire_R;
    wire_L = [wire_L(1,:); wire_L];
    wire_L(1,2) = wire_L(1,2) - 0.6 + delta_wire;
    wire_R = [wire_R(1,:); wire_R];
    wire_R(1,2) = wire_R(1,2) - 0.6 - delta_wire;
    plot(wire_L(:,1),wire_L(:,2),'r-', wire_R(:,1),wire_R(:,2),'r-');

plot(wire_L(length(wire_L),1),wire_L(length(wire_L),2),'r*',wire_R(l
ength(wire_R),1),wire_R(length(wire_R),2),'r*');
    plot(wire_L(1,1),wire_L(1,2),'ro',wire_R(1,1),wire_R(1,2),'ro');
    plot(traj(:,1), traj(:,2), 'k--');

    drawnow;
    hold off;
    F(n)=getframe;
    mov = addframe(mov,F(n));
end;

movie(F,1);
mov = close(mov);
```

B5. Pin-joint BS composed by two sub-sections (Full deflection: 275°)

This program is to simulate the pin-joint bending section to deflect to the angle of 275°. This bending section comprises two sub-sections and one pair of control wires. The control wires all the way pierce through the parts and mounted at the distal end of the bending section. Hence the whole bending section deflects if either control wire is being pulled. There are two inner radii, R_{in1} and R_{in2}, appears at full deflection. By observation, $R_{in1}>R_{in2}$.

```
mov = avifile('rivet_2_275.avi')

max_angle = 275/180*pi;

g = 0.152;
r = 1.1555;
dbeta = 0.0025;
t = 0.089;

la = 1.881;
lb = 3.048;
lc = 5.4749;
ld = 5.3345;

l_head = 1.524;
r_head = 2.8811/2;

theta = atan(g/r);
alpha = pi-2*theta;
beta  = 2*theta;

hole_r = r-0.254;
hole_w = 0.4572;
N = round(max_angle/beta);

rot_angle = 0:dbeta:beta;
req_angle = 275/180*pi;
N_90 = round(pi/2/beta);
```

```
N_need = round(req_angle/beta);

figure(1);

for k = 1:N+2 %% +2 because head and tail components

   if k == 1
      node(k).location = [0 0 1];
      node(k).body = ones(6,1)*node(k).location + [-r, -ld/2, 0; -r,
ld/2+g, 0; 0, ld/2+2*g, 0; r, ld/2+g, 0; r, -ld/2, 0; -r, -ld/2, 0];
      node(k).axis = ones(2,1)*node(k).location + [0, -ld/2, 1; 0,
ld/2+2*g, 1];
      node(k).hole = ones(12,1)*node(k).location + [-r,
g+lc/3-hole_w/2, 0; -hole_r, g+lc/3-hole_w/2, 0; -hole_r,
g+lc/3+hole_w/2, 0; -r, g+lc/3+hole_w/2, 0; r, g+lc/3-hole_w/2, 0; hole_r,
g+lc/3-hole_w/2, 0; hole_r, g+lc/3+hole_w/2, 0; r, g+lc/3+hole_w/2, 0;
r-t, g, 0; r-t, g+lc, 0; -r+t, g, 0; -r+t, g+lc, 0];
   elseif k ~= N+2

      if k <= N_90
         l = lb;
      else
         l = la;
      end;

      if k == 2
         node(k).location = node(k-1).location + [0, ld+2*g, 0];
      elseif k == N_90+1
         node(k).location = node(k-1).location + [0, lb+2*g, 0];
      elseif k == N+2
         node(k).location = node(k-1).location + [0, la+2*g, 0];
      else
         node(k).location = node(k-1).location + [0, l+2*g, 0];
      end;

      node(k).body = ones(7,1)*node(k).location + [0, 0, 0; -r, g, 0;
-r, g+l, 0; 0, l+2*g, 0; r, l+g, 0; r, g, 0; 0, 0, 0];
      node(k).axis = ones(2,1)*node(k).location + [ 0, 0, 0; 0, l+2*g,
0];
```

```
        node(k).hole = ones(12,1)*node(k).location + [-r, g+l/2-hole_w/2,
0; -hole_r, g+l/2-hole_w/2, 0; -hole_r, g+l/2+hole_w/2, 0; -r,
g+l/2+hole_w/2, 0; r, g+l/2-hole_w/2, 0; hole_r, g+l/2-hole_w/2, 0;
hole_r, g+l/2+hole_w/2, 0; r, g+l/2+hole_w/2, 0;  r-t, g, 0; r-t, g+l,
0; -r+t, g, 0; -r+t, g+l, 0];
    end;

    if k == N+2
        node(k).location = node(k-1).location + [0, la+2*g, 0];
        node(k).body = ones(12,1)*node(k).location + [0, 0, 0; -r, g, 0;
-r, lc-l_head, 0; -r_head, lc-l_head, 0; -r, lc, 0; r, lc, 0; r_head,
lc-l_head, 0; r, lc-l_head, 0; r, g, 0; -r, g, 0; -r, lc-l_head, 0; r,
lc-l_head, 0];
        node(k).axis = ones(2,1)*node(k).location + [ 0, 0, 1;  0, lc-g,
1];
        node(k).hole = ones(12,1)*node(k).location;
    end;

    axis equal;
    axis([-5 40 -30 55]);
    hold on;

end;

hold off;

F(1)=getframe;
mov = addframe(mov,F(1));

traj = [node(1).body(2,:)];

for n = 1:length(rot_angle)

    wire_L = [node(1).hole(2,:); node(1).hole(3,:)];
    wire_R = [];
    length_wire_L = 0;
    length_wire_R = 0;

    for k = 1:N+2
```

```
if k ~= 1

    if k <= N_90
        l = lb;
    elseif k ~= N+2
        l = la;
    else
        l = lc;
    end;

    if k >= N+2-N_need
        if k == 2
            node(k).location = node(k-1).location +
(Rot((k-(N+2-N_need))*rot_angle(n))*[0, ld/2+2*g, 0]')';
        elseif k == N_90+1
            node(k).location = node(k-1).location +
(Rot((k-(N+2-N_need))*rot_angle(n))*[0, lb+2*g, 0]')';
        elseif k == N+2
            node(k).location = node(k-1).location +
(Rot((k-(N+2-N_need))*rot_angle(n))*[0, la+2*g, 0]')';
        else
            node(k).location = node(k-1).location +
(Rot((k-(N+2-N_need))*rot_angle(n))*[0, l+2*g, 0]')';
        end;
    end;

    if k ~= N+2
        if k >= N+2-N_need-1
            node(k).body =
(Tran(node(k).location)*(Rot((k-(N+2-N_need)+1)*rot_angle(n))*[0, 0,
1; -r, g, 1; -r, g+l, 1; 0, l+2*g, 1; r, l+g, 1; r, g, 1; 0, 0, 1]'))';

            node(k).axis =
(Tran(node(k).location)*(Rot((k-(N+2-N_need)+1)*rot_angle(n))*[ 0, 0,
1; 0, l+2*g, 1]'))';

            node(k).hole =
(Tran(node(k).location)*(Rot((k-(N+2-N_need)+1)*rot_angle(n))*[-r,
g+l/2-hole_w/2, 1; -hole_r, g+l/2-hole_w/2, 1; -hole_r, g+l/2+hole_w/2,
```

```
1; -r, g+l/2+hole_w/2, 1; r, g+l/2-hole_w/2, 1; hole_r, g+l/2-hole_w/2,
1; hole_r, g+l/2+hole_w/2, 1; r, g+l/2+hole_w/2, 1; r-t, g, 1; r-t, g+l,
1; -r+t, g, 1; -r+t, g+l, 1]'))';
            end;

            %% ========= For the control wires ==================
            wire_L = [wire_L; node(k).hole(2,:); node(k).hole(3,:)];

            if k <= N_need+1
               wire_R = [wire_R; node(k).hole(9,:);
node(k).hole(10,:)];
            end;

            if k == N_need+1
               wire_R(2*(k-1),:) = node(k).hole(10,:);
            end;

            length_wire_L = length_wire_L +
sqrt(sum((node(k-1).hole(3,:) - node(k).hole(2,:)).^2)) +
sqrt(sum((node(k).hole(2,:) - node(k).hole(3,:)).^2));
            length_wire_R = length_wire_R +
sqrt(sum((node(k-1).hole(10,:) - node(k).hole(9,:)).^2)) +
sqrt(sum((node(k).hole(9,:) - node(k).hole(10,:)).^2));

            %% ============== End of control wires ================

         else   %% if k = N+2
            node(k).body =
(Tran(node(k).location)*(Rot((k-(N+2-N_need)+1)*rot_angle(n))*[0, 0,
1; -r, g, 1; -r, lc-l_head, 1; -r_head, lc-l_head, 1; -r, lc, 1; r, lc,
1; r_head, lc-l_head, 1; r, lc-l_head, 1; r, g, 1; -r, g, 1; -r, lc-l_head,
1; r, lc-l_head, 1]'))';

            node(k).axis =
(Tran(node(k).location)*(Rot((k-(N+2-N_need)+1)*rot_angle(n))*[ 0, 0,
1;  0, lc-g, 1]'))';

            node(k).hole =
(Tran(node(k).location)*(Rot((k-(N+2-N_need)+1)*rot_angle(n))*[-r,
```

```
g+lc/3-hole_w/2, 1; -hole_r, g+lc/3-hole_w/2, 1; -hole_r,
g+lc/3+hole_w/2, 1; -r, g+lc/3+hole_w/2, 1; r, g+lc/3-hole_w/2, 1; hole_r,
g+lc/3-hole_w/2, 1; hole_r, g+lc/3+hole_w/2, 1; r, g+lc/3+hole_w/2, 1;
r-t, g, 1; r-t, g+lc, 1; -r+t, g, 1; -r+t, g+lc, 1]'))';

            %% ========== For the control wires ==================
            wire_L = [wire_L; node(k).hole(2,:); node(k).hole(3,:)];

            wire_R = [wire_R; node(k).hole(6,:); node(k).hole(7,:)];

            length_wire_L = length_wire_L +
sqrt(sum((node(k-1).hole(3,:) - node(k).hole(2,:)).^2)) +
sqrt(sum((node(k).hole(2,:) - node(k).hole(3,:)).^2));
            length_wire_R = length_wire_R +
sqrt(sum((node(k-1).hole(7,:) - node(k).hole(6,:)).^2)) +
sqrt(sum((node(k).hole(6,:) - node(k).hole(7,:)).^2));

            %% ============== End of control wires ===============

            traj = [traj; node(k).body(5,:)];

        end;

    else  %% if k = 1
        node(k).hole = ones(12,1)*node(k).location + [-r,
ld/4-hole_w/2, 0; -hole_r, ld/4-hole_w/2, 0; -hole_r, ld/4+hole_w/2, 0;
-r, ld/4+hole_w/2, 0; r, ld/4-hole_w/2, 0; hole_r, ld/4-hole_w/2, 0;
hole_r, ld/4+hole_w/2, 0; r, ld/4+hole_w/2, 0; r-t, ld/2, 0; r-t, ld/2,
0; -r+t, -ld/2, 0; -r+t, -ld/2, 0];

    end;


    plot(node(k).body(:,1),node(k).body(:,2),'k-');

    hold on;

    if k ~= N+2
        plot(node(k).axis(2,1),node(k).axis(2,2),'ro');
```

```
        end;

        plot(node(k).hole(1:4,1),
node(k).hole(1:4,2),'r-',node(k).hole(5:8,1),node(k).hole(5:8,2),'r-
');

        axis equal;
        axis([-5 40 -30 55]);

    end;

    swept_area = swept_area + sqrt(sum((traj(n+1,:) -
node(2).location).^2))*dbeta;

    delta_wire = length_wire_L - length_wire_R;

    wire_L = [wire_L(1,:); wire_L; ];
    wire_L(1,2) = wire_L(1,2) - 18 + delta_wire;
    wire_R = [wire_R(1,:); wire_R; ];
    wire_R(1,2) = wire_R(1,2) - 18 - delta_wire;

    plot(wire_L(:,1),wire_L(:,2),'b-', wire_R(:,1),wire_R(:,2),'b-');

plot(wire_L(length(wire_L),1),wire_L(length(wire_L),2),'b*',wire_R(l
ength(wire_R),1),wire_R(length(wire_R),2),'b*');
    plot(wire_L(1,1),wire_L(1,2),'bo',wire_R(1,1),wire_R(1,2),'bo');
    plot(traj(:,1), traj(:,2), 'g--');

    drawnow;
    hold off;

    F(n)=getframe;
    mov = addframe(mov,F(n));

end;

movie(F,1);
mov = close(mov);
```

B6. Pin-joint BS composed by identical parts with 2 pairs of control wires

This program is to simulate the pin-joint bending section controlling by two pairs of wires. Which means the bending section can be able to perform two stages of active deflections.

Case 1: Red pair mounts at the 12th part (Fig. 21(a))

```
req_angle = [180 90]/180*pi; % Range of deflection for 2 sub-sections
dir = [1 1]; % Direction of deflection for 2 sub-sections, 1-clockwise
```

The pair of red wires is mounted at the 12th part of the bending section, thus it can control the first twelve parts to deflect to 180° clockwise or counterclockwise. Meanwhile, the pair of blue wires is mounted at the distal end of the bending section. It enables one to pull one of the blue wires to make the rest of the bending section deflect to the extra 90°.

Case 2: Red pair mounts at the 6th part (Fig. 21(b))

```
req_angle = [90 180]/180*pi;
dir = [1 1];
```

The red wire is firstly pulled to control the first six parts deflecting to 90° and then the blue wire controls the rest to deflect to the extra 180°

Case 3: Deflecting in opposite direction (Fig. 22)

```
req_angle = [90 180]/180*pi;
dir = [1 -1];
```

The lower sub-section of the bending section can deflect to 90° clockwise by pulling the right red wire. Next, the left blue wire is pulled until the rest of the bending section deflects to 180 ° counterclockwise.

```
mov = avifile('2p_wire.avi')

max_angle = 275/180*pi;

g = 0.00625;
l = 0.0665;
r = 0.0485;
dbeta = 0.0025;
t = 0.003;
lc = 1;
```

```
theta = atan(g/r);
alpha = pi-2*theta;
beta  = 2*theta;
R = sin(alpha/2)/sin(beta)*l;

bias_angle = 25/180*pi;
hole_r = 0.084/2*cos(bias_angle)*[0.8 1];
hole_w = 0.018;

rot_angle = 0:dbeta:beta;

req_angle = [180 90]/180*pi;
dir = [1 1];
N_need = round(req_angle/beta);

N = sum(N_need);

figure(1);

for k = 1:N+2

   if k == 1
      node(k).location = [0 0 1];
      node(k).body = ones(5,1)*node(k).location + [-r, -l, 0; -r, l+g,
0; r, l+g, 0; r, -l, 0; -r, -l, 0];
      node(k).axis = ones(4,1)*node(k).location + [ 0, 0, 0;  0, 0, 0  ;
0, l+g, 0; 0, l+2*g, 0];
      for j = 1:length(N_need)
         node(k).hole(j).location = ones(12,1)*node(k).location + [-r,
g+l/3-hole_w/2, 0; -hole_r(j), g+l/3-hole_w/2, 0; -hole_r(j),
g+l/3+hole_w/2, 0; -r, g+l/3+hole_w/2, 0; r, g+l/3-hole_w/2, 0; hole_r(j),
g+l/3-hole_w/2, 0; hole_r(j), g+l/3+hole_w/2, 0; r, g+l/3+hole_w/2, 0;
r-t, g, 0; r-t, g+l, 0; -r+t, g, 0; -r+t, g+l, 0];
      end;
   elseif k ~= N+2
      node(k).location = node(k-1).location + [0, l+2*g, 0];
      node(k).body = ones(5,1)*node(k).location + [-r, g, 0; -r, g+l,
0; r, l+g, 0; r, g, 0; -r, g, 0];
      node(k).axis = ones(4,1)*node(k).location + [ 0, 0, 0;  0, g,   0;
```

```
0, l+g, 0; 0, l+2*g, 0];
        for j = 1:length(N_need)
            node(k).hole(j).location = ones(12,1)*node(k).location + [-r,
g+l/2-hole_w/2, 0; -hole_r(j), g+l/2-hole_w/2, 0; -hole_r(j),
g+l/2+hole_w/2, 0; -r, g+l/2+hole_w/2, 0; r, g+l/2-hole_w/2, 0; hole_r(j),
g+l/2-hole_w/2, 0; hole_r(j), g+l/2+hole_w/2, 0; r, g+l/2+hole_w/2, 0;
r-t, g, 0; r-t, g+l, 0; -r+t, g, 0; -r+t, g+l, 0];
        end;
    end;

    if k == N+2
        node(k).location = node(k-1).location + [0, l+2*g, 0];
        node(k).body = ones(5,1)*node(k).location + [-r, g, 0; -r, g+2*l,
0; r, 2*l+g, 0; r, g, 0; -r, g, 0];
        node(k).axis = ones(4,1)*node(k).location + [ 0, 0, 1;  0, g, 1;
0, g, 1; 0, g, 1];
        for j = 1:length(N_need)
            node(k).hole(j).location = ones(12,1)*node(k).location + [-r,
g+l/3-hole_w/2, 0; -hole_r(j), g+l/3-hole_w/2, 0; -hole_r(j),
g+l/3+hole_w/2, 0; -r, g+l/3+hole_w/2, 0; r, g+l/3-hole_w/2, 0; hole_r(j),
g+l/3-hole_w/2, 0; hole_r(j), g+l/3+hole_w/2, 0; r, g+l/3+hole_w/2, 0;
r-t, g, 0; r-t, g+l, 0; -r+t, g, 0; -r+t, g+l, 0];
        end;
    end;


plot(node(k).axis(1:2,1),node(k).axis(1:2,2),'g-',node(k).axis(3:4,1
),node(k).axis(3:4,2),'g-');
    for j = 1:length(N_need)
        plot(node(k).hole(j).location(1:4,1),
node(k).hole(j).location(1:4,2),'g-',node(k).hole(j).location(5:8,1)
,node(k).hole(j).location(5:8,2),'g-');
    end;
    axis equal;
    axis([-0.2 1.5 -1.5 1.8]);
    hold on;
    plot(node(k).body(:,1),node(k).body(:,2),'k-');

end;
```

```
hold off;

traj = [node(1).body(4,:)];

pre_angle = 0;

N_start = 1;

delta_wire = [0 0];

for j = 1:(length(N_need)-1)
   N_start = [N_start N_need(j)+1];
end;

for i = 1:length(N_need)

   for n = 1:length(rot_angle)

      for j = 1:length(N_need)
         wire(j).L = [node(1).hole(j).location(2,:);
node(1).hole(j).location(3,:)];
         wire(j).R = [node(1).hole(j).location(6,:);
node(1).hole(j).location(7,:)];
      end;

      length_wire_L(i) = 0;
      length_wire_R(i) = 0;

      for k = 1:N+2

         if k ~= 1

            if k > N_start(i) + 1
               if k <= N_need(i)+ N_start(i)
                  node(k).location = node(k-1).location +
(Rot(pre_angle + (k-N_start(i)-1)*dir(i)*rot_angle(n))*[0, 1+2*g,
0]')';
               else
```

```
                    node(k).location = node(k-1).location +
(Rot(pre_angle + (N_need(i))*dir(i)*rot_angle(n))*[0, l+2*g, 0]')';
                end;
            end;

            if k ~= N+2
                if k > N_start(i)
                    if k <= N_need(i) + N_start(i)
                        node(k).body =
(Tran(node(k).location)*(Rot(pre_angle +
(k-N_start(i))*dir(i)*rot_angle(n))*[-r, g, 1; -r, g+l, 1; r, l+g, 1;
r, g, 1; -r, g, 1]'))';

                        node(k).axis =
(Tran(node(k).location)*(Rot(pre_angle +
(k-N_start(i))*dir(i)*rot_angle(n))*[ 0, 0, 1;  0, g,   1; 0, l+g, 1; 0,
l+2*g, 1]'))';

                        for j = 1:length(N_need)
                            node(k).hole(j).location =
(Tran(node(k).location)*(Rot(pre_angle +
(k-N_start(i))*dir(i)*rot_angle(n))*[-r, g+l/2-hole_w/2, 1; -hole_r(j),
g+l/2-hole_w/2, 1; -hole_r(j), g+l/2+hole_w/2, 1; -r, g+l/2+hole_w/2,
1; r, g+l/2-hole_w/2, 1; hole_r(j), g+l/2-hole_w/2, 1; hole_r(j),
g+l/2+hole_w/2, 1; r, g+l/2+hole_w/2, 1; r-t, g, 1; r-t, g+l, 1; -r+t,
g, 1; -r+t, g+l, 1]'))';
                        end;
                    else
                        node(k).body =
(Tran(node(k).location)*(Rot(pre_angle +
(N_need(i))*dir(i)*rot_angle(n))*[-r, g, 1; -r, g+l, 1; r, l+g, 1; r,
g, 1; -r, g, 1]'))';

                        node(k).axis =
(Tran(node(k).location)*(Rot(pre_angle +
(N_need(i))*dir(i)*rot_angle(n))*[ 0, 0, 1;  0, g,   1; 0, l+g, 1; 0,
l+2*g, 1]'))';

                        for j = 1:length(N_need)
```

```
                        node(k).hole(j).location =
(Tran(node(k).location)*(Rot(pre_angle +
(N_need(i))*dir(i)*rot_angle(n))*[-r, g+l/2-hole_w/2, 1; -hole_r(j),
g+l/2-hole_w/2, 1; -hole_r(j), g+l/2+hole_w/2, 1; -r, g+l/2+hole_w/2,
1; r, g+l/2-hole_w/2, 1; hole_r(j), g+l/2-hole_w/2, 1; hole_r(j),
g+l/2+hole_w/2, 1; r, g+l/2+hole_w/2, 1; r-t, g, 1; r-t, g+l, 1; -r+t,
g, 1; -r+t, g+l, 1]'))';
                    end;
                end;
            end;

                for j = 1:length(N_need)
                    if k <= N_start(j) + N_need(j)
                        wire(j).L = [wire(j).L;
node(k).hole(j).location(2,:); node(k).hole(j).location(3,:)];
                        wire(j).R = [wire(j).R;
node(k).hole(j).location(6,:); node(k).hole(j).location(7,:)];
                    end;
                end;

            if (k <= N_need(i)+N_start(i)) & (k > N_start(i))
                length_wire_L(i) = length_wire_L(i) +
sqrt(sum((node(k-1).hole(i).location(3,:) -
node(k).hole(i).location(2,:)).^2)) +
sqrt(sum((node(k).hole(i).location(2,:) -
node(k).hole(i).location(3,:)).^2));
                length_wire_R(i) = length_wire_R(i) +
sqrt(sum((node(k-1).hole(i).location(10,:) -
node(k).hole(i).location(9,:)).^2)) +
sqrt(sum((node(k).hole(i).location(9,:) -
node(k).hole(i).location(10,:)).^2));
            end;

        else
            node(k).body =
(Tran(node(k).location)*(Rot(pre_angle +
(N_need(i))*dir(i)*rot_angle(n))*[-r, g, 1; -r, g+2*l, 1; r, 2*l+g, 1;
r, g, 1; -r, g, 1]'))';
```

```
                node(k).axis =
(Tran(node(k).location)*(Rot(pre_angle +
(N_need(i))*dir(i)*rot_angle(n))*[ 0, 0, 1;  0, g, 1; 0, g, 1; 0, g,
1]'))';

                for j = 1:length(N_need)
                    node(k).hole(j).location =
(Tran(node(k).location)*(Rot(pre_angle +
(N_need(i))*dir(i)*rot_angle(n))*[-r, g+l/3-hole_w/2, 1; -hole_r(j),
g+l/3-hole_w/2, 1; -hole_r(j), g+l/3+hole_w/2, 1; -r, g+l/3+hole_w/2,
1; r, g+l/3-hole_w/2, 1; hole_r(j), g+l/3-hole_w/2, 1; hole_r(j),
g+l/3+hole_w/2, 1; r, g+l/3+hole_w/2, 1; r-t, g, 1; r-t, g+l, 1; -r+t,
g, 1; -r+t, g+l, 1]'))';
                end;

                traj = [traj; node(k).body(3,:)];
            end;
            plot(node(k).location(:,1),node(k).location(:,2),'go');
        end;

plot(node(k).axis(1:2,1),node(k).axis(1:2,2),'g-',node(k).axis(3:4,1
),node(k).axis(3:4,2),'g-');

        for j = 1:length(N_need)
            plot(node(k).hole(j).location(1:4,1),
node(k).hole(j).location(1:4,2),'g-',node(k).hole(j).location(5:8,1)
,node(k).hole(j).location(5:8,2),'g-');
        end;
        axis equal;
        axis([-0.2 1.5 -1.5 1.8]);
        hold on;
        plot(node(k).body(:,1),node(k).body(:,2),'k-');
    end;

    delta_wire(i) = length_wire_L(i) - length_wire_R(i);

    for j = 1:length(N_need)
        wire(j).L = [wire(j).L(1,:); wire(j).L];
        wire(j).L(1,2) = wire(j).L(1,2) - 1 + delta_wire(j);
```

```
            wire(j).R = [wire(j).R(1,:); wire(j).R];
            wire(j).R(1,2) = wire(j).R(1,2) - 1 - delta_wire(j);
        end;

            plot(wire(1).L(:,1),wire(1).L(:,2),'r-',
wire(1).R(:,1),wire(1).R(:,2),'r-');

plot(wire(1).L(length(wire(1).L),1),wire(1).L(length(wire(1).L),2),'
r*',wire(1).R(length(wire(1).R),1),wire(1).R(length(wire(1).R),2),'r
*');

plot(wire(1).L(1,1),wire(1).L(1,2),'ro',wire(1).R(1,1),wire(1).R(1,2
),'ro');

            plot(wire(2).L(:,1),wire(2).L(:,2),'b-',
wire(2).R(:,1),wire(2).R(:,2),'b-');

plot(wire(2).L(length(wire(2).L),1),wire(2).L(length(wire(2).L),2),'
b*',wire(2).R(length(wire(2).R),1),wire(2).R(length(wire(2).R),2),'b
*');

plot(wire(2).L(1,1),wire(2).L(1,2),'bo',wire(2).R(1,1),wire(2).R(1,2
),'bo');

        drawnow;
        hold off;

        F_index = (i-1)*length(rot_angle)+n;
        F(F_index)=getframe;
        mov = addframe(mov,F(F_index));
    end;

    pre_angle = sum(dir(1:i).*req_angle(1:i));
end;
movie(F,1);
mov = close(mov);
```

B7. Trajectory of a BS composed by identical parts

This program is to figure out the trajectory of the distal end of the bending section composed by identical parts and a single pair of control wires. Locations of the entire bending section for different values of the part deflection angle β are plotted too.

```
L1 = 1.8806;
l = 3.0490;
r = 1.0668;
g = 0.1392;
L = l+2*g;
m = 6;
i = 1:m;

m_beta = 2*atan(g/r);
beta = -m_beta:0.001:m_beta;

for j = 1:length(beta)
    x(j) = L*sum(cos(beta(j)*i));
    y(j) = L*sum(sin(beta(j)*i));
end;

plot(x,y,'b-');
axis equal;
axis([-1 25 -16 16]);
grid;
xlabel('\bfx(mm)');
ylabel('\bfy(mm)');

hold on;

%% Different values of beta

x0 = 0;
y0 = 0;
```

```
m_beta = 2*atan(g/r);
u_beta = m_beta*ones(m);

for k = [0 0.5 1]

   x_b(1) = L*cos(u_beta(1)*k) + x0;
   y_b(1) = L*sin(u_beta(1)*k) + y0;

   for i = 2:m
      x_b(i) = L*cos(sum(u_beta(1:i)*k)) + x_b(i-1);
      y_b(i) = L*sin(sum(u_beta(1:i)*k)) + y_b(i-1);
   end;

   plot([x0 x_b], [y0 y_b],'r-');
   plot([x0 x_b], [y0 y_b],'r*');
   plot([x0 x_b], [y0 -y_b],'r-');
   plot([x0 x_b], [y0 -y_b],'r*');

end;

hold off;
```

B8. Trajectory of a BS composed by two sub-sections

B8.1 Controlled by a single pair of wires

This program is to figure out the trajectory of the distal end of the bending section composed by two sub-sections and a single pair of control wires under three different cases. In these case studies, α and β are treated as the input and the trajectory of the distal end is the output. Locations of the bending section for different values of the part deflection angle β are plotted too. Finally the comparison between three cases and the case using single pair of control wires are plotted and the distances of trajectory are calculated as well.

Case 1:

1. The lower sub-section fully deflects.
2. The upper sub-section fully deflects.

Case 2:

1. The upper sub-section fully deflects.
2. The lower sub-section fully deflects.

Case 3:

1. The lower sub-section reaches half of its full deflection.
2. The upper sub-section fully deflects.
3. The lower sub-section deflects until it reaches the limit.

```
r = 1.0668;
g = 0.1392;
l = [3.0490 1.8806];
L = l+2*g;
n = [6 13];

p_beta = 0;

m_alpha = 2*atan(g/r);
a1 = linspace(0, m_alpha/2, 500);
a2 = linspace(m_alpha/2, m_alpha, 500);

m_beta = 2*atan(g/r);
b = linspace(0, m_beta, 1000);
```

```
time = linspace(0,10, 2000);

for u = 1:3

   switch u
      case 1
         alpha = [a1 a2 m_alpha*ones(1,1000)];
         beta  = [zeros(1,1000) b];
         figure (u);
         plot(time, alpha/pi*180, 'g-', time, beta/pi*180, 'r-',
'LineWidth', 2);
         ylabel('\bfPart Deflection Angle (Degree)')
         legend('\bfLower sub-section: \alpha','\bfUpper sub-section:
\beta');
         axis([0 11 -2 20]);
      case 2
         alpha = [zeros(1,1000) a1 a2];
         beta  = [b m_beta*ones(1,1000)];
         figure (u);
         plot(time, alpha/pi*180, 'g-', time, beta/pi*180, 'r-',
'LineWidth', 2);
         ylabel('\bfPart Deflection Angle (Degree)')
         legend('\bfLower sub-section: \alpha','\bfUpper sub-section:
\beta');
         axis([0 11 -2 20]);
      case 3
         alpha = [a1 m_alpha/2*ones(1,1000) a2];
         beta  = [zeros(1,500) b m_beta*ones(1,500)];
         figure (u);
         plot(time, alpha/pi*180, 'g-', time, beta/pi*180, 'r-',
'LineWidth', 2);
         ylabel('\bfPart Deflection Angle (Degree)')
         legend('\bfLower sub-section: \alpha','\bfUpper sub-section:
\beta');
         axis([0 11 -2 20]);
   end;

   figure(u+3);
```

```
for k = 1:length(beta)

    x0 = 0;
    y0 = 0;

    x1(1,k) = L(1)*cos(alpha(k))+x0;
    y1(1,k) = L(1)*sin(alpha(k))+x0;

    for i = 2:n(1)
        x1(i,k) = L(1)*cos(alpha(k)*i)+x1(i-1,k);
        y1(i,k) = L(1)*sin(alpha(k)*i)+y1(i-1,k);
    end;

    x2(1,k) = L(2)*cos(beta(k) + n(1)*alpha(k)) + x1(n(1),k);
    y2(1,k) = L(2)*sin(beta(k) + n(1)*alpha(k)) + y1(n(1),k);

    for j = 2:n(2)
        x2(j,k) = L(2)*cos(beta(k)*j + n(1)*alpha(k)) + x2(j-1,k);
        y2(j,k) = L(2)*sin(beta(k)*j + n(1)*alpha(k)) + y2(j-1,k);
    end;

    if (k == 1) || (k == 501) || (k == 1001) || (k == 1501) || (k ==
2000)
        plot([x0; x1(:,k)], [y0; y1(:,k)], 'g-');
        hold on;
        plot([x0; x1(:,k)], [y0; y1(:,k)], 'g*');
        plot([x1(n(1),k); x2(:,k)], [y1(n(1),k); y2(:,k)], 'r-');
        plot([x1(n(1),k); x2(:,k)], [y1(n(1),k); y2(:,k)], 'r*');
    end;

end;

compx(u,:)= x2(n(2),:);
compy(u,:)= y2(n(2),:);

plot(x2(n(2),:),y2(n(2),:),'b-');
axis equal;
axis([-12 52 -5 45]);
xlabel('\bfx(mm)');
```

```
    ylabel('\bfy(mm)');

    hold off;

end;

figure(7);
hold on;

load singlepair;

plot(x, y, 'c:', compx(1,:),compy(1,:), 'b-', compx(2,:),compy(2,:),
'r-.', compx(3,:),compy(3,:), 'g--', 'LineWidth', 2);
axis equal;
axis([-10 50 -5 45]);
xlabel('\bfx(mm)');
ylabel('\bfy(mm)');
legend('Single pair','Case 1','Case 2','Case 3');
hold off;

%% Distances of different trajectories
traj_L1 = 0;
traj_L2 = 0;
traj_L3 = 0;
traj_LS = 0;

for v = 1:length(compx(1,:))-1
    traj_L1 =
sqrt((compx(1,v+1)-compx(1,v)).^2+(compy(1,v+1)-compy(1,v)).^2)+traj
_L1;
    traj_L2 =
sqrt((compx(2,v+1)-compx(2,v)).^2+(compy(2,v+1)-compy(2,v)).^2)+traj
_L2;
    traj_L3 =
sqrt((compx(3,v+1)-compx(3,v)).^2+(compy(3,v+1)-compy(3,v)).^2)+traj
_L3;
    traj_LS = sqrt((x(v+1)-x(v)).^2+(y(v+1)-y(v)).^2)+traj_LS;
end;
```

B8.2 Controlled by two pairs of wires

This program is to figure out the trajectory of the distal end of the bending section composed by two sub-sections and two pairs of control wires under two different cases. In these case studies, α and β are treated as the input and the trajectory of the distal end is the output. Locations of the bending section for different values of the part deflection angle β are plotted too. Trajectories of the distal end under different operations of the control wires are plotted for comparison.

Case 1:

1. The lower sub-section fully deflects counterclockwise.
2. The upper sub-section fully deflects clockwise.

Case 2:

1. The upper sub-section fully deflects clockwise.
2. The lower sub-section fully deflects counterclockwise.

```
r = 1.0668;
g = 0.1392;
l = [3.0490 1.8806];
L = l+2*g;
n = [6 13];

p_beta = 0;

m_alpha = 2*atan(g/r);
a = linspace(0, m_alpha, 1000);

m_beta = 2*atan(g/r);
b = linspace(0, -m_beta, 1000);

time = linspace(0,10, 2000);

for u = 1:2

   switch u
```

```
      case 1
         alpha = [a m_alpha*ones(1,1000)];
         beta  = [zeros(1,1000) b];
         figure (u);
         plot(time, alpha/pi*180, 'g-', time, beta/pi*180, 'r-',
'LineWidth', 2);
         ylabel('\bfPart Deflection Angle (Degree)')
         legend('\bfLower sub-section: \alpha','\bfUpper sub-section:
\beta');
         axis([0 11 -20 20]);
      case 2
         alpha = [zeros(1,1000) a];
         beta  = [b -m_beta*ones(1,1000)];
         figure (u);
         plot(time, alpha/pi*180, 'g-', time, beta/pi*180, 'r-',
'LineWidth', 2);
         ylabel('\bfPart Deflection Angle (Degree)')
         legend('\bfLower sub-section: \alpha','\bfUpper sub-section:
\beta');
         axis([0 11 -20 20]);
   end;

   figure(u+2);

   for k = 1:length(beta)

     x0 = 0;
     y0 = 0;

     x1(1,k) = L(1)*cos(alpha(k))+x0;
     y1(1,k) = L(1)*sin(alpha(k))+x0;

     for i = 2:n(1)
        x1(i,k) = L(1)*cos(alpha(k)*i)+x1(i-1,k);
        y1(i,k) = L(1)*sin(alpha(k)*i)+y1(i-1,k);
     end;

     x2(1,k) = L(2)*cos(beta(k) + n(1)*alpha(k)) + x1(n(1),k);
     y2(1,k) = L(2)*sin(beta(k) + n(1)*alpha(k)) + y1(n(1),k);
```

```
        for j = 2:n(2)
            x2(j,k) = L(2)*cos(beta(k)*j + n(1)*alpha(k)) + x2(j-1,k);
            y2(j,k) = L(2)*sin(beta(k)*j + n(1)*alpha(k)) + y2(j-1,k);
        end;

        if (k == 1) || (k == 1001) || (k == 2000)
           plot([x0; x1(:,k)], [y0; y1(:,k)], 'g-');
           hold on;
           plot([x0; x1(:,k)], [y0; y1(:,k)], 'g*');
           plot([x1(n(1),k); x2(:,k)], [y1(n(1),k); y2(:,k)], 'r-');
           plot([x1(n(1),k); x2(:,k)], [y1(n(1),k); y2(:,k)], 'r*');
        end;

    end;

    compx(u,:)= x2(n(2),:);
    compy(u,:)= y2(n(2),:);

    plot(x2(n(2),:),y2(n(2),:),'b-');
    axis equal;
    if u == 1
       axis([-5 50 -5 45]);
    else
       axis([-5 50 -25 25]);
    end;
    xlabel('\bfx(mm)');
    ylabel('\bfy(mm)');

    hold off;

end;

figure(7);
hold on;

load singlepair;

plot(compx(1,:),compy(1,:), 'b-', compx(2,:),compy(2,:), 'r-.',
```

```
'LineWidth', 2);
axis equal;
axis([0 50 -30 50]);
xlabel('\bfx(mm)');
ylabel('\bfy(mm)');
legend('Case 4','Case 5');
hold off;

traj_L4 = 0;
traj_L5 = 0;

for v = 1:length(compx(1,:))-1
   traj_L4 =
sqrt((compx(1,v+1)-compx(1,v)).^2+(compy(1,v+1)-compy(1,v)).^2)+traj
_L4;
   traj_L5 =
sqrt((compx(2,v+1)-compx(2,v)).^2+(compy(2,v+1)-compy(2,v)).^2)+traj
_L5;
end;
```

- **Mathematical Functions**

B9. Translation

This function is the translation matrix. The input parameter is a 3X1 point.

```
function Translate = Tran(pt)
Translate = [[1 0 0]' [0 1 0]' pt'];
```

B10. Rotation

This function is the rotation matrix about z-axis. The input is an angle.

```
function Rotate = Rot(angle)
Rotate = [cos(angle) sin(angle) 0; -sin(angle) cos(angle) 0; 0 0 1];
```